Received: 21 June 2023 | Revised: 24 August 2023 | Accepted: 11 September 2023

DOI: 10.1002/est2.524

RESEARCH ARTICLE

ENERGY STORAGE WILEY

Hydrogen storage materials for vehicular applications

Sumita Srivastava

Government Degree College, Nainbagh, Tehri Garhwal, India

Correspondence
Sumita Srivastava, Government Degree College, Nainbagh 249186, Tehri Garhwal, India.
Email: sumita_uki1@rediffmail.com

Abstract

Hydrogen energy has been assessed as the clean and renewable energy source with the highest energy density. At present, 25% of energy demand comes from the transport sector, while 20% of greenhouse gases are produced from the transport sector at the global level. Hydrogen may be utilized in the vehicles as a fuel for fuel cell vehicles or as a hydrogen system in internal combustion engine vehicles. In both cases, hydrogen storage remains a key parameter. Various types of hydrogen storage materials have a wide range of operating conditions in terms of temperature, hydrogen plateau pressure, and hydrogen storage capacity with other relevant hydrogenation characteristics. At present, not a single hydrogen storage material is available to fulfill all the requirements of hydrogen storage for vehicles on the set target of DOE US. MgH_2 has high hydrogen storage capacity equivalent to 7 wt%, but desorption temperature is 300°C. The normal vehicles do not operate at such a high temperature. Therefore, in the present communication, combinations of metal hydrides have been studied. The first combination belongs to MgH_2 and AB_2 system and another belongs to MgH_2, $NaAlH_4$, and AB_2 system. In the calculation performed, it has been shown that the amount of heat and temperature available in the exhaust gas of a vehicle is enough to liberate the hydrogen from the high-temperature metal hydride system. The calculated specific capacity on the system basis has been found as 1.13 kWh/kg (0.034 kgH_2/kg) and 1.20 kWh/kg (0.036 kgH_2/kg) for both combinations, respectively. These values of specific capacity are very much close to the present target of DOE US.

KEYWORDS

fuel cell, hydrogen energy, internal combustion, metal hydride, specific capacity, vehicles

1 | INTRODUCTION

In the world energy scenario, the energy demand in 2019 was 606 EJ. At present, about 80% of energy comes from fossil fuel sources. According to the International Energy Association (IEA), the total electricity generation in the world was 26 936 TWh in 2019, where 63.1% share came from fossil fuels. In 2018, carbon dioxide emission during electricity generation was 1.4 t CO_2/MWh. Total world carbon dioxide emission during 2019 was 33.6 Gt compared to 15.5 Gt in 1973. In 2020, CO_2 emission was recorded as 31.5 Gt. In the world, during 2019, per capita total energy supply, electricity consumption, and CO_2 emission were 79.1 GJ, 3265 kWh, and 4.39 t, respectively.[1-3] At present, 25% of energy demand comes from the transport sector, while 20% of greenhouse gases are produced from the transport sector at the global level. In this energy scenario, the world must move from the

exhaustive use of fossil fuels. Fossil fuels have double disadvantages. On the one side, it has many detrimental effects on the environment like emission of greenhouse gases, global warming, acid rain, air pollution, and so on; on the other side, it is of non-renewable nature with limited stock on the earth.

In the search for clean, renewable, and sustainable energy sources, we have many choices like solar, wind, geothermal, biomass, hydropower, ocean, and wave energy.[4] Unfortunately, no one can be used directly in the transport sector from this list. Thus, to replace fossil fuel from the transport sector, we need another form of energy. Hydrogen energy has been assessed as the clean, green, and renewable source of energy to fulfill the demand for alternative energy in the transport sector. Hydrogen is a secondary energy carrier and has versatile applications in the energy sector as well as in other sectors. As a source of energy, hydrogen offers the highest calorific value as a fuel having the highest energy density.[5] Mostly hydrogen is produced from water through water electrolysis and converted again into water after combustion. Three-fourths of the land on the earth is covered with water, giving plenty of resources for hydrogen production. When hydrogen production through water electrolysis is coupled with other forms of renewable electricity, it offers environmentally clean and renewable fuel for society. To harness the hydrogen energy at its fullest potential, hydrogen production and storage, followed by transportation and applications, are the major issues to be looked upon. In the study covered by IEA, it has been discussed that hydrogen is firmly a suitable candidate to become a clean, secure, and affordable energy future. In 2020, hydrogen demand was 90 Mt, practically all in the refining and industrial sectors. Presently, most of the hydrogen is produced by fossil fuel and in the production of this 90 Mt hydrogen, 900 Mt of CO_2 was emitted.[6,7] Therefore, the world must adopt the clean production of hydrogen, especially through water electrolysis. If hydrogen is produced through fossil fuels, the process should be followed by carbon capture, utilization, and storage method.

Hydrogen energy has many applications other than the transport sector like industry, refinery, power production, heating purpose, and so on. The present communication is focused on the application of hydrogen in the transport sector. At present, the share of hydrogen energy in the transport sector is only 0.01% of total transportation energy. However, it has been predicted by IEA that in the Net Zero Emissions Scenario (NZES), hydrogen demand would be almost 6-fold to reach the value of 530 Mt H_2 by 2050. In this amount of hydrogen, half of the demand will be for the industry and transport sectors. Whereas the demand in the industrial sector would be nearly triple from the present, that is, from 50 Mt H_2 in 2020 to around 140 Mt H_2 in 2050, the transport sector would utilize more than 100 Mt H_2 in 2050 in comparison to less than 20 kt H_2 at present. In the Announced Pledges Scenario (APS), hydrogen and hydrogen-based fuel consumption in transport would climb to 520 PJ or 0.4% of transport energy demand in 2030. By 2050, the demand would be about 15 times higher than in 2030 for hydrogen and hydrogen-based fuels across all transport end-uses and equivalent to 6% of the transport sector's energy demand. In the NZES, hydrogen and hydrogen-based fuel deployment would be accelerated in comparison to APS and would reach the value of 2.7 EJ in 2030, covering 2.6% of transport energy demand. This would further increase by 2050 and hydrogen and hydrogen-based fuels would cover 25% of total transport energy demand in the NZE scenario.

Hydrogen energy as fuel has many advantages in comparison to other existing fuels. Hydrogen has a wide flammability range, high auto-ignition temperature, minimum ignition energy, large flame velocity, and high heating value. These combustion properties of hydrogen and other fuels are summarized in Table 1.[8]

In the transport sector, we have varieties of vehicles like passenger vehicles, trucks, forklifts, buses, logistic vehicles, aviation, marine, and e-bike. For efficient deployment of hydrogen in the transport sector, it has to meet and fulfill certain challenges as mentioned below.[9-11]

1. Safety;
2. Range of the vehicle before the next charging;
3. Performance based on high gravimetric and volumetric hydrogen storage;
4. Good reaction kinetics for fast charging-discharging of the fuel;
5. Thermodynamically operative near ambient conditions for reversible hydrogen intake and release;
6. Cold start of the vehicles;
7. Cost;
8. Infrastructure and technical adaptation;
9. Wide scalability range so that it may apply to small and large vehicles.

At present in the transport sector, two types of vehicles are available in the market: gasoline/compressed natural gas/diesel-based internal combustion engine vehicles (ICEV) and battery-operated electric vehicles (BEV). The third category is hybrid vehicles, a mixture of both methods. Hydrogen energy may be utilized as a fuel in the transport sector for vehicles in two broad ways. The first method utilizes hydrogen as a fuel in the internal combustion engine (ICE) of vehicles. The other

TABLE 1 Combustion properties of hydrogen.[8]

Property	Hydrogen	CNG	Gasoline
Density (kg/m^3)	0.0824	0.72	730
Flammability limits (ϕ)	10 to 0.14	2.5 to 0.62	1.43 to 0.25
Auto ignition temperature in air (K)	858	723	550
Minimum ignition energy (MJ)	0.02	0.28	0.24
Flame velocity (m/s)	1.85	0.38	0.37 to 0.43
Adiabatic flame temperature (K)	2480	2214	2580
Stoichiometric fuel/air ratio	0.029	0.069	0.068
Lower heating value (MJ/kg)	119.7	45.8	44.79
Research octane number	>120	140	91 to 99

TABLE 2 Comparison of hydrogen storage technologies.[16]

Storage technologies capacity (kWh/kg)	Gravimetric capacity (kWh/L)	Volumetric ($/kWh)	Cost
Chemical hydrides	1.6	1.4	8
Complex metal hydrides	0.8	0.6	16
Liquid hydrogen	2.0	1.6	6
10 000-psi gas	1.9	1.3	16
DOE goals	3.0	2.7	2

method relates to the use of hydrogen in the fuel cells of electric vehicles. In both categories, hydrogen may be deployed in many ways.[12-15] These are listed in the following:

1. Compressed hydrogen gas in a cylinder;
2. Liquid hydrogen in a cylinder;
3. Cryo-compressed hydrogen gas in a cylinder;
4. Fuel cells with any of the above sources of hydrogen as a fuel (FCEV);
5. Fuel cell with hydrogen adsorbed/absorbed in hydrogen storage material;
6. Hydrogen storage material as a source of hydrogen for ICE in vehicles.

All these methods have their advantages and disadvantages. The future will be of that, which will win the race. A comparison of all these storage technologies has been presented in Table 2.[16] For the 400 km range of passenger vehicles, 24 kg petrol is needed. The same range may be covered by 4 kg hydrogen using fuel cells in FCEV and 8 kg hydrogen in ICE vehicles.[17] On comparing the BEV and FCEV, one finds that the performance of FCEV is far better than BEV. FCEV can be refueled in less than 10 min, while BEV takes more time, even hours. Weight is significantly lower in FCEV. It is approximately 550 Wh/kg for FCEV compared to 150 Wh/kg for BEV. The cost of lithium-ion battery BEV is about 270$/kWh and 270$/kW compared to fuel cells with compressed hydrogen tanks as 15$/kWh and 100 $/kW, respectively.[18,19] Hydrogen refueling charge is estimated as $8/kg hydrogen and 0.24 $/kWh.[20] As reflected in Table 2, compressed hydrogen gas and liquid hydrogen is not viable storage system for long-term future application due to the larger weight of the tank and associated cost factor. Therefore, researchers are trying to find suitable materials for vehicular purposes.

The material-based hydrogen storage technologies have the advantage that the characteristics may highly be altered by tailoring the material. The hydrogenation properties of hydrogen storage materials are very sensitive to the synthesis route adopted for the synthesis of the material and the substituted elements in the parent material. Thus, material-based hydrogen storage technologies have a wider scope for improvement. At present, all hydrogen storage materials may be divided into four major categories.[1,10] These are described in the following.

1. Conventional metal hydrides: Conventional metal hydrides are AB, AB_2, A_2B, and AB_5 types of alloys. Here, A is the element with large hydrogen affinity and B is a commonly a transition element. Hydrogen atoms are stored at the interstitial sites of the structure forming the metallic bond with the host metal atoms. Examples are TiNi, TiFe, ZrNi, $TiMn_2$, ZrV_2, $ZrMn_2$, Mg_2Ni, Mg_2Co, Zr_2Fe, $LaNi_5$, $CeNi_5$, and $CaNi_5$.
2. Complex metal hydrides: In complex hydrides, hydrogen is covalently bonded as stable “complex” anions

TABLE 3 Comparison of hydrogenation characteristics of hydrogen storage materials for vehicles.[10]

Properties	Conventional metal hydrides	Complex metal hydrides	Sorbent systems	Chemical hydrides
Example	$LaNi_5H_6$	$NaAlH_6$	MOF-5	NH_3BH_3
Volumetric capacity	Satisfactory	Satisfactory	Improvement	Satisfactory
Gravimetric capacity	Unsatisfactory	Satisfactory	Satisfactory	Satisfactory
Reversibility	Satisfactory	Satisfactory	Satisfactory	Unsatisfactory
Thermodynamics	Satisfactory	Satisfactory	Unsatisfactory	Improvement
Kinetics	Satisfactory	Unsatisfactory	Satisfactory	Improvement
Efficiency	Satisfactory	Satisfactory	Satisfactory	Unsatisfactory
Desorption enthalpy (ΔH)	Endothermic	Largely endothermic Less exothermic	Endothermic	Largely exothermic Less endothermic

having the formula $A_xB_yH_z$. Here, A is a light element of the first and second group forming cation and B is Al, B, N, and transition elements. These are lightweight metal hydrides known as alanates and borohydrides. Examples are: $NaAlH_4$, $LiAlH_4$, $Mg(AlH_4)_2$, $NaBH_4$, $LiBH_4$, and $Mg(BH_4)_2$.

3. Sorbent systems: In this system, molecular hydrogen is physically adsorbed to the large surface area of the sorbent material. Examples are active carbon, carbon nanotubes and doped metal-organic framework (MOF).
4. Chemical hydrides: In this storage system, hydrogen is covalently bonded to the atoms of the material and this system is utilized as single-use fuel. Thus hydrogenation process is not reversible at ambient conditions. Charging of the fuel is possible off the board. Examples are NH_3, NH_3-BH_3, and AlH_3.

A comparison of the hydrogenation characteristics of these hydrogen storage systems relevant for vehicular application is presented in Table 3.[10]

The above discussions show various options to deploy hydrogen as fuel in vehicles. The material-based hydrogen systems are more advanced. It is more useful than the conventional compressed hydrogen gas cylinder. According to US DOE goals for the application of hydrogen as fuel in vehicles, at present no material fulfills all the requirements.[21,22] However few examples of $LaNi_5$, TiFe, and $TiMn_2$-based alloys have been reported to store hydrogen successfully in vehicles either for fuel cells or for internal combustion engines.[11,15,21,23] Though these materials have less gravimetric hydrogen storage capacity (1.5-2.0 wt%), they have an excellent performance to operate at near ambient conditions, easy activation, good reversibility of hydrogen, fast kinetics and necessary thermodynamic conditions. Hence, such metal hydrides with abovementioned properties are still likely to win the race until any other material comes with these primary requirements and high gravimetric and volumetric storage capacity.

In metal hydrides, the bond between metal and hydrogen is metallic. The nature of bond depends on the electronegativity of elements. For smaller electronegativity of elements, bond with hydrogen is ionic, while for larger electronegativity, bond is covalent. In between metallic bond is formed. Therefore, in metal hydrides, one element (A) of alloy ($AB/AB_5/AB_2/A_2B$) is hydride forming, while another is generally transition element (B), which is not hydride farming. Transition elements act as catalysts for dissociation of gaseous hydrogen molecules into hydrogen atoms. After dissociation, these hydrogen atoms penetrate inside the alloy and are stored in the interstitial space of the alloy. In this case, the electron energy levels of metal and hydrogen overlap sharing delocalized electrons characterized by a metallic bonding.[24] The hydrogen atom is occupied in either a tetrahedral or an octahedral void formed by metal atoms. During hydrogen desorption, reverse process occurs. Hydrogen atoms migrate from interstitial voids to the surface of alloy, where combination of atoms takes place to form hydrogen molecule. The hydrogen absorption-desorption kinetics play a crucial role for application of metal hydrides, especially for vehicular application. Several reports have shown that multiphase (disordered) materials have better kinetics in comparison to single-phase material.[25,26] It is due to the reason that disordered materials have more channels for hydrogen penetration in form of higher density of phase boundary and grain boundary. Nano version of alloys and catalyst-embedded alloys also offer better hydrogen absorption-desorption kinetics in comparison to bulk alloys.[27-29] Use of multielement composition and studies through theoretical and simulation-based investigations are new approaches in the development of metal hydrides.[30-32]

It also pertains to discuss here the comparison of BEV, FCEV, and hydrogen-based ICEV. It has been already established that FCEV is better than BEV in comparison to weight, cost, and charging time.[18-20] It has been assessed that at present, FCEVs are 40% and 90% more expensive than BEVs and gasoline-based ICEVs, respectively, on a per 100 km drive basis; by 2027, it will be less than both. The next concern is the comparison of FCEV and hydrogen-based ICEV. There are four types of fuel cells[11];

1. Alkaline Fuel Cells (AFC) and Direct Borohydride Fuel Cells (DBFC);
2. Low-temperature Proton Exchange Membrane Fuel Cells (LT PEMFC), Direct Methanol Fuel Cells (DMFC), and High-temperature Proton Exchange Membrane Fuel Cells (HT PEMFC);
3. Phosphoric Acid Fuel Cells (PAFC);
4. Molten Carbonate Fuel Cells (MCFC).

In all varieties of fuel cells, LTPEMFC is suitable for vehicular purposes operative at 60°C to 80°C. To feed the hydrogen fuel to LTPEMFC, the required hydrogen storage system must also be operative at a similar temperature. If one applies high-temperature materials like MgH_2 and $NaAlH_4$ having high hydrogen storage capacity, an extra mechanism to supply heat energy is also required. However, such high-temperature materials may be applied in ICEV as the extra heat energy may be supplied through exhaust gas. The obvious advantages of ICEV are the ready technology with small changes in gasoline ICEV. It may operate at ambient conditions in the context of fuel and air impurity. Hydrogen-based ICEV has less demand for rare earth and precious metals as in BEV and FCEV. ICEV has well-established development and production methods.[33] However, the efficiency of ICEV (40%-45%) is less than the efficiency of FCEV (50%-60%). In light of the above facts, ICEV may be a better option to serve the transport sector to replace existing fossil fuels in robustly.

The present manuscript is based on the study of ICEV operated with a metal hydride bed. The materials selected for the hydride bed are conventional metal hydrides. There is not a single material applicable for this purpose. Therefore, in the present study, combinations of alloys have been selected for this purpose. Various characteristics related to ICEV, like efficiency, compression ratio, brake thermal efficiency, output power, and exhaust gas heating value at different equivalence ratios, have been calculated on a theoretical basis. Efforts have been made to calculate the amount of heat transferred from the exhaust gas of ICEV to supply the required heat to high-temperature metal hydrides. In the present investigation, the combinations of metal hydrides applied in a metal hydride bed are Mg-hydride+AB_2-type hydride and Mg-hydride+$NaAlH_4$ hydride. Currently, no alloy is present with high hydrogen storage capacity (~6 wt%) with operation at ambient temperature and pressure. The vehicle runs at ambient temperature and pressure. Hence, in the present study, the combination of metal hydride alloy is proposed: one alloy with high hydrogen storage capacity (MgH_2) and other operative at ambient temperature and pressure ($TiMn_2$ and $NaAlH_4$). The global concern of clean environment has resulted in the scenario of Net Zero Emission (NZE) by 2050. Transport sector is responsible for 21% of carbon dioxide in the total emissions.[2] It is the need of hour to replace fossil fuel-based transport system with clean and renewable energy. Hydrogen energy may be utilized to proceed in this direction. Present study offers a mean to utilize hydrogen energy as fuel in vehicles to replace fossil fuel.

2 | METHODOLOGY

The present study is focused on the search for appropriate materials for metal hydride beds in ICEV. For onboard charging at ambient conditions, only metal hydrides fulfill the conditions to be used in the bed of ICEV. The known metal hydrides with high storage capacity (MgH_2 and $NaAlH_4$) need high temperatures for desorption of hydrogen. It has been proposed here to use a combination of metal hydrides; one operated at ambient conditions and another operated at high temperatures. The reason behind choosing the combination is that the known metal hydrides operated at ambient conditions have a low hydrogen storage capacity of 1.5 to 2.0 wt% (AB_5, AB, and AB_2), while known metal hydrides with high storage capacity of 5.0 to 7.0 wt% is operative at higher temperature (100°C-350°C). The idea is that at the ambient conditions, the first material releases the hydrogen to start the vehicle. As soon as the vehicle is started, the heat released in the exhaust gas can be supplied to another material working at higher temperatures to release the hydrogen. Calculations have been performed to check what amount of heat is available in the exhaust gas and what amount of heat can be supplied to the high-temperature material. The viability in the context of heat available in the exhaust gas has been evaluated. Together with this, various other basic operations of the IC engine have also been calculated on a theoretical basis. These are efficiency, compression ratio, brake thermal efficiency, output power, exhaust gas heating value at different equivalence ratios, and so on. The formulae and equations for calculations are described here.

2.1 | Auto-ignition temperature and thermal efficiency

During the compression of fuel in the engine, the temperature of the chamber increases. If this high temperature becomes equal to the auto-ignition temperature, the auto-ignition starts. Thus auto-ignition temperature of the fuel is an important factor to calculate the required compression ratio.[34]

$$T_2 = T_1\left(\frac{V1}{V2}\right)^{\gamma-1} \tag{1}$$

where V_1/V_2 = the compression ratio, T_1 = absolute initial temperature, T_2 = absolute final temperature, and γ = ratio of specific heats.

The compression ratio of the engine and the ratio of the specific heat of the fuel are important to decide the theoretical thermodynamic efficiency of an Otto cycle engine.[34]

$$\eta_{th} = 1 - \frac{1}{\left(\frac{V1}{V2}\right)^{\gamma-1}} \tag{2}$$

where V_1/V_2 = the compression ratio, γ = ratio of specific heats, and η_{th} = theoretical thermodynamic efficiency.

2.2 | Stoichiometric mixture and fuel/air equivalence ratio (ϕ)

For combustion in the IC engine, fuel is mixed with air. In the stoichiometric mixture, air is mixed with fuel in the amount to fulfill the complete combustion of the fuel. If the air quantity is less than the stoichiometric amount, the mixture is known as a lean mixture and if the air is more, it is known as a rich mixture.[34] For stoichiometric ratio, the combustion equation is

$$H_2 + \frac{1}{2}O_2 + 1.887\,N_2 = H_2O + 1.887\,N_2 \tag{3}$$

Let us consider the molecular weights of oxygen and atmospheric nitrogen as 32 and 28.16, respectively, and the atomic weight of hydrogen as 1.008. By weight the stoichiometric air-to-fuel ratio is

$$\frac{(0.5\times 32) + (1.887\times 28.16)}{(2\times 1.008)} = 34.3 \tag{4}$$

Hence for the stoichiometric mixture $(A/F)_S = 34.3$ (5)

At molar or volumetric basis, the ratio of fuel/air in a stoichiometric mixture is

$$\frac{\text{Number of moles of hydrogen (LHS of Eq 3)}}{\text{Total number of moles (LHS of Eq 3)}} = \frac{1}{3.387} = 0.295 \tag{6}$$

Hence, the volumetric % of hydrogen in the stoichiometric mixture is 29.5%.

Now fuel/air equivalence ratio ϕ is defined as

$$\phi = \frac{\left(\frac{F}{A}\right)_{\text{actual}}}{\left(\frac{F}{A}\right)_S} \tag{7}$$

The relative air-to-fuel ratio (λ) is the inverse of ϕ and it is defined as

$$\lambda = \frac{\left(\frac{A}{F}\right)_{\text{actual}}}{\left(\frac{A}{F}\right)_S} \tag{8}$$

For fuel-lean mixture: $\phi < 1, \lambda > 1$
For stoichiometric mixture: $\phi = 1, \lambda = 1$
For fuel-rich mixture: $\phi > 1, \lambda < 1$

2.3 | Engine power and brake thermal efficiency

Engine power is defined as the product of angular speed and torque as given in the following equation:

$$P_b\,(\text{kW}) = 2\pi\omega\left(\frac{\text{rev}}{\text{s}}\right) \times T(\text{N m}) \times 10^{-3} \tag{9}$$

where P_b = power, ω = angular speed (revolution per s), and T = torque.

In the IC engine brake thermal efficiency ($\eta_{b\text{th}}$) is defined as the ratio of the work produced to the amount of heat energy released during the combustion process.[34]

$$\eta_{b\text{th}} = \frac{P_b(\text{kW})}{m_f\left(\frac{\text{kg}}{\text{s}}\right) \times Q_{\text{LHV}}\left(\frac{\text{kJ}}{\text{kg}}\right)} \tag{10}$$

where $\eta_{b\text{th}}$ = brake thermal efficiency, P_b = power, m_f = mass flow rate of fuel (kg/s), and Q_{LHV} = lower heat value of fuel (kJ/kg).

2.4 | Heat transferred by exhaust gas

The maximum quantity of heat Q_{HT}, which can be supplied to the high-temperature hydrogen storage system, is given as[15]:

$$Q_{HT} = Q_A \frac{T_A - T_B}{T_A - T_0} \tag{11}$$

where Q_A = thermal content of the exhaust gas, Q_{HT} = the maximum quantity of heat transferred, T_A = temperature of the exhaust gas, T_B = operating temperature of hydride, and T_0 = ambient temperature.

The number of moles of hydrogen liberated by absorbing the heat Q_{HT} from high-temperature system is

$$\eta = \frac{Q_{HT}}{\Delta H} \tag{12}$$

where ΔH is the heat of desorption per mole of H_2.

Using above mentioned equations, the following properties for metal hydride-based ICEV have been calculated.

1. The compression ratio has been evaluated to get the auto-ignition temperature. Using this compression ratio, the thermal efficiency of the engine has been calculated.
2. The energy available in exhaust gas/mole H_2 combustion, the energy available in exhaust gas/mole initial mixture (before combustion), and energy available in exhaust gas/mole exhaust gas (after combustion) at different equivalence ratios (ϕ = 0.70-1.00).
3. The above data has been recalculated at different mass flow rates (m_f) of hydrogen fuel (1-40 kg H_2/h).
4. The power of the engine has been calculated at each combination of angular speed and torque by varying angular speed (500-4000 rpm) and torque (100-3000 N m).
5. The efficiency of the engine has been calculated at the fixed torque value (500 N m) at different values of ϕ (ϕ = 0.8 and 1.0) by varying the hydrogen mass flow rate m_f (1-40 kg H_2/h).
6. Combinations of high-temperature and ambient-temperature metal hydrides have been taken and the amount of heat available in the exhaust gas, the amount of heat transferred to the high-temperature storage system and the viability of the process have been calculated and studied.

3 | RESULTS AND DISCUSSIONS

In the present study, many properties related to ICEV connected with metal hydride beds have been calculated on a theoretical basis. These properties have been calculated for a wide range of input parameters. The range of the value of input parameters has been selected near to the values quoted by earlier researchers in their work.

3.1 | Auto-ignition temperature and thermal efficiency

Using Equation (1), first, the compression ratio is evaluated and then thermal efficiency is calculated at the same compression ratio.

T_2 = auto-ignition temperature of hydrogen = 858K.

T_1 = ambient temperature = 300K.

γ = specific heat ratio for hydrogen = 1.4.

Hence, the corresponding ratio of V_1/V_2 = 13.83.

The thermal efficiency η_{th} at the same compression ratio = 65.03%.

The common value of the compression ratio in ICEV is between 8.7 and 13.[15,21,33]

3.2 | Energy value of the exhaust gas

The lower heating value (LHV) for hydrogen is 120 MJ/kg, equivalent to 240 kJ/mole H_2.

At ϕ = 1, the combustion equation is

$$H_2 + \frac{1}{2}O_2 + 1.887\,N_2 = H_2O + 1.887\,N_2 \tag{13}$$

In this equation,

Number of moles of reactant mixture = 3.387.

Number of moles of exhaust mixture = 2.887.

The heating value of 1 mole of H_2 is 240 kJ.

Therefore,

The heating value of exhaust gas per reaction of 1 mole H_2 is = 240 kJ.

Heating value per mole mixture is = 240 kJ/3.387 = 70.86 kJ/mole mixture.

Heating value per mole exhaust is = 240 kJ/2.887 = 83.13 kJ/mole exhaust.

Similarly, for ϕ = 0.95, the combustion equation is

$$0.95H_2 + \frac{1}{2}O_2 + 1.887\,N_2 = 0.95H_2O + 1.887\,N_2 + 0.025\,O_2 \tag{14}$$

Now, the heating value of 1 mole of H_2 (or per reaction) is only 228 kJ due to lean mixing.

In this equation,

Number of moles of reactant mixture = 3.37.

Number of moles of exhaust mixture = 2.862.

Therefore,

TABLE 4 Heating content of exhaust gas in ICEV.

Equivalence ratio (ϕ)	Energy/mole H_2 (kJ)	Energy content/mole mixture (kJ)	Energy content/mole exhaust (kJ)
1.0	240	70.86	83.13
0.95	228	67.66	79.66
0.90	216	65.71	76.14
0.85	204	63.02	72.55
0.80	192	60.24	68.89
0.75	180	57.38	65.17
0.70	168	54.42	61.38

Abbreviation: ICEV, internal combustion engine vehicle.

Heating value of exhaust gas per reaction of 1 mole H_2 is = 228 kJ.

Heating value per mole mixture is = 228 kJ/3.37 = 67.66 kJ/mole mixture.

Heating value per mole exhaust is = 240 kJ/2.862 = 79.66 kJ/mole exhaust.

All such results corresponding to $\phi = 1.0$, 0.95, 0.90, 0.85, 0.80, 0.75, and 0.70 are presented in Table 4.

In the literature wide range of hydrogen mass flow rates (m_f) has been mentioned. The value of m_f ranges from 0.7 to 40 kg/h. Hence, the exhaust heating amount has been calculated at various values of m_f ($m_f = 1$, 2, 3, 4, 5, 10, 15, 20, 25, 30, 35, and 40 kg/h). For a particular value of m_f, exhaust heating value has been calculated at different equivalence ratios ($\phi = 1.0$, 0.95, 0.90, 0.85, 0.80, 0.75, and 0.70). These values are given in Tables 5 and 6 for different values of ϕ. These tables show the heating value of exhaust gas at various mass flow rates and fuel/air ratios. The heat content of the exhaust gas depends on the proportion of air and is an average of approximately 75 to 80 kJ/mole mixture.[15] In another report, the volumetric heat value of the hydrogen-air mixture is reported as 2890 J/L. This volumetric value is equivalent to 64.74 kJ/mole mixture.[34]

3.3 | Power and brake thermal efficiency

Power and brake thermal efficiency have been calculated using Equations (9) and (10). The calculated theoretical power has been presented in Table 7 at various values of angular speed (500-4000 rpm) and torque (100-3000 N m). The values of torque mentioned by researchers in their reports are 19, 51, and 300 N m.[21,34] In a similar way reported values of angular speed are 1000 to 6000 rpm.[21,34] The values of rated power output in various examples of ICEV are mentioned as 30, 50, 90, and 100 kW.[15,21] Taking the values of output power, the brake thermal efficiency of ICEV has been evaluated at different fuel mass flow rates (1-40 kg/h) at the torque value 500 N m for ϕ values 1.0 and 0.8. The calculated values of efficiency corresponding to ϕ values 1.0 and 0.8 are indicated in Tables 8 and 9.

Considering all these values of efficiency, the value of fuel mass flow rate has been taken as equivalent to 50% efficiency. For further calculation of the amount of heat transferred to the hydrogen storage system mass flow rate of 10 kg/h has been considered.

3.4 | Heat transferred by exhaust gas to the storage system

Literature review shows that, for the 400 km range of vehicles, 8 kg of hydrogen is needed. In the combination of two metal hydrides, the mass of both materials has been taken in the ratio, such that hydrogen outflows from materials are in the ratio of their weight % hydrogen storage capacity. It is considered that in the combination of alloys, one must be operative at ambient conditions, so that the initial amount of hydrogen at the start of the vehicle can be released by this alloy. After the first combustion of the hydrogen coming from room temperature alloy, the heat will be transferred from the exhaust gas to the high-temperature alloy and then hydrogen flow will be more from high-temperature alloy. Thus, the circle of hydrogen will be maintained in this way.

3.4.1 | Combination of MgH_2 and $TiMn_2$-based alloys

The properties of these alloys are:

MgH_2 (high temperature).[22]

Reversible wt% hydrogen storage capacity = 7 wt%,

Operating temperature = 300°C,

Operating pressure = 1 bar,

Heat of hydrogen desorption = −75 kJ/mole H_2.

TABLE 5 Heating content of exhaust gas at $\phi = 1.0$, 0.95, 0.90, and 0.85 for various value of mass flow rate of hydrogen.

Mass flow rate of H_2 (kg H_2/h)	Mass flow rate of H_2 (moleH_2/h)	$\phi = 1.0$			$\phi = 0.95$			$\phi = 0.90$			$\phi = 0.85$		
		Energy value/mole H_2 (J/s)	Energy value/mole mixture (J/s)	Energy value/mole exhaust (J/s)	Energy value/mole H_2 (J/s)	Energy value/mole mixture (J/s)	Energy value/mole exhaust (J/s)	Energy value/mole H_2 (J/s)	Energy value/mole mixture (J/s)	Energy value/mole exhaust (J/s)	Energy value/mole H_2 (J/s)	Energy value/mole mixture (J/s)	Energy value/mole exhaust (J/s)
Value for 1 mole													
H_2 ⟶		**240**	**70.86**	**83.13**	**228**	**67.66**	**79.66**	**216**	**65.71**	**76.14**	**204**	**63.02**	**72.55**
1	0.138	33.12	9.78	11.47	31.46	9.34	10.99	29.81	9.07	10.51	28.15	8.70	10.01
2	0.276	66.24	19.56	22.94	62.93	18.67	21.99	59.62	18.14	21.02	56.30	17.39	20.02
3	0.414	99.36	29.34	34.41	94.39	28.01	32.98	89.42	27.20	31.52	84.46	26.09	30.04
4	0.552	132.48	39.11	45.89	125.86	37.35	43.97	119.23	36.27	42.03	112.61	34.79	40.05
5	0.69	165.6	48.89	57.36	157.32	46.69	54.97	149.04	45.34	52.54	140.76	43.48	50.06
10	1.38	331.2	97.79	114.72	314.64	93.37	109.93	298.08	90.68	105.07	281.52	86.97	100.12
15	2.07	496.8	146.68	172.08	471.96	140.06	164.90	447.12	136.02	157.61	422.28	130.45	150.18
20	2.76	662.4	195.57	229.44	629.28	186.74	219.86	596.16	181.36	210.15	563.04	173.93	200.24
25	3.45	828.0	244.47	286.80	786.6	233.43	274.83	745.2	226.70	262.68	703.8	217.42	250.30
30	4.14	993.6	293.36	344.16	943.92	280.11	329.79	894.24	272.04	315.22	844.56	260.90	300.36
35	4.83	1159.2	342.25	401.52	1101.24	326.80	384.76	1043.28	317.38	367.76	985.32	304.39	350.42
40	5.52	1324.8	391.15	458.88	1258.56	373.48	439.72	1192.32	362.72	420.29	1126.08	347.87	400.48

TABLE 6 Heating content of exhaust gas at $\phi = 0.80$, 0.75, and 0.70 for various value of mass flow rate of hydrogen.

		$\phi = 0.80$			$\phi = 0.75$			$\phi = 0.70$		
Mass flow rate of H_2 (kg H_2/h)	**Mass flow rate of H_2 (moleH_2/h)**	**Energy value/ mole H_2 (J/s)**	**Energy value/mole mixture (J/s)**	**Energy value/mole exhaust (J/s)**	**Energy value/ mole H_2 (J/s)**	**Energy value/mole mixture (J/s)**	**Energy value/mole exhaust (J/s)**	**Energy value/ mole H_2 (J/s)**	**Energy value/mole mixture (J/s)**	**Energy value/ mole exhaust (J/s)**
Value for 1 mole										
H_2 ⟶		**192**	**60.24**	**68.89**	**180**	**57.38**	**65.17**	**168**	**54.42**	**61.38**
1	0.138	26.50	4.16	9.51	12.42	7.92	8.99	23.18	7.51	8.47
2	0.276	53.00	16.63	19.01	49.68	15.84	17.99	46.37	15.02	16.94
3	0.414	79.49	24.94	28.52	74.52	23.76	26.98	69.55	22.53	25.41
4	0.552	105.98	33.25	38.03	99.36	31.67	35.97	92.74	30.04	33.88
5	0.69	132.48	41.57	47.53	124.2	39.59	44.97	115.92	37.55	42.35
10	1.38	264.96	83.13	95.07	248.4	79.18	89.93	231.84	75.10	84.70
15	2.07	397.44	124.70	142.60	372.6	118.78	134.90	347.76	112.65	127.06
20	2.76	529.92	166.26	190.14	496.8	158.37	179.87	463.68	150.20	169.41
25	3.45	662.4	207.83	237.67	621.0	197.96	224.84	579.6	187.75	211.76
30	4.14	794.88	249.40	285.20	745.2	237.55	269.80	695.52	225.30	254.11
35	4.83	927.36	290.96	332.74	869.4	277.15	314.77	811.44	262.85	296.47
40	5.52	1059.84	332.52	380.27	993.6	316.74	359.74	927.36	300.40	338.82

TABLE 7 Calculation of theoretical power.

Torque (N m) → / Speed (rpm) ↓	Power (kW)									
	100	**200**	**300**	**400**	**500**	**1000**	**1500**	**2000**	**2500**	**3000**
500	5.23	10.47	15.70	20.92	26.17	52.34	78.51	104.68	130.85	157.02
1000	10.46	20.94	31.40	41.84	52.34	104.68	157.02	209.36	261.70	314.04
1500	15.69	31.41	47.10	62.76	78.51	157.02	235.53	314.04	392.55	471.06
2000	20.92	41.88	62.80	83.68	104.68	209.36	314.04	418.72	523.40	628.08
2500	26.15	52.35	78.50	104.60	130.85	261.7	392.55	523.40	654.25	785.10
3000	31.38	62.82	94.20	125.52	157.02	314.04	471.06	628.08	785.10	942.12
3500	36.61	73.29	109.90	146.44	183.19	366.38	549.57	732.76	915.95	1099.14
4000	41.84	83.76	125.60	167.36	209.36	418.72	628.08	837.44	1046.8	1256.16

TABLE 8 Calculation of thermal efficiency at $\phi = 1.0$ and torque 500 N m.

Speed (rpm) → / Mass flow rate of H_2 (kg/h) ↓	Thermal efficiency							
	500	**1000**	**1500**	**2000**	**2500**	**3000**	**3500**	**4000**
1	79.02	158.04	237.06	316.08	395.10	474.12	553.14	632.16
2	39.51	79.02	118.53	158.04	197.55	237.06	276.57	316.08
3	26.34	52.68	79.02	105.36	131.70	158.04	184.38	210.72
4	19.76	39.52	59.28	79.04	98.80	118.56	138.32	158.08
5	15.80	31.60	47.40	63.20	79.0	94.80	110.60	126.40
10	7.90	15.80	23.70	31.60	39.50	47.40	55.30	63.20
15	5.27	10.54	15.81	21.08	26.35	31.62	36.89	42.16
20	3.95	7.90	11.85	15.80	19.75	23.70	27.65	31.60
25	3.16	6.32	9.48	12.64	15.80	18.96	22.12	25.28
30	2.63	5.26	7.89	10.52	13.15	15.78	18.41	21.04
35	2.26	4.52	6.78	9.04	11.30	13.56	15.82	18.08
40	1.98	3.96	5.94	7.92	9.90	11.88	13.86	15.84

$TiMn_2$-based alloys (ambient temperature).[23]

Reversible wt% hydrogen storage capacity = 1.5 wt%,

Operating temperature = ambient temperature 20°C,

Operating pressure = 10 bar,

Heat of hydrogen desorption = −27 kJ/mole H_2.

Let us consider,

Mass flow rate of hydrogen = 10 kg/h = 1.38 mole/s,

$\phi = 1.0$,

Energy released = 240 kJ/mole H_2,

Total energy released = 331.2 kJ/s,

Taking efficiency 50%, heat content of exhaust gas is = 165.6 kJ/s.

Exhaust gas temperature[22] = 650°C.

Heat transferred to the Mg system is (using Equation 11):

$Q_{Mg} = 165.6 \frac{923-573}{923-300} = 92.76$ kJ/s.

The number of moles of H_2 liberated from this heat = 92.76/75 = 1.24 mole H_2/s.

To maintain the flow rate of 1.38 mole H_2/s, the number of moles of hydrogen required by another alloy is = 1.38-1.24 = 0.14 mole H_2/s.

To liberate 0.14 mole H_2 from AB_2 alloy, energy needed is = 0.14 × 27 = 3.78 kJ/s.

Since AB_2 alloy is operative at room temperature, it can itself release the initial amount of hydrogen as 1.38 mole/s.

In this way, it is clear that enough amount of heat content is present in the exhaust gas which can be utilized for hydrogen release from high-temperature alloys of high hydrogen storage capacity.

TABLE 9 Calculation of thermal efficiency at $\phi = 0.8$ and torque 500 N m.

Speed (rpm) → / Mass flow rate of H_2 (kg/h) ↓	Thermal efficiency							
	500	1000	1500	2000	2500	3000	3500	4000
1	98.80	197.60	296.40	395.20	494.00	592.80	691.60	790.40
2	49.40	98.80	148.20	197.60	247.00	296.40	345.80	395.20
3	32.90	65.80	98.70	131.60	164.50	197.40	230.30	263.20
4	24.70	49.40	74.10	98.80	123.50	148.20	172.90	197.60
5	19.75	39.50	59.25	79.00	98.75	118.50	138.25	158.00
10	9.88	19.76	29.64	39.52	49.40	59.28	69.16	79.04
15	6.58	13.16	19.74	26.32	32.90	39.48	46.06	52.64
20	4.94	9.88	14.82	19.76	24.70	29.64	34.58	39.52
25	3.95	7.90	11.85	15.80	19.75	23.70	27.65	31.60
30	3.29	6.58	9.87	13.16	16.45	19.74	23.03	26.32
35	2.82	5.64	8.46	11.28	14.10	16.92	19.74	22.56
40	2.47	4.94	7.41	9.88	12.35	14.82	17.29	19.76

For the 400 km range, the amount of hydrogen required is 8 kg. Dividing this 8 kg hydrogen in the ratio of wt% hydrogen capacity of two alloys.

Hydrogen liberated from Mg-based alloy = 6.59 kg.

Hydrogen liberated from AB_2 alloy = 1.41 kg.

The amount of Mg-based alloy to release 6.59 kg hydrogen is = 94.14 kg.

The amount of AB_2-based alloy to release 1.41 kg hydrogen is = 94 kg.

Total weight of both alloys = 188.14 kg.

Let us consider an extra 25% weight as metal hydride tank weight.

Hence, total system weight = 235.175 kg.

Corresponding energy of 8 kg hydrogen is = 8 kg × 120 MJ/kg = 960 MJ = 266.66 kWh.

Therefore specific energy of this combined metal hydride system is = 1.13 kWh/kg = 0.034 kgH_2/kg.

According to US DOE, the present target of system-specific capacity is 1.5 kWh/kg and 0.045 kgH_2/kg.[22] The present calculation is very much close to the US DOE present target.

3.4.2 | Combination of MgH_2, $NaAlH_4$, and $TiMn_2$-based alloys

The properties of these alloys are:

MgH_2 (high temperature).[22]

Reversible wt% hydrogen storage capacity = 7 wt%,

Operating temperature = 300°C,

Operating pressure = 1 bar,

Heat of hydrogen desorption = −75 kJ/mole H_2.

$NaAlH_4$ (high temperature).[35]

Reversible wt% hydrogen storage capacity = 5 wt%,

Operating temperature = 100°C,

Operating pressure = 1 bar,

Heat of hydrogen desorption = −47 kJ/mole H_2.

$TiMn_2$-based alloys (ambient temperature).[23]

Reversible wt% hydrogen storage capacity = 1.5 wt%,

Operating temperature = ambient temperature = 20°C,

Operating pressure = 10 bar,

Heat of hydrogen desorption = −27 kJ/mole H_2.

Let us again consider,

Mass flow rate of hydrogen = 10 kg/h = 1.38 mole/s.

$\phi = 1.0$,

Energy released = 240 kJ/mole H_2.

Total energy released = 331.2 kJ/s.

Taking efficiency 50%, heat content of exhaust gas is = 165.6 kJ/s.

Exhaust gas temperature[15] = 650°C.

Heat transferred to the Mg system is (using Equation 11):

$Q_{Mg} = 165.6 \frac{923-573}{923-300} = 92.76$ kJ/s.

The number of moles of H_2 liberated from this heat = 92.76/75 = 1.24 mole H_2/s.

Remaining heat content in the exhaust gas after heat transfer to the Mg system = 165.6−92.76 = 72.84 kJ/s.

Now, heat transfer to the $NaAlH_4$ system is:

$Q_{NaAlH_4} = 72.84 \frac{923-373}{923-300} = 64.30$ kJ/s.

The number of moles of H_2 liberated using this heat from $NaAlH_4$ is = 64.30/47 = 1.37 mole H_2.

In this combination of three materials, initially at the time of the first start, hydrogen is liberated by the AB_2 alloy, operated at ambient conditions. After the combustion, energy will be released in the exhaust gas and further hydrogen will be released from the other high-temperature materials also. In this way, the hydrogen release cycle will be maintained in the combined system of three alloys.

The ratio of the amount of hydrogen outflow (8 kg) from three materials is in the ratio of their hydrogen storage capacity: 7:5:1.5.

Amount of hydrogen released from the MgH_2 system = 4.15 kg.

Amount of hydrogen released from the $NaAlH_4$ system = 2.96 kg.

Amount of hydrogen released from AB_2 system = 0.89 kg.

Required weight of the Mg system to liberate 4.15 kg hydrogen = 59.29 kg.

Required weight of the $NaAlH_4$ system to liberate 2.96 kg hydrogen = 59.2 kg.

Required weight of the AB_2 system to liberate 0.89 kg hydrogen = 59.3 kg.

Total weight of metal hydrides = 177.79 kg.

Adding 25% extra weight for the metal hydride tank, the system weight is = 222.24 kg.

Corresponding energy of 8 kg hydrogen is = 8 kg × 120 MJ/kg = 960 MJ = 266.66 kWh.

Therefore specific energy of this combined metal hydride system is = 1.20 kWh/kg = 0.036 kgH_2/kg.

According to US DOE, the present target of system-specific capacity is 1.5 kWh/kg and 0.045 kgH_2/kg.[22] This combination of the metal hydrides is even more close to the US DOE present target.

In the present study, calculations have been performed by taking a simple metal hydride of the parent family; however, any substituted and tailored metal hydride of the corresponding family with enhanced properties may offer better results in this context. Here, the amount of heat and the temperature required for hydrogen desorption have been supplied by the exhaust gas. During refueling and charging of the hydrogen to the metal hydride system, the temperature may be maintained at the refueling center by some external system.

4 | CONCLUSIONS

In the search for a better hydrogen storage system for ICEV, it has been found that there are varieties of potential materials available to fulfill the requirements of vehicles. Still, at present, no material is in accordance with the present, near future, and ultimate targets set by the DOE of the US government. The gravimetric hydrogen storage capacity of the system, operation at ambient conditions, medium heat of desorption, and fast hydrogen absorption-desorption kinetics are fundamental requirements of hydrogen storage systems to be utilized in vehicles. In the present study, it has been shown that by taking the combination of metal hydrides, the present target may be achieved. In combination, at least one material should be operated at the ambient conditions to release the hydrogen at the first start of the vehicles spontaneously. After that, the heat from the exhaust gas may be transferred to the high-temperature metal hydride system to release the hydrogen further. The calculation performed in the present study shows the feasibility and viability of the combined metal hydride system in ICEV.

5 | THE CHALLENGES AND FUTURE PROSPECTS

The major challenge during implementation of hydrogen-driven vehicles is the cost of hydrogen itself. The production, storage, and transportation of hydrogen are key challenges to be solved. According to the Global Hydrogen Review 2021 of IEA, many countries have started to focus on viable and green methods of hydrogen production through large electrolyzers.[7] Use of solar electricity for hydrogen production may cut down the cost of hydrogen as \$1/kg H_2.[6] The scenario of NZE by 2050 has targeted the production of low-emission hydrogen as 450 Mt in comparison to 1 Mt of the present value.[7] Several materials are available for hydrogen storage, with different hydrogen storage capacities and different characteristics for hydrogenation. For winning the race, material should be of low cost, but at the same time should have high hydrogen storage capacity at ambient temperature and pressure. Many countries have started to invest in hydrogen infrastructure including filling stations.[7] To attain the NZE scenario by 2050, the compromise shall not be on use of hydrogen energy, rather than it shall be on cost. All these combined efforts at global level will form golden era of hydrogen energy to save the earth.

ACKNOWLEDGEMENTS

The author is grateful to Late Prof. O. N. Srivastava (BHU, INDIA) and Prof. I. P. Jain (Rajasthan University, INDIA) for helpful discussions.

CONFLICT OF INTEREST STATEMENT

The authors declare no conflicts of interest.

DATA AVAILABILITY STATEMENT

Data sharing not applicable to this article as no datasets were generated or analysed during the current study.

ORCID

Sumita Srivastava https://orcid.org/0000-0002-1600-4335

REFERENCES

1. Dematteis EM, Barale J, Corno M, Sciullo A, Baricco M, Rizzi P. Solid-state hydrogen storage systems and the relevance of a gender perspective. *Energies*. 2021;14:6158.
2. IEA (2021), *Key World Energy Statistics 2021*, IEA, Paris. https://www.iea.org/reports/key-world-energy-statistics-2021. Accessed January 10, 2022.
3. World Energy Outlook 2022.
4. Selvam P. Energy and environment—an all time search. *Int J Hydrogen Energy*. 1991;16:35-45.
5. Harder EL. *Fundamentals of Energy Production*. New York: John Wiley & Sons, Inc; 1982.
6. IEA (2019), *The Future of Hydrogen*, IEA, Paris. https://www.iea.org/reports/the-future-of-hydrogen. Accessed December 22, 2022.
7. IEA (2021), *Global Hydrogen Review 2021*, IEA, Paris. https://www.iea.org/reports/global-hydrogen-review-2021. Accessed December 22, 2022.
8. Chatterjee A, Dutta S, Mandal BK. Combustion performance and emissioncharacteristics of hydrogen as an internal combustion engine fuel. *J Aeronaut Automot Eng*. 2014;1(1):1-6.
9. Mori D, Hirose K. Recent challenges of hydrogen storage technologies for fuel cell vehicles. *Int J Hydrogen Energy*. 2009;3:4569-4574.
10. Yang J, Sudik A, Wolverton C, Siegelwa DJ. High capacity hydrogenstorage materials: attributes for automotive applications and techniques for materials discovery. *Chem Soc Rev*. 2010;39:656-675.
11. Lototskyy MV, Tolj I, Pickering L, Sita C, Barbir F, Yartys V. The use of metal hydrides in fuel cell applications. *Prog Nat Sci Mater Int*. 2017;27:3-20.
12. Dell RM, Rand DAJ. Energy storage—a key technology for global energy sustainability. *J Power Sources*. 2001;100:2-17.
13. Andrews J, Shabani B. Re-envisioning the role of hydrogen in a sustainable energy economy. *Int J Hydrogen Energy*. 2012;37:1184-1203.
14. Modi P, Aguey Zinsou KF. Room temperature metal hydrides for stationary and heat storage applications: a review. *Front Energy Res*. 2021;9:616115.
15. Toepler J, Bernauer O, Buchner H. The use of hydrides in motor vehicles. *J Less Common Met*. 1980;74:385-399.
16. Zheng J, Wang CG, Zhou H, et al. Current research trends and perspectives on solid-state nanomaterials in hydrogen storage. *Research*. 2021;2021:3750689.
17. Schlapbach L, Zuttel A. Hydrogen-storage materials for mobile applications. *Nature*. 2002;414:353-358.
18. Tajitsu N, Shiraki M. *Toyota Plans to Expand Production, Shrink Cost of Hydrogen Fuel Cell Vehicles in Business News*. London: Reuters; 2018.
19. Rivard E, Trudeau M, Zaghib K. Hydrogen storage for mobility: a review. *Materials*. 2019;12:1973.
20. Brown EG. *Joint Agency Staff Report on Assembly Bill 8: Assessment of Time and Cost Needed to Attain 100 Hydrogen Refueling Stations in California*. USA: California Energy Commission; 2015.
21. Hosseini SE, Butler B. An overview of development and challenges in hydrogen powered vehicles. *Int J Green Energy*. 2020;17:13-37.
22. Abe JO, Popoola API, Ajenifuja E, Popoola OM. Hydrogen energy, economy and storage: review and recommendation. *Int J Hydrogen Energy*. 2019;4:15072-15086.
23. Davids MW, Lototskyy M, Malinowski M, et al. Metal hydride hydrogen storage tank for light fuel cell vehicle. *Int J Hydrogen Energy*. 2019;4:29263-29272.
24. Nagar R, Srivastava S, Hudson SL, et al. Recent developments in state-of-the-art hydrogen energy technologies—review of hydrogen storage materials. *Solar Compass*. 2023;5:100033.
25. Kumar A, Yadav TP, Mukhopadhyay NK. Notable hydrogen storage in Ti–Zr–V–Cr–Ni high entropy alloy. *Int J Hydrogen Energy*. 2022;47:22893-22900.
26. Yadav TP, Verma A, verma SK, Mukhopadhaya NK. High-entropy alloys for solid hydrogen storage: potentials and prospects. *Trans Indian Natl Acad Eng*. 2022;7:147-156.
27. Verma SK, Shaz MA, Yadav TP. Enhanced hydrogen absorption and desorption properties of MgH2 with graphene and vanadium disulfide. *Int J Hydrogen Energy*. 2023;48:21383-21394.
28. Verma SK, Bhatnagar A, Shaz MA, Yadav TP. Mechanistic understanding of the superior catalytic effect of Al65Cu20Fe15 quasicrystal on de/re-hydrogenation of NaAlH4. *Int J Hydrogen Energy*. 2023;48:9762-9775.
29. Panwar K, Srivastava S. Enhancement in hydrogenation properties of ball-milled AB5-type hydrogen storage alloy through catalyst. *J Phys Conf Ser*. 2022;2267:012052.
30. Panwar K, Srivastava S. Theoretical model on the electronic properties of multi-element AB5-type metal hydride. *Int J Hydrogen Energy*. 2021;46:10819-10829.
31. Panwar K, Srivastava S. On structural model of AB5-type multi-element hydrogen storage alloy. *Int J Hydrogen Energy*. 2019;44:30208-30217.
32. Panwar K, Srivastava S. Investigations on calculation of heat of formation for multi-element AB5-type hydrogen storage alloy. *Int J Hydrogen Energy*. 2018;43:11079-11084.
33. Sterlepper S, Fischer M, Claben J, Huth V, Pischinger S. Concepts for hydrogen internal combustion engines and their implications on the exhaust gas aftertreatment system. *Energies*. 2021;14:8166.
34. Naresh P, Hari Babu AV, Reddy BVA, Reddy MS. Analysis of a hydrogen fuelled internal combustion engine. *WWJMRD*. 2016;2:27.
35. Dornheim M. In: Moreno JC, ed. *Thermodynamics—Interaction Studies—Solids, Liquids, Gases*. London: InTech; 2011:891.

How to cite this article: Srivastava S. Hydrogen storage materials for vehicular applications. *Energy Storage*. 2023;e524. doi:10.1002/est2.524

Solar Compass 5 (2023) 100033

Contents lists available at ScienceDirect

Solar Compass

journal homepage: www.elsevier.com/locate/solcom

Recent developments in state-of-the-art hydrogen energy technologies – Review of hydrogen storage materials

Rupali Nagar[a], Sumita Srivastava[b], Sterlin Leo Hudson[c], Sandra L. Amaya[d], Ashish Tanna[e], Meenu Sharma[f], Ramesh Achayalingam[c], Sanjiv Sonkaria[g], Varsha Khare[g], Sesha S. Srinivasan[h,*]

[a] *Nanomaterials for Energy Applications Lab, Applied Science Department, Symbiosis Institute of Technology (SIT), Symbiosis International (Deemed University), Lavale, Pune 412 115, Maharashtra, India*
[b] *Government Degree College, Nainbagh 249186 Tehri Garhwal, India*
[c] *Department of Physics, Banaras Hindu University, Varanasi 221005, UP, India*
[d] *Institución Universitaria Pascual Bravo, Facultad de Ingeniería, Grupo de Investigación e Innovación en Energía GIIEN, Calle 73 No 73A 226, CP 050001, Medellín, Colombia*
[e] *Department of Physics, RK University, Bhavnagar Highway, Tramba, Gujarat 360020, India*
[f] *Mechanical Engineering, Energy Systems Research Laboratory, Indian Institute of Technology Gandhinagar, Gujarat 382355, India*
[g] *Soft Foundry Institute, Seoul National University, Kwanak-gu, Seoul, 39-131, South Korea*
[h] *Department of Engineering Physics, Florida Polytechnic University, 4700 Research Way, Lakeland, FL, USA*

ARTICLE INFO

Keywords:
Hydrogen energy technologies
Hydrogen storage
Metal hydrides
Carbonaceous
Nanoparticles
Metal organic frameworks
Perovskites
Fuel cells

ABSTRACT

Hydrogen energy has been assessed as a clean and renewable energy source for future energy demand. For harnessing hydrogen energy to its fullest potential, storage is a key parameter. It is well known that important hydrogen storage characteristics are operating pressure-temperature of hydrogen, hydrogen storage capacity, hydrogen absorption-desorption kinetics and heat transfer in the hydride bed. Each application needs specific properties. Every class of hydrogen storage materials has a different set of hydrogenation characteristics. Hence, it is required to understand the properties of all hydrogen storage materials. The present review is focused on the state-of–the–art hydrogen storage materials including metal hydrides, magnesium-based materials, complex hydride systems, carbonaceous materials, metal organic frameworks, perovskites and materials and processes based on artificial intelligence. In each category of materials' discovery, hydrogen storage mechanism and reaction, crystal structure and recent progress have been discussed in detail. Together with the fundamental synthesis process, latest techniques of material tailoring like nanostructuring, nanoconfinement, catalyzing, alloying and functionalization have also been discussed. Hydrogen energy research has a promising potential to replace fossil fuels from energy uses, especially from automobile sector. In this context, efforts initiated worldwide for clean hydrogen production and its use via fuel cell in vehicles is much awaiting steps towards sustainable energy demand.

Abbreviations: IPHE, International Partnership for Hydrogen and Fuel Cells in the Economy; IEA, International Energy Agency; CEM, Clean Energy Ministerial; MI, Mission Innovation; MT, Million Tons; IRENA, International Renewable Energy Agency; AEO, Annual Energy Outlook; US-DOE, United States Department of Energy; LCOE, Levelized Cost of Electricity; SMR, Steam Methane Reforming; KWh, Kilo Watt-hour; MOF, Metal Organic Frameworks; FCTO, Fuel Cell Technologies Office; AI, Artificial Intelligence; ML, Machine Learning; SWCNT, Single Wall Carbon Nanotube; MWCNT, Multiwall Carbon Nanotube; ANI, Artificial Narrow Intelligence; AGI, Artificial General Intelligence; HSA, Hydrogen Storage Alloys; IMC, Intermetallic Compounds; Pa, Pascal; MPa, Mega Pascals; Atm, Atmosphere; BCC, Body Centered Cubic; SS, Solid Solution; Ni-MH, Nickel-Metal Hydride; P-C-T (or PCT), Pressure Composition Temperature; Wt% (or wt%), weight percentage; kJ, Kilo Joules; PEM, Proton Exchange Membrane; H/M, Hydrogen to metal ratio; CRMM, Controlled Reactive Mechanical Milling; HRBM, High-Energy Ball Milling; NPs, Nanoparticles; PMMA, Poly(methyl methacrylate; CA, Carbon Aerogels; 2D and 3D, Two and Three Dimension; DFT, Density Functional Theory; RHC, Reactive Hydride Composite; K, Kelvin (Temperature scale); C (or °C), Degree Celsius (Temperature scale); CC, Creative Commons; LOHC, Liquid Organic Hydrogen Carriers; MWNT, Multiwall Nanotubes; GDY, Graphdiyne; TM, Transition Metal; H–H, Hydrogen-Hydrogen; FCEV, Fuel Cell Electric Vehicle.

* Corresponding author.
E-mail address: ssrinivasan@floridapoly.edu (S.S. Srinivasan).

https://doi.org/10.1016/j.solcom.2023.100033
Received 7 December 2022; Received in revised form 23 January 2023; Accepted 25 January 2023

1. Introduction - overview and background of hydrogen energy technologies

An unprecedented raise of global mean temperature over the several decades and associate *global warming* lead both developed and developing countries to device strategies for containing the global CO_2 emissions [1]. As it is known to everyone that conventional energy resources like fossil fuels such as petroleum products and coal have been used for a long time and created an impact on the environment especially *greenhouse effect* due to large production of CO_2 gasses during the combustion of these fuels [2]. Due to this fact, researchers have focused on alternate source of energy which should be environmentally friendly and easily available [3]. One of the sources is solar energy though due to efficiency of solar cell and sturdiness inspire research fraternity to find another source which could be mobile and economical for the future prospectus [4]. In this review article, focus area is *hydrogen as a fuel*. The lightest and most available material on the earth is hydrogen which can be useful as energy source. The hydrogen is a fuel with less or almost zero emission of toxics as well non-polluting gas when it burns or used as renewable energy sources [5]. As hydrogen is an alternate source has extremely useful as a green fuel for the current time. The hydrogen fuel is more than double efficiency than the other fuels like gasoline [6,7]

There are number of techniques available to produce hydrogen and utilize those with suitable aspects. Main source of hydrogen is the industrial steam reforming method [7], where 96% of hydrogen is produced. It is a well-established technology to extract hydrogen from fossil fuel stocks [8]. Almost 10 million tons of hydrogen requirements of U.S. is fulfilled using steam reforming every year [8]. While remaining 4% of hydrogen can be produced via electrolysis process [9]. Electrolysis process is the most important and emerging technology, in this method, water can be split into hydrogen/oxygen using the electrical energy. other methods like thermochemical, wind, biomass gasification and solar radiation are to be considered although those are under preliminary research level hence needs more experimental proof for the quantitative production of hydrogen [8]. One can consider hydrogen as a prospective fuel, but it requires a huge effort to make it commercially viable. Though, in recent era researchers have made significant contributions in the production of hydrogen gas, intermediate storage, and utilization in PEM fuel cells by state-of-art methodologies (Fig. 1) [8]. The hydrogen storage is the bottleneck in implementing the hydrogen technologies to its fullest potential [10–12]. Looking into this, researchers are required to focus on storage of the hydrogen gas as a fuel. One of the solutions to this problem is the reversible storage of hydrogen in solid state materials. There are a number of solid materials available which have properties like microporous with high surface area, moisture sensitive complex hydrides and gas sorption can be utilized [13].

2. Hydrogen energy technologies – an international perspectives

The US administration's bold "*Hydrogen Earthshot*" initiatives, "One-for-One-in-One", otherwise simply, "111" is driving and reviving the hydrogen-based research and development to realize for the generation of "clean hydrogen" at the cost of $1.00 for one kilogram in one decade [14]. This initiative triggers not only to develop "US Hydrogen Hubs" but also catalyze the international hydrogen research. Another bold goal of this process on the international stage, a net zero or 100% renewable energy consumption (or 100% clean grid) must be achieved by 2050 with a short-term to realize the 50% of set-forth goals by 2030 [15]. Another bold initiative from the EU Commission to adopt renewable hydrogen to decarbonize at the cost-effective manner that is strategically developed by the REPowerEU; this leads to the "*hydrogen accelerator*" where a domestic hydrogen production of 10 MT (million tons)

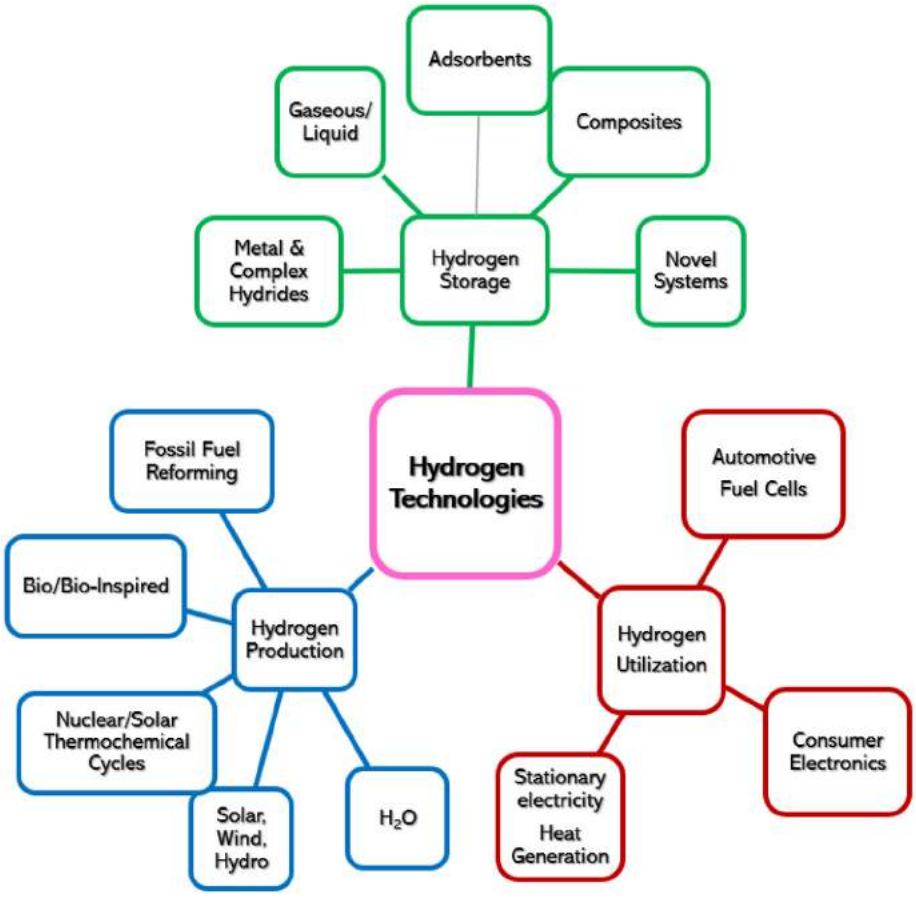

Fig. 1. Hydrogen Energy Technologies.

by 2030 [16]. Africa-EU Green Energy initiatives are on the horizon in developing 40 GW (Gigawatts) of electrolyzer capacity to generate renewable hydrogen and critical raw materials to support the green and digital technologies [17]. In 2021, the IPHE (International Partnership for Hydrogen and Fuel Cells in the Economy), the IEA (International Energy Agency), and the CEM (Clean Energy Ministerial)/MI (Mission Innovation) have collectively addressed the four issues and developed the strategies for scaleup, accelerate and deploy the hydrogen energy technologies that not only enhance the reduction of carbon footprints but also enable sustainable infrastructure [18].

On the Asia-Pacific initiatives towards implementing hydrogen energy technologies, very recently, China announced its first ever bold plan to reach its fullest potential of generating 100,000 tons to 200,000 tons of clean hydrogen and hence that lead to the reduction of CO_2 emissions of 1MT to 2MT per year by 2025. By 2035, China seeks the country's major energy consumptions that are catered by the green sources, especially hydrogen [19]. According to the 2019 IEA/IRENA's report, South Korea's bold plan and road map in volume production of at least 6.2 million fuel-cell electric vehicles, commissioning 1200 hydrogen-enabled refilling stations and at least 15 GW of fuel cell for power generation by 2040 [20]. The road map of Japan has been pushing the boundaries to cut down the cost of hydrogen by 2030 and by encouraging the deployment of ammonia in thermal power generation as a low-carbon transition fuel. Japan also strategically attempting to establish an integrated and international supply chain by 2030 for up-streaming (production), mid-streaming (storage and transportation) and down-streaming (utilization or consumption) the clean hydrogen [20]. India's bold hydrogen initiatives that propose to at least infuse four percent of hydrogen in the national energy mix by 2030 and at least 10 developmental projects on nation-wide deployment of hydrogen energy technologies [22]. Based on the statistics and overview, it is undoubtedly clear that the hydrogen energy technologies are the future vectorial strategies that can fully replace the much-depleted fossil fuels, especially gasoline for automotive transportation and stationary power generation.

3. Hydrogen: a green and sustainable energy resource

The steady decline and depletion of natural energy resources has placed considerable demands for the alternative energy sources. In addition, while an emerging climate crisis driven by global warming from greenhouse gas emissions [23,21] poses an imminent threat to modern-day society, the energy shortfall must be met by sustainability for a growing global population and secure the imbalance to the environment with clean energy. The inherent fluctuations associated with wind or solar energy as renewable sources may have an impact on sustainability requiring a constant and steady supply from the source. Further, the lack of long-term energy storage capabilities with existing technologies underlines the growing importance for alternative strategies which can work alongside renewable forms. Hence, an alternative sustainable but continual energy source is necessary for power generation while renewable technology evolves. In this quest, hydrogen is the most promising candidate for the cleaner energy as a plentiful resource for zero-carbon emission [22–24]. Interestingly, hydrogen emits pure water vapor upon reaction with oxygen or upon combustion therefore, hydrogen-based technologies is likely to be one of the most significant determinants in reducing the carbon emission and thus playing an unprecedented role in driving fuel economy.

The Hype cycle methodology has been instrumental in understanding current and future impact of the most pivotal and exciting technological fields by estimating technological growth and maturation points. In view of the insight from the Garner Hype and Amara Hype cycle analysis for energy storage technology put forward by Khodayari et al. and Fredrik Uddenfeldt [25,26] which suggests that chemical hydrogen storage technology is still at the innovation stage (Figs. 2a and 2b), the projected low cost of hydrogen as a fuel source in comparison could be an attractive and real alternative (Fig. 2c and d) [27]. Further, based on survey and interview with hydrogen council member experts, Mckinsey & Company predictively proposes increasing efforts to apply the use hydrogen energy to various sectors of society with the expectation that by 2050, hydrogen will be accepted as the main energy source for mass transportation and will become the next generation green energy technology (Fig. 2e) for power/electricity generation [26]. US Department of energy (DOE) in its Annual Energy Outlook (AEO) of 2020 projected threefold increases in the electricity generation based on renewable energy storage systems [28].

Energy economy heavily depends on energy storage systems which is a key player between supplies and utilization. As efficient energy storage system boosts the efficiency by reducing potential losses. As an excellent and cost-effective intermittent energy storage systems requires extensive research in a short space of time to achieve rapid solutions for climate change and exhausting resources. However, energy generation from electricity or gas energy sectors does not require storage. However, storing the excess supply would help in supplementing the shortfall. In their analysis spanning a period of years, M. Wieliczko et al. highlighted the development of potential impact of technologies with low to high storage capacities on a timescale of ranging from seconds to months for the energy and climate problems [29]. Although such technologies namely supercapacitors, superconducting magnets, flywheels, pumped hydel storage, compressed air energy storage and batteries offer solutions for a variety of applications (depending upon the requirements), but the challenge here is that no single technology can be used for a given range of applications [30]. Interestingly, among these technologies, hydrogen is the only one energy technology which can fulfill the requirements of various sectors as shown in Fig. 3a.

In addition, role of hydrogen becomes even more important because it can be produced not only by conventional SMR methods but also by harnessing other renewable sources such as solar, wind and geothermal among others. However, in spite of its advantage as a high specific energy material, safety, and elevated cost due to its low energy density (Fig. 3b) are the biggest challenges for hydrogen technology [31]. Hydrogen storage systems are classified into two categories based on the type of stored hydrogen (Fig. 3c). In physical storage system which are mainly liquid, or gaseous, free, or elemental hydrogen is stored. Another challenge is liquefaction of hydrogen which requires a high energy input (8–12 kW/h) [32].

For gaseous hydrogen although the density is much lower than liquid hydrogen, the high cost of containment to store at high pressures pose major safety are concerns [33–35]. On the other hand, in materials-based hydrogen storage system hydrogen atom bonded to materials are stored. Fig. 3d and e shows a comparative study done by the Fuel Cell Technologies Office (FCTO) on the materials in terms of hydrogen gravimetric capacity as a function of hydrogen release temperature [36,37]. It took many years of investigations to develop these materials which are still facing challenges of cost, reproducibility, and recyclability along with high temperature desorption. Despite all these years of explorations material with desired thermodynamic, kinetic, and physical properties combination is missing. This suggest that in place of trial and error using periodic table a well-trained investigation based on AI (Artificial Intelligence) and ML (Machine Learning) are required. *AI/ML will help not only to identify the elemental, structural combinations but also will provide us the pathway for efficient synthesis.*

4. AI/ML concepts in hydrogen storage materials' design

Increasing role of AI in changing our life is of paramount importance. AI is helping us to live in more comfortable and safer world. Fig. 4a suggests that AI has three main stages: artificial narrow intelligence (ANI), artificial general intelligence (AGI) and artificial super intelligence (ASI). Out of these three stages first stage of AI is safe and useful for humankind. Recently research using ANI has become increasingly important in all sectors of research and development including hydrogen storage research (Fig. 4b). Khare et al. have outlined the impor-

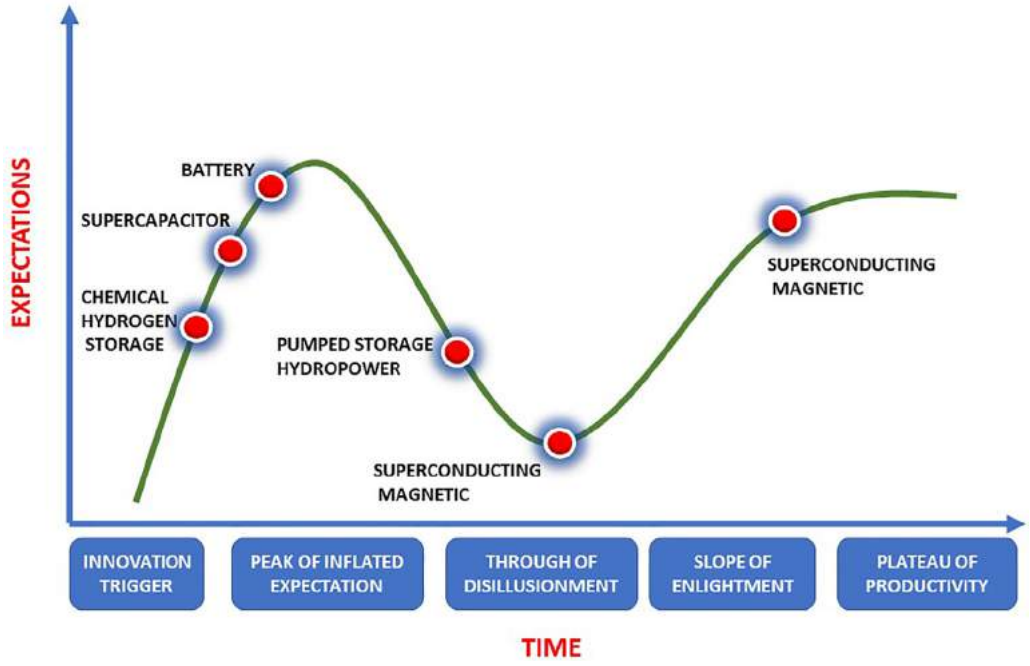

Fig. 2. (a) Chemical Hydrogen Storage at the Innovation Stage of the industrial revolution

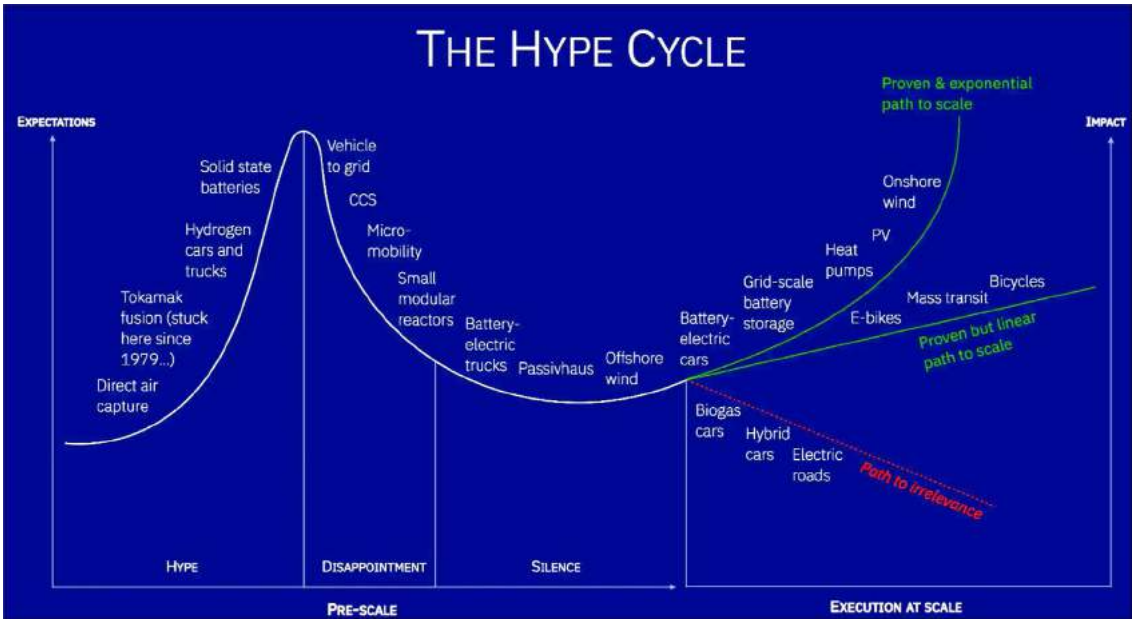

Fig. 2. (b) The HYPE cycle.

tance of interconnectivity of disciplines and further utilizing this transdisciplinary approach in AI to enhance the utility of AI for materials discovery [38]. Web of science search with the keywords of hydrogen storage technology and AI suggests that research on AI for hydrogen storage technology triggered in all areas of importance. However, there are only 95 publications so far in past 10 years but frequency of publications in recent 3–4 years has increase manifold. There have been many algorithm techniques (Fig. 4c) to predict materials and properties of the hydrogen storage system (Fig. 4d).

Thornton et al. utilized the findings of a very inspiring project called 'The Materials Genome' where millions of materials were predicted based on sequencing and modeling. In their work Thornton et al., targeted hydrogen storage system using a materials genome database to understand and identify the performance limits of hydrogen storage system [39]. In this work, the prediction of two hypothetical MOFs were shown to be associated with superior capability compared to the best performing MOFS synthesized to date. Interestingly, hypothetical MOFS predicted to enhance the net deliverable of energy by 30% when filled in a tank at cryo-compression condition (20k, 100 atm.) resulting in 30% increase in volumetric capacity. Further Jager et al. have worked on a different scale i.e. on nanosized clusters for optimizing the prediction methods for assessing conditions for best property optimization. In their work using machine learning algorithms, Jager et al. scanned a single and multiple nanoclusters applying atomic structural descriptors (SOAP, MBTR and ACSF) and this was predicted to be the best descriptor for the prediction of hydrogen adsorption (free) energy. This study con-

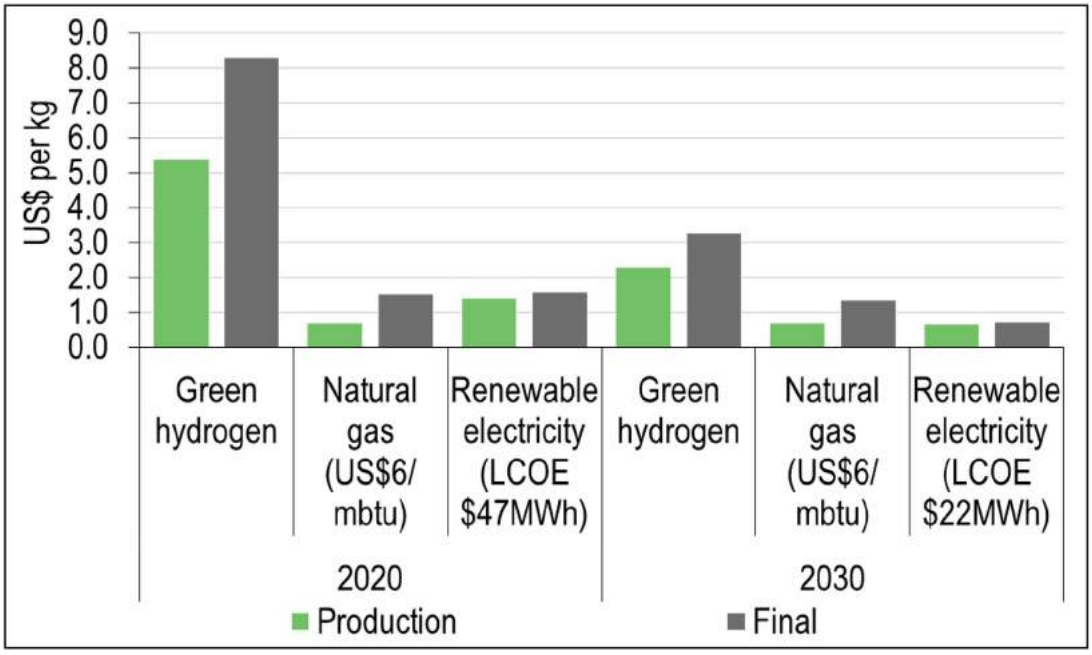

Fig. 2. (c) Cost analysis of green hydrogen (US$ per kg) with natural gas and renewable electricity.

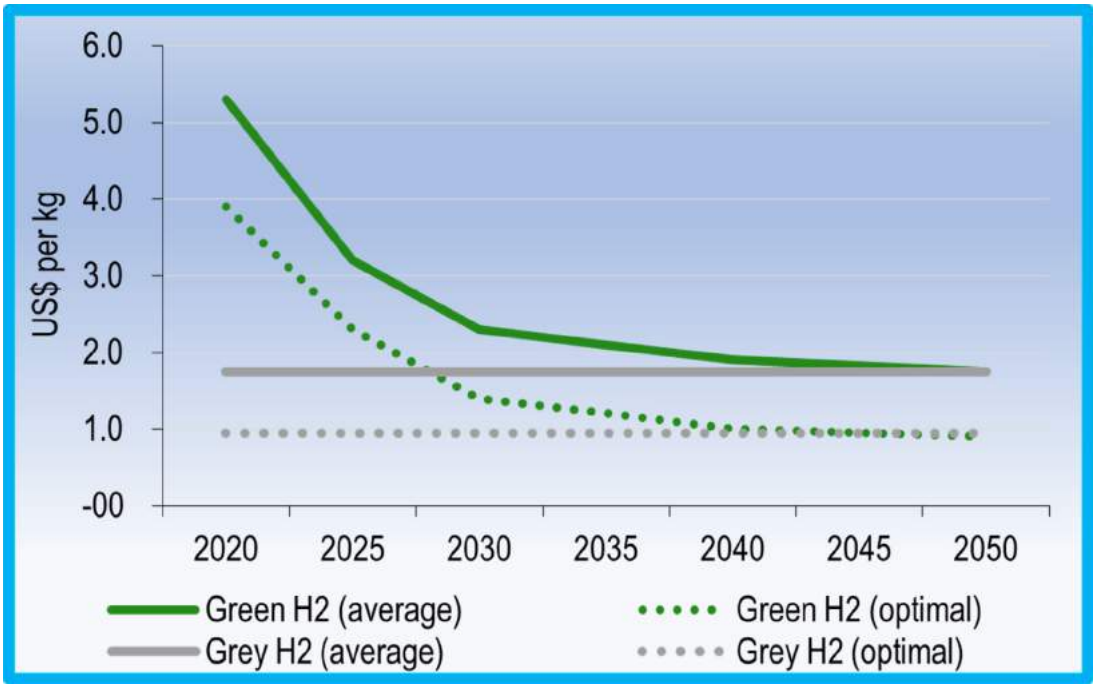

Fig. 2. (d) Timeline chart of green and gray hydrogen cost of production (US$ per kg).

cludes that the local symmetry is important for descriptor methods and therefore near-symmetric systems are ideal for the descriptor methods [40]. In an extensive work published in two volumes by Rahnama and co-workers have combined statistical analysis with supervised machine learning algorithms to obtain the best machine learning algorithms for quick identification for a desired class of materials with optimized properties such as hydrogen absorption wt.% [41,42]. More research efforts have been implemented for the prediction of components of hydrogen energy storage system which will be reviewed in detail in our future work with a focus on AI for the components of hydrogen energy storage systems.

5. Hydrogen energy storage – a bird's eye view

The reversible hydrogen storage can be realized using metal hydrides and adsorbent materials. The hydrogen sorption capacity of materials is the most important factor to do hydrogen storage. Looking into the storage part, the thermodynamic properties affect including the enthalpy of molecular hydrogen adsorption and the enthalpy of hydride formation or decomposition [13]. Hence, the kinetics of hydrogen adsorption, the activation energy, the hydrogen diffusion coefficient and the apparent rate of hydrogen absorption and desorption would be the key factors. There are quite a few good techniques available to measure gas sorp-

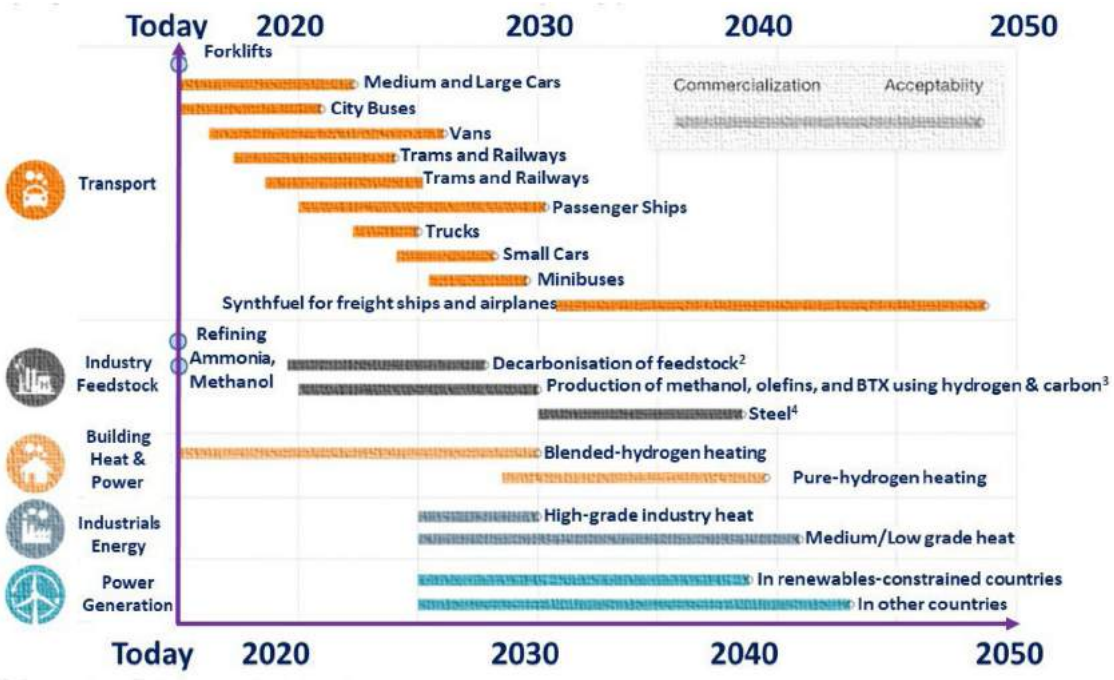

Fig. 2. (e) Timeline chart of mass energy transportation and power generation.

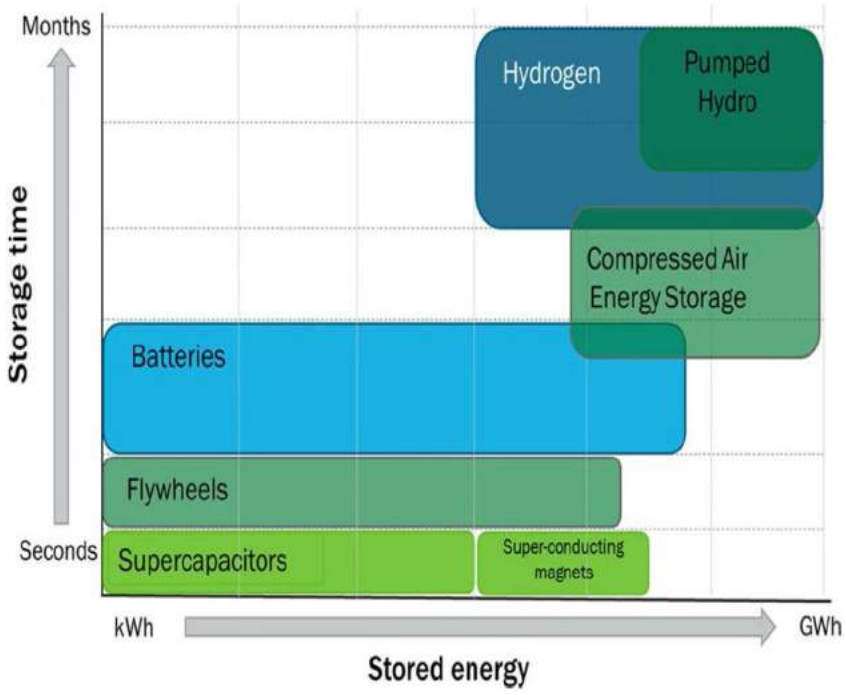

Fig. 3. (a) Stored energy vs. storage time for various energy technologies.

tion at laboratory scale which could be useful to determine the hydrogen storage capacity of the materials. Not only the storage capacity of the materials but also other physical and chemical properties are very important to optimize the hydrogen storage solid specimens which includes the microstructural properties using X-ray diffraction and electron microscopy. The spectroscopic studies can be used to analyze various chemical and molecular properties of the targeted storage materials. Though, the analysis data of the targeted specimens are not enough to give final sorption capacity of the potential storage materials for the hydrogen [13]. A very recent comprehensive review on the prospects of hydrogen storage and related issues have been discussed especially metal hydrides for sustainable energy applications [43].

6. Metal hydrides and related systems

Compounds formed between metals and hydrogen are termed metal hydrides. Here the metal can be in form of an element, an alloy, or a metal complex. The nature of bonding between metal and hydrogen depends on the electronegativity of the metal, which is responsible for the type of electrons shared among metal and hydrogen. For low elec-

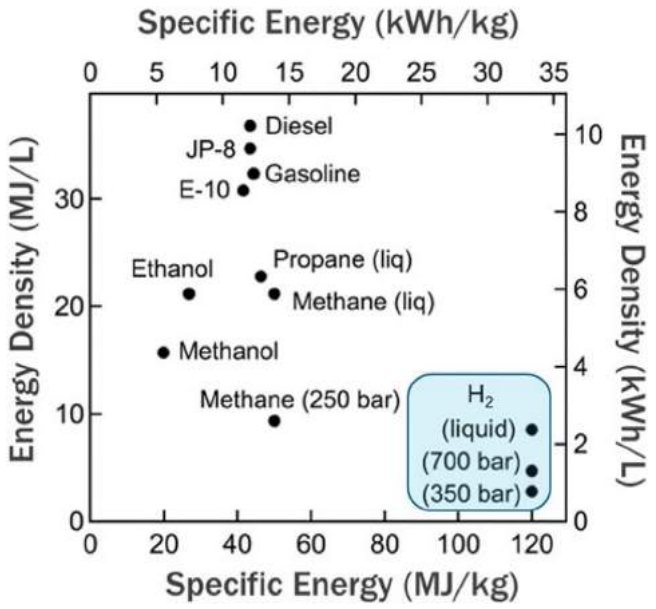

Fig. 3. (b) Specific energy density vs volumetric density of number of fuel sources.

tronegative metals alkali (Group 1a) or alkaline earth metals (Group 2a), the electron is transferred from the metal to the hydrogen and thus the ionic bond is formed. With the increase in the electronegativity of the metal, the metal-hydrogen bond is metallic. With the even higher value of electronegativity of metal, the bond becomes covalent in nature. Metallic metal hydrides are formed from transition metals, lanthanides, and actinides. In this case, the electron energy levels of metal and hydrogen overlap sharing delocalized electrons characterized by a metallic bonding. The hydrogen atom is occupied in either a tetrahedral or an octahedral void formed by metal atoms.

As mentioned above, in metal hydrides metal may be in form of an element, alloy or intermetallic compound (IMC). Metal hydrides formed by an element have limited properties. There is the large scope and greater flexibility for tailoring the hydrogenation characteristics through alloys and intermetallic compounds with a wider range of applications. Alloys and intermetallic compounds may be binary, ternary, quaternary, and more complicated systems. The class of alloys capable of storing hydrogen is also known as hydrogen storage alloys (HSA). The major binary IMC systems used as HSA are AB_5 ($LaNi_5$), AB_2 ($TiMn_2$), A_2B (Mg_2Ni) and AB (TiFe) (Table 1). The few other classes are A_3B (Nb_3Sn), AB_3 ($LaNi_3$), A_2B_7 (Nd_2Ni_7), A_2B_{17} (La_2Mg_{17}), A_6B_{23} (Ho_6Fe_{23}) etc. There may be more than one stable crystal structure for each system. The characteristics of the binary IMC may not be always available for a particular application. In such cases, partial substitution at A, B or both sites with elements containing the same or the similar number of outer shell electrons can be done. This substitution

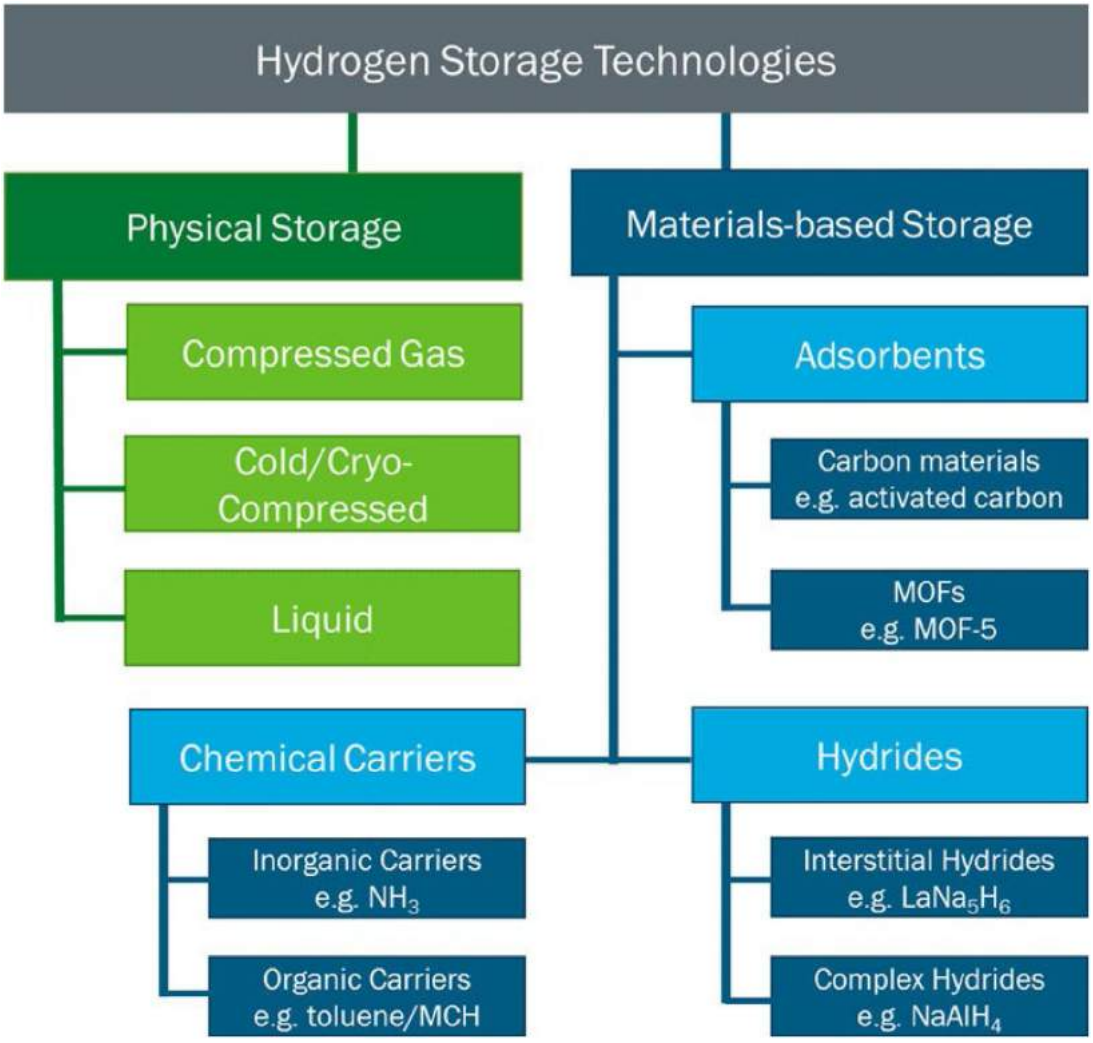

Fig. 3. (c) Types of hydrogen storage technologies.

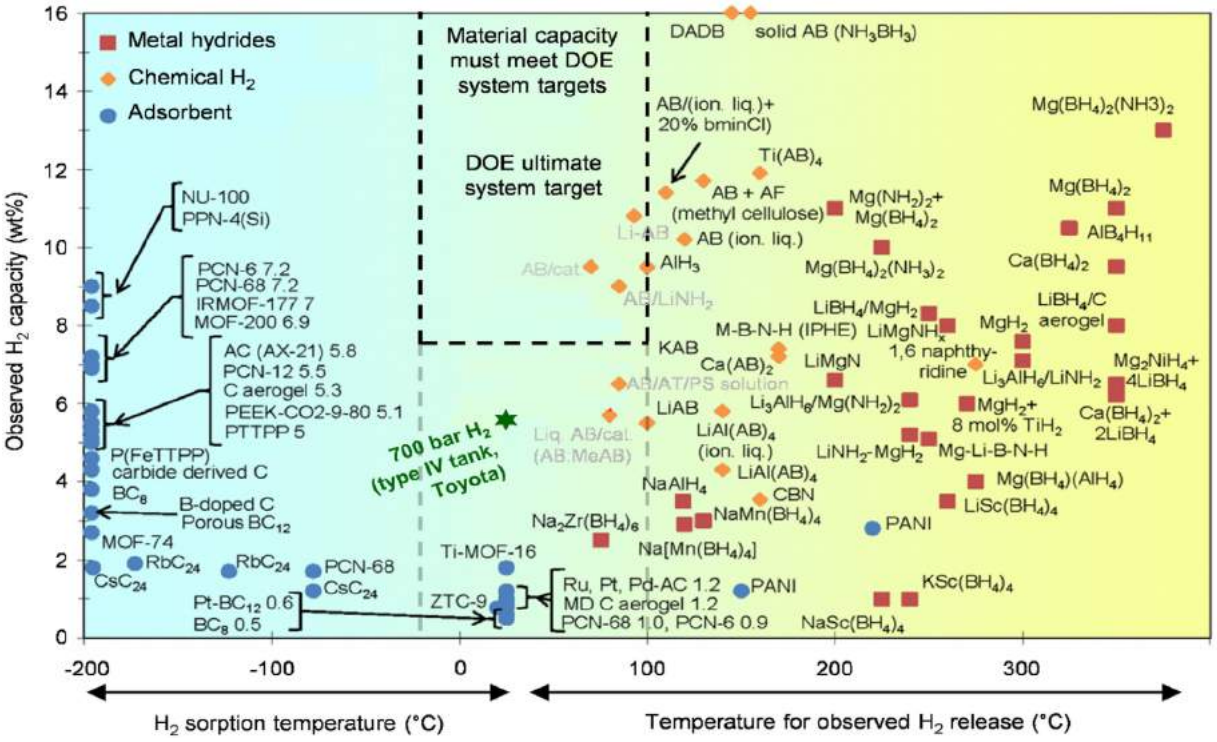

Fig. 3. (d) metal hydrides, chemical hydrogen, and adsorbents temperature of operation with respect to the hydrogen storage capacity

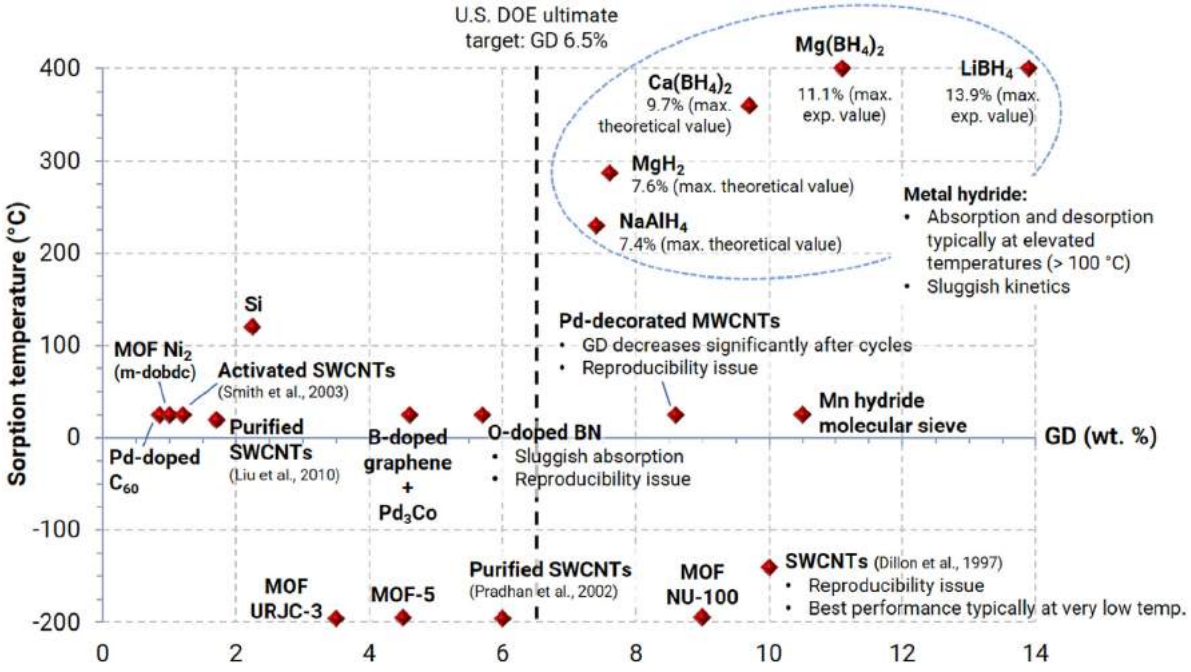

Fig. 3. (e) Sorption temperatures of various soft materials and complex hydrides with respect to hydrogen storage capacities.

may specifically tailor the IMC for required hydrogenation properties (Table 2). One more popular metal hydride corresponds to vanadium-based solid solution. In the following, each class of IMC and their progress (Fig. 5) will be discussed one by one.

6.1. AB_5 system

It is the most easily operated intermetallic compound with the application at ambient conditions. In the AB_5 system, A usually comes from the rare earth (lanthanide) elements (at. no. 57–71) including Ca and B is a transition element basically Ni. It is synthesized through vacuum induction melting. This type of intermetallic compound is very brittle and easily reduced to the granular or powder form to fill hydride containers. The hydrogen storage capacity of $LaNi_5$ corresponds to 1.4 wt% with plateau pressure ~ 0.5 MPa. The heat of formation of $LaNi_5H_7$ is 7.3 kcal per mol H_2 [44].

6.1.1. Crystal structure

AB_5-type IMCs have $CaCu_5$-type hexagonal structure with space group P6/mmm. Here the unit cell is hexagonal with one formula unit

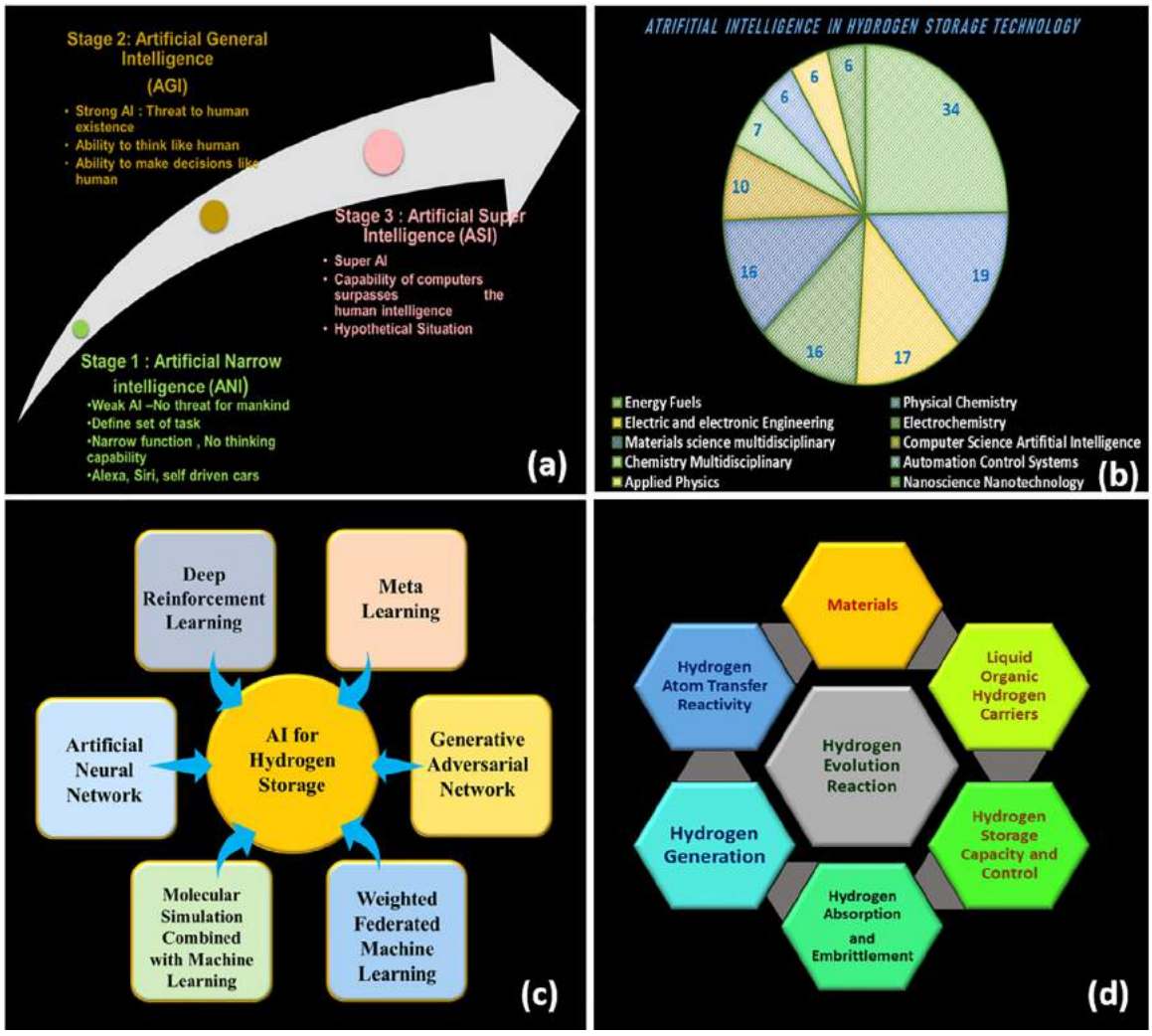

Fig. 4. (a) Three main stages of AI, (b) AI in hydrogen storage technology, Different techniques of AI to predict (c) materials and (d) properties of the hydrogen storage systems.

Table 1
Types of metal hydrides.

S.N.	Class	Crystal structure	Representative compound				
			Composition	Hydrogen Storage capacity wt%	Plateau pressure (MPa)	Operating temperature °C	Heat of hydride formation kcal (mol H_2)$^{-1}$
1	AB_5	Hexagonal $CaCu_5$	$LaNi_5$	1.5	0.5	Room temperature	7.3
2	AB_2	C14 Hexagonal	$TiMn_2$	2.0	1.4	Room temperature	7.2
3	A_2B	C16 Hexagonal	Mg_2Ni	3.8	0.1	300	15.3
4	AB	BCC	FeTi	1.9	0.5	40	6.7
5	Solid Solution (SS)	BCC	$(V_{0.9}Ti_{0.1})_{0.95}Fe_{0.05}$	1.8	0.05	25	10.3

Table 2
Comparison of hydrogenation properties of metal hydrides.

Activation	AB_5	>	AB_2	>	SS	>	A_2B	>	AB
Kinetics	AB_5	>	AB_2	>	SS	>	A_2B	>	AB
Cyclic stability	AB_2	>	SS	>	AB_5	>	AB	>	A_2B
Cost	AB_5	>	AB_2	>	SS	>	A_2B	>	AB
Reversible hydrogen storage capacity	AB_2	>	AB	>	SS	>	A_2B	>	AB_5
Operating conditions	AB_5	>	AB_2	>	SS	>	AB	>	A_2B
Sensitivity to impurity	AB	>	A_2B	>	SS	>	AB_5	>	AB_2

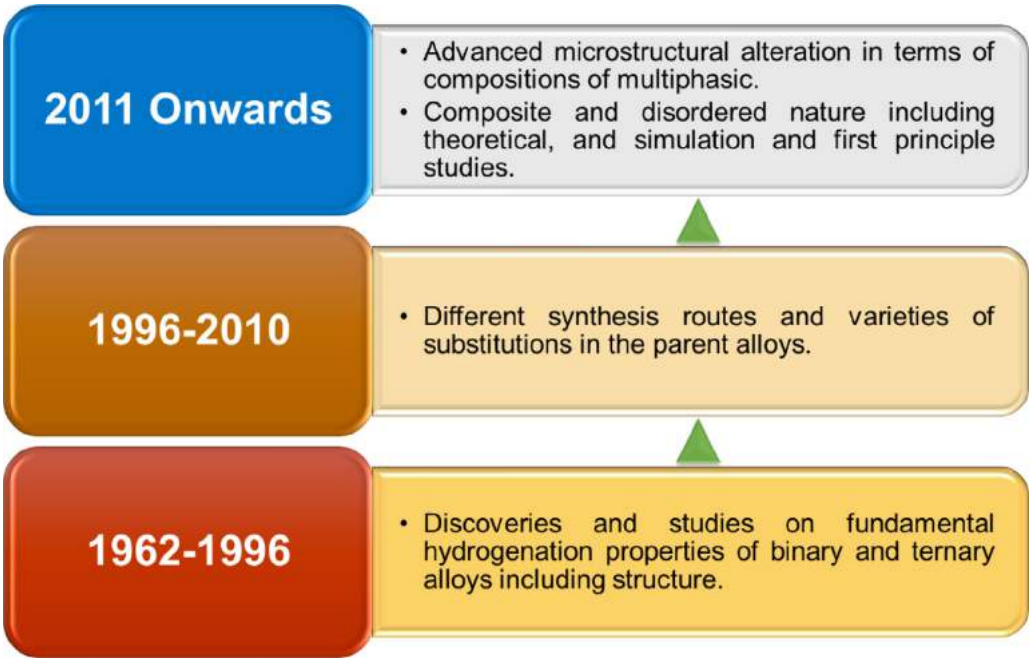

Fig. 5. Progress in metal hydride-based research.

per cell. The calcium atoms occupy the positions (0,0,0) and copper atoms are found at positions (1/3, 2/3,0), (2/3, 1/3, 0), (1/2, 0, 1/2), (0, 1/2, 1/2) and (1/2, 1/2, 1/2) [45]. The representative compound of this family corresponds to $LaNi_5$. The $CaCu_5$-type of structure is relatively common in AB_5 compounds when the atomic diameter of the B atom is smaller than that of the A atom. It happens within a range of radius ratio r_A/r_B from 1.3014 ($NbBe_5$) to 1.7656 ($RbAu_5$). In this hexagonal structure, the lanthanum atoms occupy the 1a crystallographic site in the basal plane, while the nickel atoms occupy the 2c site in the basal (N_I) and the 3 g site in the $Z = 1/2$ plane (N_{II}). Each lanthanum atom is surrounded by six lanthanum atoms in the basal plane at distances of 5.01 Å and by two lanthanum atoms in the c-direction located at about 3.98 Å. These La-La distances are to be compared with $d_{La\text{-}La}$: 3.75 Å in the pure fcc lanthanum lattice. The Ni_{II} atoms are surrounded by four Ni_{II}atoms at 2.46 Å, four Ni_{II} atoms ($d_{NiII\text{-}NiII}$ = 2.508 Å) and four lanthanum atoms ($d_{NiI\text{-}La}$ = 3.202 Å). It should be noted that these Ni-Ni distances are comparable with $d_{Ni\text{-}Ni}$ = 2.45 Å in the fcc nickel lattice in which the coordination number is 12, thus much larger than in $LaNi_5$.There are in total 34 tetrahedral holes in one AB_5 unit [46]. These are B_4 tetrahedral holes (4 in subgroup 4 h), AB_3 tetrahedral holes Type I (12 in subgroup 12o), AB_3 tetrahedral holes Type II (12 in subgroup 12n), A_2B_2 tetrahedral holes (12 in subgroup 12n). In the hexagonal AB_5 structure, 9 sites are most probable for hydrogen occupancy.

- 3 clusters of 4 type-II AB_3holes, centroids with subgroup 3f (H_I site)
- 6 clusters of 1 A_2B_2 hole and 2 type-I AB_3 holes, centroids with subgroup 6 m (H_{II} site)

6.1.2. Discovery

AB_5 IMC was accidentally discovered at the Philips Eindhoven Labs about 1969 during work on AB_5 permanent magnet materials $SmCo_5$ [47]. To study the positions of the H-atoms in $SmCo_5$ hydride by NMR, AB_5 compound $LaNi_5$ was selected. The reaction of $LaNi_5$ with H_2 was remarkable compared to $SmCo_5$ [48]. The reversible hydrogenation was confirmed with H/M > 1 at ambient temperature at a pressure of less than 2.5 atm. Low hysteresis and fast kinetics were observed and $LaNi_5$ could also be easily activated at room temperature. Thus, a new and exciting hydrogen storage alloy $LaNi_5$ was discovered. Later on its cost-effective version, $MmNi_5$ evolved. Mm represents an unrefined rare earth mixture commonly known as mischmetal. Mm usually contains the four main rare earth elements Ce, La, Nd and Pr. The actual composition of mischmetal depends on the mineral and ore body from which it is derived. The typical composition (in weight%) corresponds to 48–50% Ce, 32–34% La, 13–14% Nd, 4–5% Pr and 1.5% other rare earth. $MmNi_5$ had been synthesized in early 1973 at Brookhaven National Lab for H_2 separation trials and a high-pressure H_2 source tank [49]. The choice of Mm for La results in very high plateau pressures and hysteresis. This may be adjusted by substitution at Mm and Ni.

6.1.3. Development

For lowering the high hysteresis and high plateau pressure, initially, partial ternary substitutions were done to both the Mm and Ni sides of $MmNi_5$ [50,51]. At the B site other transition elements were tried as Al, Fe, Co, Si, Mn etc.[52–57] Almost up to 2010 AB_5-type compounds were investigated for ternary substitutions at A, B and both sites for the study of their basic hydrogenation characteristics. The earlier study was focused on material development for NiMH cells and storage purposes. Within the last decade many more applications have been coming forward. To accommodate all these applications, the trends of multi-element substitutions have increased. The nano version of the compound and the mixing of alloys were also tried by researchers. A computer simulation study has thrown new insights at the understanding level.

The substitution at the B site is more common and has more options. Each substituted elements plays a specific role in hydrogenation properties according to the specific application. The substitution of Al at the Ni site lowers the plateau pressure of $MmNi_5$ from 1.4 MPa to around 0.2 MPa ?????[58,59]. Mn and Si are substituted for improvement in cyclic performance [60–62]. Co stops the corrosion of metal hydride electrodes [63,64]. To improve the hydrogenation properties, melt-spun versions of IMC were also studied, which resulted in improved kinetics [65–67]. Melt-spun versions reflected higher storage capacity, fast kinetics, and fast activation in comparison to conventional induction melting. It has been noticed that more substitution at the Ni site reduces the hydrogen storage capacity of the parent alloy from 1.4 wt% to 1.0 wt% [65–67]. Fe substitution has a reverse effect on hydrogen storage capacity. It increases the storage capacity due to the presence

of unfilled d-orbital [68]. The Ca substitution at A site is also known to enhance the storage capacity because of its lightweight [69]. However, the plateau pressure has been noticed to increase drastically. To lower this high plateau pressure simultaneous substitution was done at the Ni site also by Al and Fe. A series of IMCs were studied on Ca substitution [70,71]. High hydrogen storage capacity of 2.2 wt% was reported following the composite pellet formation route for the synthesis of the alloy. The multiphasic alloys have shown enhancements in all the hydrogenation characteristics of the $LaNi_5$ alloy with a major phase of $LaNi_5$ and minor phases of $LaNi_3$ and La_2Ni_7 [72–75].

Nowadays multi-element substitutions are preferred to achieve the required properties for specific applications [76–78]. Especially in Ni-MH electrode material, various substitutions are done at Ni sites, with the roles of each element. Such multi-element substitutions give stability to the electrode in alkaline electrolyte and lessen the pulverization, thus increasing cyclic stability with enhanced energy density[79–82].

In the recent decades, the nano-version of alloys has shown improvement in hydrogenation properties due to the larger surface area exposed to the hydrogen. This is achieved through mechanical alloying or ball-milling of the bulk synthesized alloy [83–86]. Ball-milling has resulted in improved hydrogen storage capacity with fast activation process and fast kinetics [87]. The use of a catalysts during ball milling has been found to improve the hydrogenation properties further [88–92]. Widely used catalyst in AB_5 compound corresponds to transition elements. Catalysts are known to favor hydrogen molecule dissociation and more entrance channel for hydrogen atom diffusion into the material at interstitial sites.

Several theoretical calculations and simulations works were also performed to expose the researchers to a better understanding of properties[93–95]. Density functional theory has been proven to reveal information about energy levels and the positions occupied by hydrogen in the metal hydride [45,80,96,97]. Theoretical models have been developed to predict the heat of formation, structural properties, and electronic properties [44,98–104]. Recently AB_5-type IMCs have been applied in many new applications like actuators [102] and thermal management systems [103]. $LaNi_5$ has been reported in other forms as well for hydrogen storage purposes. Spray-dried composite microparticles of polyetherimide and $LaNi_5$ have been studied as versatile materials for hydrogen storage applications [104]. $LaNi_5$ has shown an excellent catalytic effect on the hydrogen storage properties of aluminum hydride at mild temperatures [105]. Hydrogen absorption by ~5 kg $LaNi_5$ has been studied in a metal hydride reactor through simulation studies to show that 290 and 375 s are required for 80% and 90% hydrogen storage saturation level in the reactor, respectively [106]. A monolayer model treated by statistical physics was applied employing the grand canonical ensemble to describe P-C-T isotherms for absorption of hydrogen by $LaNi_{3.6}Mn_{0.3}Al_{0.4}Co_{0.7}$ alloy to correlate with the experimental results [107].

6.2. AB_2 system

The A elements in the AB_2 system are from the IVA group (Ti, Zr, Hf) and/or rare earth series (at. no. 57–71) or Th. The B-elements can be a variety of transition or non-transition metals with a preference for atomic numbers 23–26 (V, Cr, Mn, Fe). In this system also, a wide variety of substitutions are possible for both A- and B-elements. Substitutions may help in developing materials with hydrogenation properties for specific requirements.

6.2.1. Crystal structure

The class of practical AB_2 intermetallic compounds for hydrogenation purposes belongs to the Laves phase. Laves phase structures have three varieties: C14, C15 and C36 [108]. The C14 and C15 are the most important structures. The C14 phase has hexagonal structure, with 4 AB_2 formula units per equivalent trigonal unit cell (4 A-atoms and 8 B-atoms). A representative hydriding C14 phase is $ZrMn_2$. The C15 phase has a cubic structure with eight AB_2 formula units per unit cell (8 A-atoms and 16 B-atoms). A representative C15 hydriding phase is ZrV_2. In both cases, H-atoms tend to occupy $[A_2B_2]$ tetrahedral interstices [109]. The AB_2 intermetallics may have some homogeneity range (i.e., A: B need not be exactly 1:2), unlike the AB_5 line compounds. $ZrMn_2$ and ZrV_2 have hydrogen storage capacities of 1.0 and 2.1 wt% respectively [110]. The heat of the formation of hydrides of $ZrMn_2$ and ZrV_2 have values close to 12.7 and 35.9 kcal per mole H_2 [111,112].

6.2.2. History

The first intentionally studied report on AB_2 intermetallic compounds is the formation of two AB_2 hydrides: $ZrCr_2H_{3.6}$ and $ZrV_2H_{4.14}$ [113]. This early study was focused mostly on high temperature (>538 °C) properties. Several years later the 1956 report of Trezeciak et al. [113], a major pioneering hydriding survey of many binary intermetallic compounds was reported by Beck in 1962 [110]. However, AB_2 hydride activity was virtually dormant for the next decade and became quite active at several laboratories in the late 1970s.

6.2.3. Development

In the AB_2 system hydrogen storage capacities are not much if heavy A-atoms are incorporated (e.g., the rare earth elements or Zr). Using the lighter Ti as the A-element helps with a higher weight percent of hydrogen storage capacity [114]. The practically popular alloy of the AB_2 class is $TiMn_2$ having a C14 structure. Plateau pressure, hydrogen storage capacity and other properties can be adjusted by substituting Zr for Ti and Cr for Mn. Zr substitution decreases the plateau pressure and storage capacity [115]. For this alloy, plateau pressure is 1.4 MPa with a hydrogen storage capacity of 2.0 wt%. Several studies have been reported on the substitution of Ti with Zr and the substitution of Mn with Co, Cu, V, Fe, Ni and Cr. The hydrogen storage capacity for these alloys corresponds to 1.5 to 2.0 wt%, while plateau pressure is below 1.0 MPa at ambient temperature. Sometimes a multi plateau is also seen in this system. $TiMn_{1.5}$ and $Ti_{0.98}Zr_{0.02}V_{0.43}Fe_{0.09}Cr_{0.05}Mn_{1.5}$ are popular compositions in the AB_2 system [116–119].

Melt-spun alloys have been prepared to improve the hydrogenation properties and electrochemical properties for application in Ni-MH cells [120,121]. High catalytic activity disorder in multi-component alloys has also been shown to improve the electrochemical capacity of 440 $mAhg^{-1}$ [122]. It has been reported that the hydrogen absorption capacity of the $TiMn_2$-based alloys is mainly governed by the atomic composition and atomic arrangement of the alloy within the $TiMn_2$ phase [121]. The degradation of the cyclic property of the alloy actively depends on the substituted elements in the hexagonal $TiMn_2$ Laves phase [123]. Centrifugal casting and gas atomization processes were applied to multiple-phase AB_2 alloys by Young et al. [124]. They reported that the centrifugal casting process provided the better cycle life. The gas atomization process has lower production cost but suffers from higher bulk oxygen content and thicker surface oxide, and thus inferior in all battery performance characteristics other than cycle life and charge retention. Various changes in the structure incorporated through phase abundance, defect and off stoichiometric have direct effects on the hydrogenation characteristics of the AB_2 alloy [125–127]. Phase abundance has shown higher gas phase and electrochemical storage capacities, lowering of the hydrogen equilibrium pressure, decrease in the half-cell high rate dischargeability, improvement of both charge retention and cycle life [102]. Defect in C15 $Zr_{0.9}Ti_{0.1}V_2$ alloy improved the hydrogen absorption-desorption properties [103].

In a separate study carried out by Kazemipour et al.$Ti_{0.72}Zr_{0.28}Mn_{1.6}V_{0.4}$ alloy was synthesized using mechanical alloying and innovative vacuum copper boat induction melting. They showed that the samples consisted of two main phases, the C14 Lave phase and the V-base solid solution phase. The hydrogen capacity of the induction melted samples was higher than that of the samples produced by the mechanical alloying method [128]. Studies through density functional theory on the total energy, electronic structure and

bond of $Zr(Cr_{0.5}Ni_{0.5})_2$ alloy and its hydrides showed that A_2B_2 sites are preferentially occupied in the structure, followed by the AB_3 while B_4 remains empty. Among hydrogenations, the main contribution to the density of states is due to the d electrons of all components of the structure [129]. $TiMn_2$ has been reported to enhance the hydrogenation properties of MgH_2 nanocomposites synthesized through reactive ball-milling [130]. Several recent studies have pointed out the effective application of AB_2 alloys in electrochemical storage, compressor, and easy activation for storage purposes [131,132]. High entropy alloy has further enhanced the electrochemical capacity [133]. Qin et al. devoted their studies to demonstrating that $ZrFe_2$-based alloys with a small Ga or Al substitution are suitable for high-pressure hydrogen storage applications [134]. Few researchers reported the hydrogenation characteristics of AB_2 alloys based on machine learning [135,136].

Normally freshly crushed AB_2 materials activate at room temperature. Sometimes heating at a few 100 ˚C temperatures in a hydrogen atmosphere is needed for activation. The kinetics of hydrogen absorption-desorption is high. The intrinsic kinetics is faster than the heat transfer [94]. Less than 5% of capacity loss was seen in commercial alloy $Ti_{0.98}Zr_{0.02}V_{0.43}Fe_{0.09}Cr_{0.05}Mn_{1.5}$ during 2000 absorption-desorption cycles with high purity H_2 (0.1–5.0 MPa, 20–80 ˚C) [94]. The AB_2s are considerably less expensive than the AB_5s.

6.3. A_2B system

In the A_2B system, PCT data does not fall in the 0–100 ˚C temperature range and 0.1–1.0 MPa pressure range for most of the IMC of this class. Hence it is less useful for ambient condition applications. Mg_2Ni is the representative hydride phase with an H/M value of 1.33, a hydrogen storage capacity of 3.6wt%, 15.4 Kcal $(mol\ H_2)^{-1}$heat of hydride formation 0.32 MPa plateau pressure at the temperature of 299 ˚C [137].

6.3.1. Structure

Mg_2Ni has an Al_2Cu-type C16 hexagonal structure. It may be noted that Mg_2NiH_4 is not a metallic hydride in the sense of the other intermetallic compounds [138]. It is a more complicated hydride. Mg_2NiH_4 is not an interstitial hydride. Here Mg donates electrons to stabilize an $[NiH_4]^{-4}$ complex. 4 hydrogen atoms are bonded with a single Ni atom and the two electrons are donated by two Mg atoms each to stabilize the $[NiH_4]^{-4}$ transition metal complex. The structure of Mg_2NiH_4 is quite different from the starting Mg2Ni structure. Mg_2FeH_6 and Mg_2CoH_5 A_2B stoichiometries are present only as hydride complexes. Mg_2Fe and Mg_2Co phases do not exist without hydrogen in the binary metal systems.

6.3.2. History

Historically Mg_2Ni was one of the earliest intermetallic compounds that were reported to be usable as a rechargeable hydride [115]. Mg_2Ni can absorb up to 3.8 wt% hydrogens [139]. This capacity is very large in comparison to AB_5 and AB_2-type alloys [140]. Ni is known to improve the hydrogenation absorption-desorption capacity of Mg [141]. During reaction with Mg, Ni forms Mg_2Ni and $MgNi_2$ alloy. $MgNi_2$ alloy does not absorb hydrogen, but Mg_2Ni absorbs a good quantity of hydrogen.

E:\Vendor–2\backup\FEB-2023\2-FB\SOLCOM100033The A2B system has desorption pressure usually less than 0.1 MPa. To increase the desorption pressure various substitutions have been done at the A and B sites. Partial substitution of Al for Mg and Zn for Ni does lower the desorption temperatures of Mg_2Ni a little, but it is difficult to reach the pressure of 0.1 MPa at 100 ˚C [142]. The metallurgy and the basic chemistry of the hydrides of A_2B systems are fundamentally different compared to the AB_5, AB_2 and AB families. Together with the principal plateaux at very low pressures, Zr_2Pd, Hf_2Pd and Hf_2Cu have additional plateaux at very high pressures (100 MPa) at room temperature [143]. These interesting intermetallics have the "non-close-packed" tetragonal Cl_{lb} $MoSi_2$ structure with various available interstitial sites [144]. The additional plateaux cover about 0.3–0.6 H/M, i.e., a relatively small part of the maximum capacity. Generally During the synthesis of Mg_2Nifinal product is typically a three-phase mixture of Mg_2Ni, $MgNi_2$ and Mg. It may be noted that the $MgNi_2$ phase does not hydride. Hence the alloy is usually melted to slightly higher Mg levels than the stoichiometric Mg_2Ni. Single-phase Mg_2Ni can be made by mechanical alloying (high-energy ball milling) of elemental Mg and Ni powders [145] and by the reaction of Ni powder with Mg vapor [146].

Zaluski et al. reported on the synthesis of Mg_2Ni through mechanical alloying using a high energy ball mill to enhance the kinetic and activation properties [147]. In a similar work reported by Singh et al., the nano version of Mg_2Ni alloy prepared through ball milling has been found to show easy activation by annealing at 300 ˚C in a vacuum for 30 min [148]. Mechanical alloying has also revealed the enhancement in hydrogen diffusion and charge transfer reaction [149]. In a separate work on ternary $Mg_2Ni_{0.75}M_{0.25}$????(M = Ti, Cr, Mn, Fe, Co, Cu and Zn) alloys synthesized by the ball milling; hydrogen desorption capacity reached the highest value after only two adsorption-desorption cycles after fluorination treatment [150]. In these alloys, 3.3 wt.% hydrogen desorption was measured at 250 ˚C. Replacement of Ni by Cr, Mn and Co has lowered the decomposition plateau pressure; while Ti and Cu had the opposite effect and Fe and Zn had little effect. Mg_2Ni and Mg_2NiH_4 have been reported showing the catalytic effects on the hydrogen desorption characteristics of MgH_2 [151]. The catalytic efficiency of Mg_2NiH_4 was found considerably higher than pure Ni and Mg_2Ni phase. Cr doping to result in the alloy $Mg_2Ni_{0.9}Cr_{0.1}$ showed stable absorption capacity, and improvement in absorption/desorption rates after cycling [152]. The use of MWCNTs coupled with TiF_3 during the ball milling process has improved the hydrogen desorption property of Mg_2NiH_4 reasonably [153]. It was noticed that in the presence of above-mentioned catalysts, the dehydrogenation temperature, and the activation energy of Mg_2NiH_4 were reduced to 230 ˚C from 244 ˚C and 53.24 kJ/mol from 90.13 kJ/mol respectively. Hence the addition of proper catalysts has been proven to be an effective strategy to decrease the desorption temperature and activation energy of Mg_2NiH_4 hydrides.

Studies on the first-principle calculation have been performed to evaluate the hydrogen absorption energy on the Mg_2Ni surface and in the bulk alloy [154]. Reduction in hydrogen absorption enthalpy was observed through an ab initio study by substitution of Al, Ga, In, Si, Ge and Sn at the Ni site in Mg_2Ni alloy [155]. Mg_2NiH_4 powder was used for hydrogen generation via hydrolysis reaction in different types of solutions. The extremely intense hydrogen kinetics was observed using an acidic solution [156]. Moreover, Mg_2NiH_4 powder stored for two months disclosed almost identical hydrogen generation volume as-received Mg_2NiH_4 powder. The hydrolysis reaction between Mg_2NiH_4 and the acidic solution was also applied for electricity production via the PEM fuel cell. Vanadium doping in Mg_2Ni during the ball milling process has resulted in improved hydrogenation-dehydrogenation kinetics with extended plateau region as compared to pure-Mg_2Ni [157]. A few other A_2B-type alloys have also been reported for hydrogen absorption properties. Partial substitution of Mo for Ti increased the hydrogen storage capacity to 2.23 wt%. It was due to decreased dihydride stability after Mo substitution [158]. Density functional theory calculations have been employed to study the improvement in the adsorption, dissociation and diffusion of hydrogen on the $Zr_2Fe(101)$ surface through Mn doping [159]. Zn substitution in Mg_2Ni alloy for Ni has shown a lowering in the activation energy as 17.01 kJ/mol in comparison to 46.07 kJ/mol for the Zn-free Mg_2Ni. The equilibrium hydrogen pressure in the PCT curve of alloys was increased with increasing Zn content [160].

6.4. AB system

Most of the practical AB compounds are based on TiFe and therefore represent low raw materials costs. They are historically important to the early development of ambient temperature hydrides and their application to the first H_2-fueled vehicles.

6.4.1. Crystal structure

The common AB structure corresponds to B1 CrB-type structure. Among AB compounds, practically applied alloys have simple B2 structure. It has a body-centered-cubic cell with one formula unit per unit cell. One A-atom is shared by the cell corners and one B-atom resides at the center of the cubic cell. Each cell contains 12 tetrahedral and 6 octahedral interstices. H atoms occupy only the octahedral sites with the preference of [Ti_4Fe_2] co-ordination. [Ti_2Fe_4] octahedral sites may also be filled at high H/M value [161].

6.4.2. History

The first member of the AB hydride group was reported as ZrNi in 1958 as reversible hydride $ZrNiH_3$ desorption plateau pressure of 0.1 MPa at 300 °C [162]. This material was not studied for one more decade due to the high temperature of 300 °C. The first practical room-temperature AB hydride was TiFe, discovered at Brookhaven National Lab in the U.S. around 1969 [163]. Two distinct hydrides (TiFeH and $TiFeH_{1.95}$) resulted in two separate plateaus. In this class, most of the members have multi-plateau PCT curves.

6.4.3. Development

TiFe has a hydrogen storage capacity of 1.9 wt%, the heat of hydride formation is 6.72 Kcal(mol H_2)$^{-1}$ and plateau pressure of 0.5 MPa at 40 °C. In the AB system useful IMC are ZrNi, TiFe and TiCo, among which TiFe is the most popular one [164,165]. In TiFe IMC Zr can be partially substituted for Ti and Mn, Ni, V, Nb and Si can be substituted for Fe [166–168]. TiFe and $TiFe_{0.85}Mn_{0.15}$ were the best-reported compounds during 1990 in the AB metal hydride system.

Chiang et al. studied the hydrogenation properties of TiFe, $TiFe_2$ and pure Ti during high-energy ball milling in a hydrogen atmosphere. Through ball milling, TiFe could absorb hydrogen without activation treatment [169]. To overcome the deterioration of the hydrogen absorption performances of TiFe-based hydrogen storage materials, surface modifications have been reported by the deposition of metals (including Palladium). This technique facilitated the hydrogenation of the material even after its exposure to air [170]. Benyelloul et al. found that the insertion of hydrogen into the FeTi crystal structure causes an increase in the bulk modulus. Using density functional theory they observed that the FeTi compound and its hydrides are ductile and that this ductility changes with changing the concentration of hydrogen [171]. In separate research, plastic deformation created in intermetallics of TiFe using groove rolling and high-pressure torsion has resulted in 1.7–2 wt% of hydrogen absorption in the first few cycles thus improving the activation process significantly [172]. The samples were not deactivated by long-time exposure to the air. To further improve the activation process and hydrogen storage capacity Cu and Y were incorporated in Ti-Fe-Mn alloy as $Ti_{0.95}Y_{0.05}Fe_{0.86}Mn_{0.05}Cu_{0.05}$ [173]. The melted alloy had a TiFe matrix with a Cu_2Y secondary phase. The addition of element Y enhanced the hydrogen storage capacity as 1.85 wt% at 20 °C. The activation and kinetic properties of the hydrogenated alloy were improved due to the presence of the secondary phase Cu_2Y. Due to its lightweight and low-cost TiFe was compared with $LaNi_5$ for their application in metal hydride beds [174]. Heat exchange was higher in the TiFe bed as compared to $LaNi_5$ filled in a similar tank. Silva et al. reported their work on Mg - 40 wt% TiFe nanocomposite prepared by high-energy ball milling. This process has improved hydrogen absorption at room temperature [175]. To produce active nanocrystalline TiFe compound TiH_2 and Fe powders were dry co-milled in a planetary ball mill for 5–40 h [176]. All samples absorbed hydrogen at 2 MPa without additional thermal activation cycles. Milling for Shorter time of 10 h resulted in easy hydrogen absorption during the first cycle. However, the samples milled for longer times (25 and 40 h) have shown better results in terms of reversible and storage capacities (0.73 and 0.94 wt.%, respectively). In separate research carried out by Lv et al. hydrogen storage properties of air exposed TiFe + x wt.% (Zr+2 V) (x = 0, 4, 5 and 6) alloys were studied [177]. Doped samples had bcc TiFe main phase and hcp secondary phase. The samples showed the fastest hydrogenation kinetics, highest hydrogen capacity and good cycling stability corresponding to x = 4.

Another report focused on the effect of air exposure on the first hydrogenation kinetics of TiFe +4 wt% Zr +2 wt% Mn alloy [178]. In this study researchers observed that the air-exposed alloy could be successfully hydrogenated after ball milling and after cold rolling with some loss in hydrogen storage capacity. To improve the hydrogen storage performances of TiFe-based alloys, $TiFe_{0.8-m}Ni_{0.2}Co_m$ (m = 0, 0.03, 0.05 and 0.1) alloys were synthesized. All the alloys were composed of the majority phase of TiFe and the non-hydrogenated phase of Ti_2Fe. The secondary phase favored the lowering of activation temperature [179]. Zeaiter et al. have reported the effect of mechanical milling on the morphological, structural and hydrogen sorption properties of powdered $TiFe_{0.9}Mn_{0.1}$ alloy [180]. Ball milling has lowered the activation temperature and increased the hydride stability with a sloppy plateau in the PCT curve. Mn in TiFe alloy acted as a sacrificial element to prevent the bulk oxidation of alloys [181]. A very interesting study was reported by Patel et al. on the easy activation of TiFe alloy at room temperature [182]. They showed that the chunks of the alloy under hydrogen pressure can be activated without any additional grinding media. They termed their process as self-shearing reactive milling and observed the full hydrogenation of FeTi alloys. In another study, TiFeMn has been reported as a useful metal hydride for forklifts using numerical simulation [183]. The density functional theory studies made on hydrogen adsorption over TiFe surface and doped TiFe surface reflected that even a very small amount of dopant can influence the hydrogen adsorption properties of TiFe alloy [184].

Density functional theory calculations were applied to investigate the effect of Al, Be, Co, Cr, Cu, Mn and Ni in the TiFe system. Enthalpy of formation was approximated in terms of changes in lattice parameters without the need for Van't Hoff plot [185]. $TiFe_{0.85}Mn_{0.05}$ alloy has been applied as a hydrogen carrier for an industrial hydrogen storage plant of about 50 kg of hydrogen [186]. In general, TiFe is very difficult to activate. It needs heating at a higher temperature of 300–400 °C for activation to break the oxygen layer present at the surface. The intrinsic kinetics of TiFe and related alloys are slower than the AB_5 compound, but heat transfer is rapid.

6.5. Solid solution alloy hydrides

The term "solid solution alloy" designates a primary element used as a solvent into which one or more minor elements in form of solutes are dissolved. In the case of a solid solution, the solute need not be present at an integer or near-integer stoichiometric for the solvent. This feature is entirely different from the intermetallic compounds discussed here. The solute is present in a random (non-ordered) substitutional or interstitial distribution within the basic crystal structure. Various solid solution alloys have been reported as reversible hydrides, in particular, those based on the solvents Pd, Ti, Zr, Nb and V. Pd, Ti and Zr Solid Solutions represent the largest family of solid solution hydrides consisting of the face-cantered-cubic (A1)Pd-based alloys. Many of the Pd solid solution alloys have PCT properties within the range of 0.1–1.0 MPa at 0–100 °C with a low hydrogen storage capacity of 1.0 wt.%, but they are costly.

Hydrides of Ti- and Zr-base solid solution alloys are very stable. Nb and V solid solutions have simple body-centered cubic (A2) crystal structures and their dihydrides generally form a face-cantered cubic structure. In vanadium-based solid solution various elements Ni, Cr, Fe, Mo, Ge, Si, Sn, Ti, Mn and Zr were used [187]. A representative alloy $(V_{0.9}Ti_{0.1})_{0.95}Fe_{0.05}$ was reported with PCT properties as 0.05 MPa pressure at 25 °C, the heat of hydride formation as 10.3 kcal(mol H_2)$^{-1}$ with a hydrogen storage capacity of 3.7 wt% and reversible capacity of 1.8 wt% [188].

Investigations were made on the interaction of hydrogen for the mechanochemically synthesized composition of $Ti_{45}Zr_{38}Ni_{17}$ solid solution alloy. The hydrogenation in this alloy started in the very first

cycle even at a hydrogen pressure of less than 0.1 MPa [189].Gao et al. studied the pulverization mechanism of the multiphase Ti–V-based hydrogen storage alloy consisting of a V-based solid solution phase of the BCC structure and a C14 Laves phase of the composition $Ti_{0.8}Zr_{0.2}V_{2.7}Mn_{0.5}Cr_{0.6}Ni_{1.25}Fe_{0.2}$ alloy [190]. Fe substitution in hydrogen storage alloy $Ti_{12}Cr_{23}V_{65}$ leading to the composition $Ti_{12}Cr_{23}V_{64}Fe_1$ resulted in the increase of the lattice strain and the decrease of the crystallite size by hydrogen absorption and desorption thus improving the cyclic durability [191]. $Ti_{52}V_{12}Cr_{36}$ alloy was investigated by Kamble et al. for the first hydrogenation cycle [192]. They observed that doping of 4% Zr and reduced particle size had a direct effect on lowering the incubation time. In separate research, studies were performed on microstructural details of hydrogen diffusion and storage in $Ti_{25}V_{50}Cr_{25}$ and $Ti_{10}V_{75}Cr_{15}$ alloys activated through the surface and bulk severe plastic deformation [193]. Liu et al. have correlated the order of entropy of alloy with hydrogen absorption and reversible hydrogen desorption capacity on the alloys $V_{35}Ti_{30}Cr_{25}Fe_{10}$, $V_{35}Ti_{30}Cr_{25}Mn_{10}$, $V_{30}Ti_{30}Cr_{25}Fe_{10}Nb_5$ and $V_{35}Ti_{30}Cr_{25}Fe_5Mn_5$ [194]. The partial substitution with niobium and iron in $Ti_{25}Cr_{50}V_{25}$ hydrogen storage alloy increased the cyclic durability of the alloy [195]. In high entropy alloy TiVZrHfNb, it was observed that lower particle size had affected improving the kinetics of hydrogen absorption-desorption, while higher temperature decreased the incubation time for activation [196]. The hydrogen storage alloy specified by the composition $Ti_{10+x}V_{80-x}Fe_6Zr_4$ (x = 0, 5, 10, 15) resulted in the lowest incubation time of 12 s and the highest storage capacity of 3.6 wt% [197]. High entropy equiatomic intermetallic alloy TiZrVCrNi has shown a stable reversible hydrogen storage capacity of 1.52 wt% [198]. A hydrogen storage capacity of 3.5 and 6 wt% H_2 was noticed in nearly equimolar alloys TiVCrMo and TiZrNbH with Mg addition [199].

The disordered and amorphous materials have certain more specific advantages in context to hydrogenation characteristics. A disordered material lacks long-range order in both composition and structure. Such disordered and multiphasic materials lie in between crystal and amorphous materials. Due to the increasing degree of disorder in the metal hydride following trends in hydrogenation characteristics may be observed:

- The hydrogen storage capacity may increase.
- The plateau region in the pressure–concentration isotherm becomes short and slanted.
- Lattice expansion upon hydrogenation becomes less and results in less pulverization during hydride/dehydride cycling.
- In disordered material more surface-active sites are available to facilitate chemical/electrochemical reactions.

6.6. Metal hydrides - summary

Thus, metal hydrides offer varieties of materials for hydrogen storage and their applications accordingly. All the classes of metal hydrides may be summarized as given in Table 1. Different classes of metal hydrides have different hydrogenation characteristics. Some have high storage capacity, while others may have easy activation at ambient conditions. A comparison of important hydrogenation properties among metal hydrides is presented in Table 2. Hence, based on the requirement of specific properties, metal hydrides may be chosen for applications. The metal hydride-based research development has been completed for almost 60 years (1962–1922). These 60 years may be divided into three phases of progress (Fig. 2). The first or early phase within the time range 1962–1995 includes the discovery and studies on fundamental hydrogenation properties like pressure-composition isotherm, hydrogen absorption-desorption kinetics, hydrogen storage capacity, the heat of formation, the structure of parent member and their ternary counterparts. In the middle phase (1996–2010) investigations were focused on the adoption of different synthesis routes mainly ball-milling, reactive ball-milling, melt-spinning etc. with emphasis on varieties of substitutions in the parent alloy. The present ongoing era (2011 onwards) is the witness to advanced microstructural alteration in terms of composition and structure. Nowadays multi-element compositions of multiphasic, composite, and disordered nature are preferred over simple parent alloys. Various theoretical, simulation and first principle calculations based on density functional theory have also come forward. The research on metal hydrides had some recession within the time frame of 2014–2020 due to their less hydrogen storage capacity in comparison to complex hydrides. But the ease of operation at normal temperature and pressure has proven metal hydrides as more feasible candidates for application point of view. Therefore, the research on metal hydrides has again gained a boom for the last few years.

7. Magnesium-based and related systems

Magnesium (the 7th most abundant element in the curst of the Earth with an abundance of 2.3%) and hydrogen (the universe's most common element) reacts together and form the stable magnesium hydride (MgH_2).

$$Mg+H_2 \leftrightarrow MgH_{2+}\Delta H$$

Where, ΔH is the enthalpy of reaction, describing the thermodynamic stability of hydride. The theoretical gravimetric and volumetric hydrogen content of MgH_2 is 7.6 wt.% and 110 kgm^{-3}, respectively. This is at par with the required US-DOE target for onboard storage of hydrogen for vehicular applications [200]. Due to this high gravimetric and volumetric hydrogen density, MgH_2 is considered as a potential candidate for solid state hydrogen storage. However, the high thermodynamic stability of MgH_2 (enthalpy and entropy values are 74.7 kJ mol^{-1} and 130 $JK^{-1}mol^{-1}$) hinders its hydrogen release/absorption (de-/hydrogenation) kinetics at low temperatures [201]. This is due to the fact that the bonding of hydrogen in MgH_2 is partially ionic and partially covalent in nature [202]. Moreover, the factors affecting the de-/hydrogenation behavior of MgH_2 are (i) surface oxide layer formation, (ii) slow hydrogen diffusion rate in the bulk Mg, (iii) poor hydrogen chemisorption on Mg, and (iv) low thermal conductivity [203]. Till date, researchers have adopted several strategies to improve MgH_2's hydrogen storage properties and achieved significant improvement. Methods such as (i) nanostructuring; reduction of grain size providing shorter diffusion path for hydrogen [204,205] (ii) mechanical alloying; destabilize the hydride phase by alloy formation [206] (iii) nanoconfinement; preventing the grain growth by confining in porous scaffolds [207] (iv) additives; forming pathways that facilitate hydrogen diffusion through the diffusion barriers [208] have been employed for improving the MgH_2's hydrogen storage behavior. So far, several techniques have been developed for the synthesis of MgH_2, such as mechanical milling, thin film deposition, melt spinning, electrochemical deposition etc. [209]. Herein, we describe some of the recent progress made on MgH_2 for improving its hydrogen storage behavior.

7.1. Nanostructuring

The properties of materials in the nano dimension may differ significantly when compared to their bulk form. Nanoparticles (NPs) exhibits (i) increased in surface to volume ratio, resulting in increased exposure of surface atoms (ii) reduced diffusion path (iv) closer proximity between different reacting solids, (iv) increased in the number of grain boundary atoms [210]. Due to the larger volume contribution of phase boundaries, nanocrystalline solids exhibit a higher level of disorder [211]. Hence, nanosizing of MgH_2 leads to reduced grains with high active interface/surface and short hydrogen diffusion path, which can accelerate the de-/hydrogenation kinetics of MgH_2/Mg. Nanosizing of MgH_2 not only increases the hydrogen diffusion rate but also increases the surface exposure of MgH_2 NPs [212]. Nanosizing affects

the stability of Mg-H bond resulting in an improvement in the thermodynamic behavior of MgH_2. Theoretical studies predict that MgH_2 NPs may have reduced reaction enthalpy with improved kinetics when the size of the particle is below 50 nm. However, significant improvement in the thermodynamics of MgH_2 NPs was observed for < 5 nm size particles [176,213,]. In general, the methods employed for nanoscaling of MgH_2 are mechanical milling, hydrogenolysis, melt infiltration, physical and chemical vapor deposition, chemical reduction, electrochemical deposition and thermolysis of Grignard reagents [214,215]. Mechanical milling [216] is one of the most widely used methods for the particle size reduction and distribution of catalysts for MgH_2. Mechanical milling introduces a number of changes in the pulverized material, such as particle size reduction up to the order of few nanometers, an increase in specific surface area, a decrease in the crystallite size in the order of nanometers, increase in the crystal lattice defects and grain boundary volume fraction, and the formation of oxide-free surfaces that aid in hydrogen chemisorption [217].

Zaluska et al. [218,219] first reported the improved hydrogen storage behavior of ball milled MgH_2. It was observed that the hydrogen sorption has dramatically improved due to the combined effect of surface modification and nanocrystalline structure of MgH_2. Depending on the ball milling condition, the onset temperature (T_{ON}) for hydrogen desorption has been lowered by 100 °C. Varin et al. [220] have demonstrated the synthesis of nanostructured MgH_2 from elemental magnesium powder in a hydrogen environment using controlled reactive mechanical milling (CRMM). The nanocrystalline MgH_2 with an average particle size of 338 nm shows a significant change in enthalpy from 74 $kJmol^{-1}$ H_2 (for commercial polycrystalline MgH_2 having an average particle size of 35.9 μm) to 57 $kJmol^{-1}$ H_2 (for nanocrystalline MgH_2). Hence, the T_{ON} for hydrogen desorption has decreased from 409.4 °C (for commercial MgH_2) to ~325 °C (for nanocrystalline MgH_2). T_{ON} for hydrogen desorption was found to be decreased with decrease in the particle size of MgH_2. It has been observed that the nanostructuring of MgH_2, leads to the formation of metastable γ-MgH_2 phase. The presence of γ-MgH_2 improves the hydrogen kinetics and significantly modifies the thermodynamic parameters of MgH_2. Shen C. et al. [221] have observed that the presence of γ-MgH_2 leads to a significant reduction in hydrogen reaction enthalpy with Mg from 74. 8 to 57.7 $kJmol^{-1}$ H_2 with improved hydrogen sorption kinetics. Recently, Lototskyy et al. [222] synthesized MgH_2 NPs using high-energy reactive ball milling (HRBM) of Mg in the hydrogen atmosphere. The MgH_2 NPs synthesized by HRBM shows improved hydrogen reaction kinetics and the T_{ON} for dehydrogenation was lowered to 302 °C. However, with additives the T_{ON} for dehydrogenation of MgH_2 NPs synthesized using HRBM was reduced significantly to 200 °C. More recently, Baran et al.[223] employed high temperature, high pressure reactive ball milling (HTPRBM) for the synthesis of MgH_2 NPs. A special milling jar with the capability of temperature control and pressure sensor was used for HTPRBM. Huang et al. [224]described the synthesis of MgH_2 NPs on 40% graphene sheets by a one-step solvent-free hydrogenolysis method. The growth of MgH_2 NPs on graphene sheets is achieved by the hydrogenolysis of $(C_4H_9)_2Mg$ through the following reaction

$$(C_4H_9)_2Mg + 2H_2 \rightarrow MgH_2 + 2C_4H_{10}$$

Here, the size of MgH_2 NPs can be controlled by adjusting the MgH_2 to graphene sheets mass ratio. The T_{ON} for dehydrogenation of MgH_2 NPs dispersed uniformly on graphene sheets is lowered to 270 °C. Whereas, MgH_2 NPs synthesized by the same method without graphene addition exhibits T_{ON} for dehydrogenation at 300 °C.

Since the addition of 40% graphene acts as deadweight to the system, the hydrogen storage capacity is reported to be ~4.5 wt.%, which is significantly less than that of pure MgH_2. Recently, Huang et al. [225] synthesized MgH_2 NPs with an average particle size of 8.9 nm by combining ball milling and thermal hydrogenolysis of di-*n*-butylmagnesium, $(C_4H_9)_2Mg$ through the following reaction.

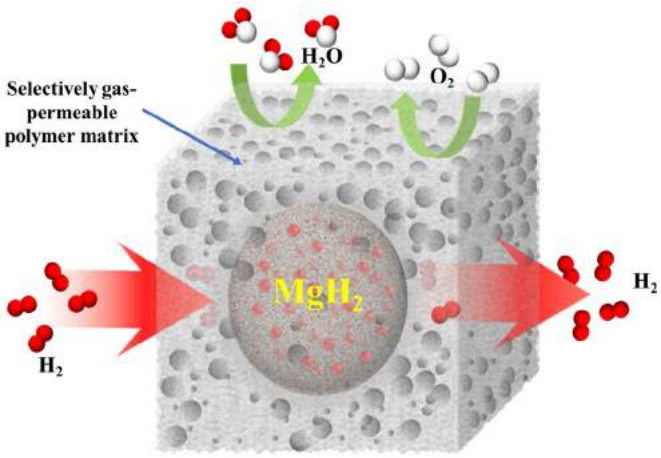

Fig. 6. Schematic of Mg NPs encapsulated by a polymer matrix, which is selectively gas permeable [226].

$$(C_4H_9)_2Mg \rightarrow MgH_2 + 2C_4H_8$$

With the effect of ball milling, the hydrogenolysis temperature was significantly reduced to 100 °C. The nano-size effect significantly alters the thermodynamic properties of MgH_2 with enthalpy value of 69.78 $kJmol^{-1}$ H_2 and the T_{ON} for dehydrogenation was observed at 225 °C.

Rambhujan et al. [215] have found that the MgH_2 NPs obtained by the thermolysis of di-tert-butylmagnesium exhibits two-staged hydrogen desorption attributed due to the presence of two MgH_2 phases; the thermodynamically stable β-MgH_2 and the metastable γ-MgH_2 phase, leading to a lower hydrogen desorption temperature with improved hydrogen sorption kinetics.

Even though several approaches have been proposed for the synthesis of Mg NPs, the high reactivity of Mg NPs in air leads the synthesis process to be a challenging task. Jeon et al.[226] synthesized an air-stable composite of Mg nanocrystals encapsulated in a polymer PMMA [poly(methyl methacrylate)] matrix, which permit only hydrogen and not O_2 or H_2O, thereby reactivity of Mg nanocrystals with air is prevented (Fig. 6). The Mg nanocrystals were synthesized by using organometallic Mg precursor bis(cyclopentadienyl) magnesium (Cp_2Mg) and lithium naphthalide as a reducing agent. The PMMA encapsulation not only protects the reactivity of Mg nanocrystals with air but also effectively increases the hydrogen storage behavior without the use of any heavy metal catalysts.

The MgH_2 NPs undergo structural changes during hydrogen release and uptake cycles. The grain/particle size of MgH_2 is reported to increase during hydrogen release and uptake cycles, resulting in an agglomeration of particles leading to macroscopic phase segregation [227,228]. The macroscopic phase formation affects the hydrogen sorption kinetics. To prevent the macroscopic phase segregation, MgH_2 NPs can be scaffolded in porous materials.

7.2. Nanoconfinement

Nanoconfinement is the method of scaffolding nano dimensional particles inside the permanent nano dimensional pores of the host scaffolds. Nanoconfinement includes two aspects: nanosizing and confinement [229]. Recently, nanoconfinement or nano-scaffolding of hydrides has emerged as an interesting field of research for altering reaction pathways and tuning the thermodynamic and kinetic parameters of metal hydrides at the nanoscale [230]. This method of scaffolding hydride NPs inside the porous networks can effectively enhance the gas-solid interface, shorten the hydrogen diffusion distance, and restricts particle sintering and macroscopic phase segregations, thus overcoming both the

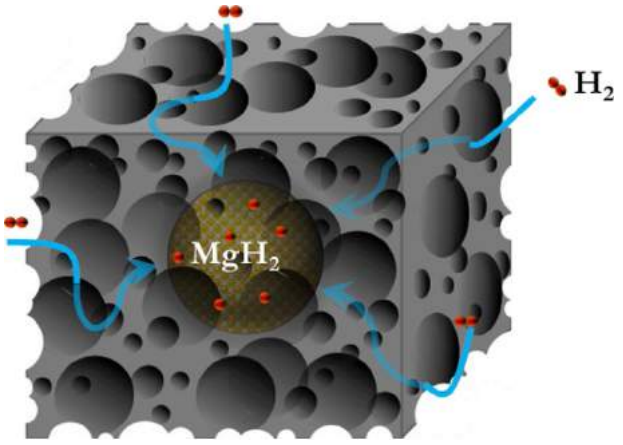

Fig. 7. Schematic representation of MgH_2 NPs confined inside the pores of scaffolding material. The scaffold restricts the movement of Mg/MgH_2 during de-/hydrogenation cycles and prevents the segregation of macroscopic phases.

kinetic and thermodynamic barriers associated with MgH_2 NPs during de-/hydrogenation cycling. Here, the dimension of pores determines the dimension of particles confined in it. Experimental conditions such as the application of external temperature and pressures may cause structural deformation of scaffolding materials, affecting the pore structures. For nanoconfinement of hydrogen storage materials, porous materials which has high specific surface area, uniform distribution of pore sizes, chemical inertness and possess structural stability during the multiple de-/hydrogenation cycles are considered (Fig. 7). Moreover, the scaffolds function as a deadweight to the hydrogen storage system and hence lightweight materials are preferred. The most commonly used scaffolds are carbon aerogels [231], activated porous carbons [232], metal-organic frameworks [233], porous polymer etc. [208]

Several methods have been adopted to infiltrate the MgH_2 NPs inside the pores of the scaffolding materials such as (i) melt impregnation (ii) solvent impregnation (iii) solution impregnation (iii) reactive gas evaporation (iv) sol-gel auto combustion and solution mixture [234] etc.

In the melt impregnation method, the molten state of MgH_2 is infiltrated into the pores of scaffolds by capillary condensation. With the benefit of physicochemical adaptability, carbon-based materials are often used as scaffolds. Generally, Carbon based porous scaffolds are considered for melt impregnation due to the wide range of porosity and chemical inertness during de-/hydrogenation cycles [235]. Gross et al.[236] employed melt infiltration method to confine MgH_2 NPs inside the micro and mesopores of carbon aerogels. The infiltration of molten Mg inside the pores of carbon aerogels (CA) followed by hydrogenation leads to the formation of confined MgH_2 NPs in CA scaffolds. The CA scaffolds have an average pore size of ~13 nm and since the confined MgH_2 particles are in the range of 13 nm, no significant change in enthalpy of MgH_2 is observed. However, significant improvement in the dehydrogenation kinetics of the confined MgH_2 is observed. Furthermore, nanoconfinement of MgH_2 in CA improves the efficacy of catalyst additive. Liu et al.[237] employed a solvent infiltration method for the confinement of MgH_2 NPs inside CA scaffold. The Mg NPs in the size range of 5 to 20 nm confined in CA were derived by hydrogenation of infiltrated dibutyl-magnesium. The 'nanosize effect' of Mg leads to a significant reduction in the thermodynamic stability of MgH_2 with improved kinetic behavior. The hydrogen absorption/desorption enthalpies of Mg/MgH_2 in CA is estimated to be -65.1 ± 1.56 kJmol^{-1} H_2 and 68.8 ± 1.03 kJmol^{-1} H_2, respectively.

Recently, nanoconfinement of MgH_2 with catalyst additives are becoming an interesting area of research for improving the kinetics and tuning the thermodynamics of MgH_2. Ma et al. [238] have described the nanoconfinement effect of MgH_2 NPs in mesoporous CoS nanoboxes scaffold. The confined MgH_2 NPs were in the size range of 5 to 10 nm. The mesoporous CoS nono-boxes was first synthesized from ZIF-67 MOF then the MgH_2 NPs in CoS nano-boxes was derived by vacuum assisted impregnation of dibutyl magnesium solution followed by hydrogenation at 180 °C under 48 atm. hydrogen pressure. The hydrogenation and dehydrogenation enthalpies of Mg/MgH_2 in CoS nanoboxes derived through solvent impregnated method is estimated to be -65.6 ± 1.1 kJmol^{-1} H_2 and 68.1 ± 1.4 kJmol^{-1} H_2, respectively. The enthalpy values are similar to that observed for the nanoconfined 5 to 20 nm MgH_2 NPs in CA [198]. Apart from lowering the thermodynamic parameters of MgH_2, the CoS nano-boxes scaffold plays an important role on providing active catalyst for enhancing the hydrogen sorption kinetics of Mg/MgH_2. Ren et al. [239] synthesized nanoconfined MgH_2 in the slit pores of 2D graphene like TiO_2 nanosheets. The MgH_2/TiO_2 nanosheets heterostructure was synthesized by hydrogenation of Mg NPs derived by impregnating dibutyl magnesium solution in the slit pores of TiO_2 nanosheets. The confined MgH_2 in TiO_2 nanosheets has T_{ON} for dehydrogenation at 180 °C. Additionally, the confined MgH_2 exhibits superior hydrogen sorption kinetics and good cyclic stability with negligible degradation even after 100 cycles of de-/hydrogenation. Zhu et al. [240] investigated MgH_2 NPs confined in 3D architecture of $Ti_3C_2T_x$ MXene nanosheets. The synergistic nanosize effect and catalytic effect by MXene leads to a significant reduction in the MgH_2 T_{ON} for dehydrogenation to 140 °C with good cyclic stability without loss in kinetics. Ren et al. [241] demonstrated the confinement effect of MgH_2/Ni NPs in MOF derived from N-doped hierarchically porous carbon nanofiber. The T_{ON} for desorption of MgH_2/Ni NPs in MOF is lowered to 200 °C and hydrogen absorption occurs at 100 °C. Thus the 'nanosize effect' of the confined Mg/MgH_2 plays a vital role for improving the reaction kinetics and modifying the thermodynamic parameters of MgH_2, which is favorable for hydrogen storage.

7.3. Catalyzing

Catalyst doping is one of the most effective ways to enhance the hydrogen storage characteristics of MgH_2. Catalyst provides an alternative reaction path with lower reaction energy barrier. Research efforts on catalyst-assisted de-/hydrogenation behavior of MgH_2 have made significant progress on improving the thermodynamics, kinetics, and reversibility of MgH_2. Till date several catalysts such as transition metals [242,243], metal oxides [244–246], metal halides [247–250] metal carbide [251], metal sulfide [252,253] metal and oxide nanoparticles [208,254–263] quantum dots [261], additives supported by carbon structures [230,264–272]s et al. have been investigated by researchers. Among the various catalyst additives, Nb_2O_5 is one of the most effective and widely investigated catalyst precursors for MgH_2. With Nb_2O_5 additive, the dehydrogenation temperature of MgH_2 was significantly reduced to a peak temperature at 230 °C and the hydrogen absorption in Mg catalyzed by Nb_2O_5 takes place even at 40 °C. This is attributed to the reduction of Nb_2O_5 during hydrogenation of dehydrogenated MgH_2 which leads to the formation of a catalytically active state. As Nb_2O_5 reduces further its catalytic activity in MgH_2 increases. Therefore, during de-/hydrogenation cycles more reduction of Nb_2O_5 occurs, resulting in further reduction in hydrogen absorption temperature. It has been found that the chemical state of Nb and the initial structural stability of Nb_2O_5 is vital for realizing superior catalytic activity in MgH_2 [270]. Shinzato et al. [271] observed that the meta stable phase of Nb_2O_5 exhibiting pillar crystallite morphology and pyrochlore structure show superior catalytic effect in improving the de-/hydrogenation kinetics of MgH_2. Zhang et al. [272] found that the hydrogen desorption/absorption kinetics of MgH_2/Mg are greatly improved by the superior catalytic effect of NbN NPs (~20 nm size). The NbN catalyzed MgH_2 released nearly 6.0 wt.% hydrogen in 12 min at 275 °C and the sample absorbs 6.0 wt.% hydrogen within 24 min at 100 °C. The Nb^{3+}-N and Nb^{5+}-N valence state of Nb_4N_3 may be the key factor for increasing MgH_2's hydrogen storage capabilities. The catalytic effect of in-situ NbN and Nb_2O_5 from N-doped Nb_2C supported Nb_2O_5 (N–Nb_2O_5@Nb_2C) on MgH_2 was in-

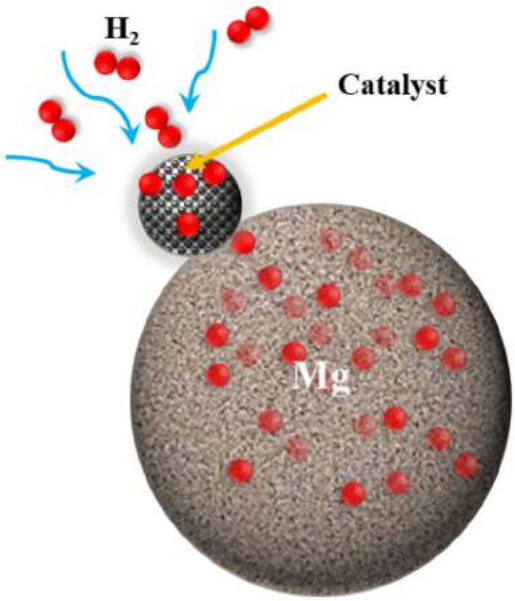

Fig. 8. Schematic representation of hydrogen spillover process during the hydrogen absorption process of Mg.

vestigated by Lan et al. [273] They observed that the catalyzed MgH_2 sample exhibit T_{ON} for hydrogen desorption at 178 °C and the hydrogen absorption temperature has been reduced to 90 °C. The catalyst additive also helps to maintain a good de/redydrogenation cyclic stability.

Recently, catalytically active hydrogen spillover receptors have gained significant research interest for enhancing the hydrogen sorption kinetics of MgH_2 (Fig. 8). Here, during hydrogen spillover process, the molecular hydrogen will get initially adsorbed on the surface of the spillover receptor and get dissociated into atoms and the atomic hydrogen can easily diffuse into Mg, which is generally poor for hydrogen chemisorption [274].

Hou et al. [275] have employed Ni/C as a catalyst for improving the hydrogen storage properties of MgH_2. They observed that the addition of 9 wt.% Ni/C with MgH_2 leads to a significant reduction in the hydrogen release temperature to 195 °C and with improved hydrogen sorption kinetics and good cyclic stability. The in-situ formation of Mg_2Ni/Mg_2NiH_4 serves as a 'hydrogen pump' in MgH_2 for enhancing the hydrogen diffusion during de-/hydrogenation cycles. Shao et al. [276] explored the catalytic activity of TiO_2 NPs (5 – 10 nm) supported on 3D ordered macropores (3DOM) as a catalyst for enhancing the hydrogen storage behavior of MgH_2. It has been observed that 5 wt.% 3DOM-TiO_2 as an additive improves the de-/hydrogenation behavior of MgH_2. The in-situ formed multiple valence state Ti helps to destabilize MgH_2 and the dehydrogenated sample shows hydrogen uptake at 100 °C with reasonably good kinetics. Recently, catalyst nanoparticles derived metal organic framework (MOF) and 2D Metal Carbides and Nitrides (MXenes) have gained enthusiastic research interest due to its unique structure, rich element composition and functional surface. [277] Gao et al. [278] reported the catalytic activity of Ni derived from MOF.

Yang et al. [279] used Ni@C derived from trimesic acid-Ni based metal organic framework (TMA-Ni MOF) as a catalyst for enhancing the hydrogen storage characteristics of MgH_2. The formation of the Mg_2NiH_4 phase serves as a 'hydrogen pump' for improving the thermodynamic and kinetic parameters of MgH_2. Lakhnik et al. [280] synthesized MgH_2/Ti_3AlC_2 MAX-phase composite by reactive ball milling followed by hydrogenation of Mg. The dehydrogenation temperature of MgH_2/7 wt.% Ti_3AlC_2 MAX-phase composite is observed at 236 °C. Zhang et al. [281] have investigated the MOF-derived bimetallic Co@NiO as catalyst for enhancing MgH_2's hydrogen storage behavior. The formation of Mg_2NiH_4/Mg_2CoH_5 interfaces lowers the energy barrier of H diffusion channels, promoting the hydrogen desorption and absorption kinetics of MgH_2/Mg. Gao et al. [282] have employed self-assembled TiO_2 NPs (15 - 20 nm in size) intercalated between layers of $Ti_3C_2T_x$ MXene as a catalyst for improving MgH_2's hydrogen storage characteristics. The interfaces not only serve as lower energy barrier for hydrogen diffusion channels but also serve as a conduction path for the electrons released from the multiple valence transition state of Ti. In another study, Geo et al.[277] have described the facet dependent catalytic effect of $Ti_3C_2T_x$ MXene. The active edge facets have a stronger affinity towards hydrogen than basal facets of $Ti_3C_2T_x$ MXene, resulting in the formation of more catalytically active metallic Ti from edge facets of $Ti_3C_2T_x$. The T_{ON} for dehydrogenation of 5 wt.% edge facet exposed $Ti_3C_2T_x$ MXene catalyzed MgH_2 was observed at 199 °C, which is 101 °C lower than that of ball milled MgH_2 without any additives. Haung et al. [283] described the catalytic effect of carbon-wrapped Ni and Co NPs (8 - 16 nm) as catalysts in the MgH_2. Among the two catalysts, carbon-wrapped Ni (Ni/C) exhibits superior effect in improving the de-/hydrogenation kinetics of MgH_2. The 6 wt.% Ni/C catalysed MgH_2 sample has peak desorption temperature at 275.7 °C, which is 142.7 and 54.2 °C lower than that of pristine MgH_2 and ball milled MgH_2. Furthermore, the Ni/C catalysed dehydrogenated MgH_2 sample reabsorbs 5.0 wt.% H_2 within 20 s at 100 °C. It has been observed that higher concentration of Ni/C in MgH_2 further improves MgH_2's de-/hydrogenation behavior. Ma et al. [284] showed the superior catalytic effect of carbon supported Ni NPs (Ni@C) towards improving the de-/hydrogenation properties of MgH_2. The T_{ON} for hydrogen desorption of 5 wt.% Ni@C catalyzed MgH_2 has been reduced to 187 °C, which is 113 °C lower than that of ball milled MgH_2 without any additives.

Chen et al. [285] described the catalytic effect of carbon-encapsulated ZrO_2 (C/ZrO_2) NPs (5 – 10 nm) in MgH_2. It has been observed that with carbon encapsulation ZrO_2 exhibits superior catalytic effect for improving the hydrogen release kinetics of MgH_2. The T_{ON} for hydrogen desorption of C/ZrO_2 catalyzed MgH_2 is observed at 208 °C, which is 40 and 101 °C lower than that of ZrO_2 and additive-free MgH_2. Wang et al. [286] reported the superior catalytic effect of uniformly dispersed Ni NPs on porous hollow carbon nanospheres (Ni@PHCNSs) towards the de-/hydrogenation of MgH_2. The T_{ON} for dehydrogenation of 5 wt.% Ni@PHCNSs catalyzed MgH_2 was lowered to 190 °C. Moreover, the dehydrogenated sample absorbed hydrogen at 150 °C with improved kinetics. Wang et al. [256] demonstrated the catalytic effect of vanadium oxide NPs on cubic carbon nanoboxes (nano-V_2O_3@C) towards the de-/hydrogenation of MgH_2. The 9 wt.% nano-V_2O_3@C catalyzed MgH_2 exhibits T_{ON} for hydrogen desorption at 215 °C, which is 60 °C lower than that of MgH_2 without any additives. The dehydrogenated sample reabsorbed hydrogen even at room temperature under 50 atm hydrogen. Lan et al. [287] studied the catalytic effect of nanoporous carbon encapsulated Ni and V_2O_3 NPs ((Ni-V_2O_3)@C) for enhancing the de-/hydrogenation kinetics of MgH_2. The 10 wt.% (Ni-V_2O_3)@C catalysed Mg/MgH_2 sample absorbs hydrogen even at room temperature. Zhao et al. [288] have employed core-shell CoNi@C as a catalyst for improving the hydrogen sorption properties of MgH_2. The 8 wt.% core-shell CoNi@C catalyzed MgH_2 exhibits T_{ON} for dehydrogenation at 173 °C and the dehydrogenated sample absorbs 6 wt.% of hydrogen at 150 °C within 200 s. Ren et al. [289] studied the catalytic activity of core-shell structure of Ni/Fe_3O_4 in porous metal carboxylate salts, MIL (Ni/Fe_3O_4@MIL) as a catalyst for improving the hydrogen storage properties of MgH_2. The T_{ON} for dehydrogenation of MgH_2 with Ni/Fe_3O_4@MIL additive was observed at 244 °C. The formation of Mg_2Ni/Mg_2NiH_4 in Ni catalyzed MgH_2 serve as a 'hydrogen pump' to improve MgH_2's hydrogen storage behavior [244,281,284,290,292,293].

7.4. Alloying

Another strategy to destabilize MgH_2 and modify the reaction pathway and thermodynamics is through the addition of reactive additives.

The reactive additive reversibly reacts with Mg and forms a new phase, whose reaction enthalpy with hydrogen will be lower than that of the formation reaction of MgH_2. Thus, the alloying additive destabilizes the Mg-H bond and reduces the enthalpy of MgH_2 through formation of new phase, thereby decreasing the dehydrogenation temperature of MgH_2.

Zhong et al. [291] have described the use of Al as a reactive additive to destabilize MgH_2. Supersaturated Mg(Al) solid solution alloy was prepared by ball milling and it was found that during hydrogenation and dehydrogenation, Mg(Al) solid solution and $Mg_{17}Al1_2$ intermetallic compound were formed reversibly. This transition of Mg(Al) solid solution and $Mg_{17}Al_{12}$ leads to the thermodynamic destabilization of MgH_2. Thus, the dehydrogenation enthalpy of 5 and 10 at.% Al in Mg(Al) solid solution was estimated to be 72.1 and 70.8 kJ mol^{-1}. The addition of Al forms numerous hetero interfaces with high interfacial energy, which could improve hydrogen diffusion and speed up the formation of Mg/MgH_2, thereby lowering the hydrogenation/dehydrogenation enthalpy. Furthermore, the addition of Al increases the thermal conductivity of Mg/MgH_2 and improves the hydrogen sorption kinetics. Cermak et al. [292] studied the hydrogen storage properties of Mg-In-amorphous carbon (Mg-In-CA) alloy synthesized by ball milling and observed that the dehydrogenation enthalpy of MgH_2 was decreased down to 51.5 $kJmol^{-1}$ attributed to the formation of MgIn phase. The enthalpy value was found to decrease with increase in concentration owing to the phase changes from Mg_2In to Mg_3In. Ershova et al. [293] observed that T_{ON} for desorption of hydrogenated Mg-Al-Fe alloy was observed at 250 °C, which is 65 °C lower than that of Mg without any additives. More recently, Lu et al. [294] have investigated the hydrogen storage behavior of carbon covered nanocrystalline Mg_2Ni. The hydrogenation of sample was achieved at room temperature and the T_{ON} for hydrogen desorption was lowered to 180 °C. The hydrogenation and dehydrogenation activation energy of carbon covered nanocrystalline Mg_2Ni were estimated to be significantly lower than that of pristine MgH_2. The hydrogen desorption enthalpy of carbon covered nanocrystalline Mg_2NiH_4 was determined to be 67.0 ± 0.5 kJ mol^{-1}. Thus, the combined effect of nanocrystalline strategy, carbon encapsulation/support and alloying help to improve the MgH_2's hydrogen storage properties. Thus, alloying of Mg with reactive additives helps to lower the hydrogen reaction enthalpy and enhances the hydrogen sorption kinetics of MgH_2.

8. Complex hydrides and related systems

In Section 6 of the present paper discussion started with the metal hydrides of AB_5, AB, A_2B, AB_2 types for hydrogen storage. Ideally, the metal hydrides shows either interstitial or substitutional hydrogen intercalation where that enhances at least 25% volumetric expansion that leads to reversible hydrogen sorption behavior. Therefore, the volumetric hydrogen storage capacity in metal hydrides is much greater when compared the gravimetric densities. The drawback with such metal hydrides is in addition to the low gravimetric hydrogen storage capacities, they are prepared by the combination of two, three or multi elements from the periodic table, that are heavy, for examples, elements from lanthanide group (La, Ce, Mm, etc.) and from transition metals (Ni, Co, Fe, Ti, V etc.) [295]. For transportation and other automotive applications, the candidate materials supposed to have light weight with high gravimetric energy storage. Hence, in search of light weight metal hydrides, the Section 5 of this article demonstrated the magnesium hydrides and related systems which are not only possess the highest hydrogen storage capacity of 7.6 wt% but also, shows less weight penalty. However, these lightweight magnesium hydrides and systems offer the high reversibility at an expense of high temperatures, ~325 °C and pressures close to sever tenths of atmosphere of hydrogen [296].

The alloying, complex formation, catalytic doping, and nanoparticle formation of these magnesium greatly demonstrated the sorption behavior at affordable temperatures and pressures, but these modified versions of hydrides still involved the usage of heavy metals such as transition metals [297] and in some cases lanthanide group metals [298]. For example, magnesium-iron based complex hydrides and related systems (for example, Mg catalyzed with neodymium oxides) showed of at least 5–6 wt% reversible hydrogen storage capacities at temperatures close to 200 °C and exhibited longer life cycles and are deployed in hydrogen energy applications, in heat pumps, and automotive [298]. Though the so called, the birth of complex hydrides evolved with the emergence of Mg-based complex hydrides, that are known to the scientific community, the real breakthrough research in developing lightweight, high-capacity complex hydrides based on alkali, alkaline, metalloids and other non-metals combinations [299]. In 1990s, Bogdanovic and coworkers discovered lightweight sodium aluminum tera- and hexa- hydrides with few moles of catalytic transition metals/compounds doping [300,301,303] that triggers the hydrogen storage community for researching and exploring new sodium aluminum hydrides [301], lithium aluminum hydrides [302], and magnesium based complex hydrides [297] and related systems that are not only push the boundaries of both thermodynamics and kinetics but also addressed the requirement of lightweight materials for PEM fuel cells driven vehicles.

In a very recent comprehensive review published from the international group of hydrogen experts of the Task 40, of the Hydrogen Energy Technologies Program of the IEA, the advantages of the complex hydrides and tunable systems are detailed with respect to their materials' design, synthesis, characterization and scale-up for hydrogen enabled applications [303]. In general, the complex hydrides, are categorized according to their bonding characteristics. such as (i) alanes and alanates [304], (ii) borohydrides [305] and borates [306], (iii) amides and imides [307,308], (iv) ammines, and (v) reactive hydride complexes (RHCs) and (vi) other novel complex hydride systems. The reactive hydride complexes are in general composed of multinary complex hydride systems with the presence of core-shell catalytic nanoparticles, one such system is reported based on the synthesis process, and DFT calculations where the Ti (core) and Mg(shell) with hydrogen bonding are shown in Fig. 9 [309]. The pristine and modified RHCs are currently under investigation by the author of this review article. These RHCs are proposed to enhance the hydrogen storage characteristics based on the nanocatalytic effects of TiH_2/MgH_2 core-shell effects in the candidate complex multinary hydrides. The chemical reactions below demonstrate the pristine and modified RHCs and with enhancement of hydrogen uptake and release from 6 to 9 mol of hydrogen (Table 3). Table 4 represents different types of complex hydrides and their hydrogen storage capacities at specific operating temperatures.

9. Carbonaceous and related systems

This section discusses the uniqueness of carbon as an element and then specific applications in the field of hydrogen storage.

9.1. Carbon: the extraordinary canvas

Carbon is one of the special and unique elements in the Periodic Table. It has atomic number 6 with electronic configuration of $1s^2\ 2s^2\ 2p^2$ which gives it enormous options of formation of covalent bonds with itself or other elements of the Periodic Table. It forms bonds through hybridization that can involve sp^3, sp^2 and/or sp^1 combinations. Its chemically inert nature, good physical strength, mechanical flexibility, light weightiness, and different allotropes gives researchers a canvas that can be engineered in various ways. For instance, it can be transformed into many forms namely, zero-dimensional fullerenes, one-dimensional carbon nanotubes, two-dimensional graphene, three-dimensional graphite, hybrid structures thereof, activated carbon, etc., can be chemically modified by attaching functional groups, decorated by nanoparticles of metals/metal oxides or non-metal nanoparticles, and doped by elements like N, B, etc. [338–341] Thus, a vast number of possibilities exist for researchers to explore '*carbon*' as a material. Further, the high surface to volume ratio of the carbon nanomaterials gives them the edge of possessing very high specific surface areas. The porosity along with high

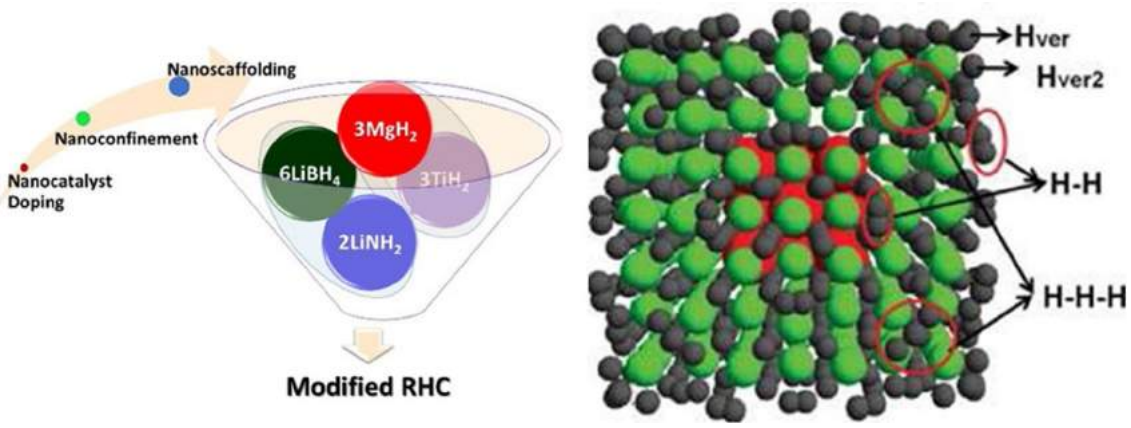

Fig. 9. (a) Synthesis process and (b) DFT calculations of the structure of modified RHCs. Reprinted with permission from Tao, S. X., Notten, P. H. L., van Santen, R. A., Jansen, A. P. J., First-principles predictions of potential hydrogen storage materials: Nanosized Ti(core)/Mg(shell) hydrides, Physical Review B 83 (2011) 195,403. 10.1103/PhysRevB.83.195403.by the American Physical Society. [309].

Table 3
Dehydrogenation and rehydrogenation reactions of RHCs.

Pristine *reactive hydride complex* - $2[n(LiBH_4) + 3n(LiNH_2)] + 3n(MgH_2)$ . . . . *(1)*

Modified *reactive hydride complex* - $2[n(LiBH_4) + 3n(LiNH_2)] + 3n[(MgH_2) + (nTiH_2)]$ *.(2)*

Dehydrogenation reaction:

$$6LiNH_2 + 2LiBH_4 \xrightarrow{3MgH_2} 2Li_4BN_3H_{10} + \rightarrow 2LiBH_4 + 3Li_2Mg(NH)_2 + 6H_2 \quad \ldots\ldots (3)$$

Rehydrogenation reaction:

$$3Li_2Mg(NH)_2 + 2LiBH_4 + 6H_2 \rightarrow 2Li_4BN_3H_{10} + 3MgH_2 \quad \ldots\ldots (4)$$

"n" signifies nano-form of host hydride.

Table 4
Types of complex hydrides, their hydrogen storage capacities, and operating temperatures.

Amides, imides and multinary complex hydrides		Capacity (wt.%)	Temperature [C]	References
$LiNH_2 + 2LiH = Li_2NH + LiH + H_2 = Li_3N + 2H_2$	$LiNH_2 + 2LiH$	10.5	300	T. Ichikawa et al. [310]
$CaNH+CaH_2=Ca_2NH+H_2$	$CaNH+CaH_2$	2.1	500	Roshan et al. [311]
$Mg(NH_2)_2 + 2LiH = Li_2Mg(NH)_2 + 2H_2$	$Mg(NH_2)_2 + 2LiH$	5.6	175	Chen et al.[312, 313]
$3Mg(NH_2)_2 + 8LiH = 4Li_2NH + Mg_3N_2 + 8H_2$	$3Mg(NH_2)_2 + 8LiH$	6.9	225	Aoki et al. [314]
$Mg(NH_2)_2 + 4LiH = Li_3N + LiMgN + 4H_2$	$Mg(NH_2)_2 + 4LiH$	9.1	225	Leng et al. [315]
$2LiNH_2 + LiBH_4 = "Li_3BN_2H_8" = Li_3BN_2 + 4H_2$	$2LiNH_2 + LiBH_4$	11.9	250	Pinkerton et al. [316]
$Mg(NH_2)_2 + 2MgH_2 = Mg_3N_2 + 4H_2$	$Mg(NH_2)_2 + 2MgH_2$	7.4	20	Hu et al. [317]
$2LiNH_2 + LiAlH_4 = LiNH_2 + 2LiH + AlN + 2H_2 = Li_3Al + N_2 + 4H_2$	$2LiNH_2 + LiAlH_4$	5	500	Xiong et al. [318]
$3Mg(NH_2)_2 + 3LiAlH_4 = Mg3N_2 + Li_3AlN_2 + 2AlN+12H_2$	$3Mg(NH_2)_2 + 3LiAlH_4$	8.5	350	Xiong et al. [319]
$Mg(NH_2)_2 + CaH_2 = MgCa(NH)_2 + 2H_2$	$Mg(NH_2)_2 + CaH_2$	4.1	500	Yongfeng et al. [320]
$NaNH_2 + LiAlH_4 = NaH + LiAl_{0.33}NH + 0.67Al + 2H_2$	$NaNH_2 + LiAlH_4$	5.2	200	Chua et al. [321]
$2LiNH_2 + CaH_2 = Li_2Ca(NH)_2 + 2H_2$	$2LiNH_2 + CaH_2$	4.5	215	Wu et al. [322]
$4LiNH_2 + 2Li_3AlH_6 = Li_3AlN_2 + Al + 2Li_2NH + 3LiH + 15/2H_2$	$4LiNH_2 + 2Li_3AlH_6$	7.5	300	Kojima et al. [323]
$2Li4BN_3H_{10} + 3MgH_2 = 2Li_3BN_2 + Mg_3N_2 + 2\ LiH + 12H_2$	$2Li_4BN_3H_{10} + 3MgH_2$	9.2	250	Niemann et al. [324]
Borohydrides				
$2LiBH_4 = 2LiH + 2B + 3H_2$	$2LiBH_4 + 2LiH$	13.6	375	Zuttel et al. [325]
$2LiBH_4 + MgH_2 = 2LiH + MgB_2 + 4H_2$	$2LiBH_4 + MgH_2$	11.5	355	Soulie et al. [326]
$3Mg(BH_4)_2{\_}NH_3 = Mg_3B_2N_4 + 2BN + 2B + 21H_2$	$3Mg(BH_4)_2$	15.9	250	Nakamori et al. [327, 328], Soloveichik et al. [329]
$Ca(BH_4)_2 = CaH_2 + 2B + 3H_2$	$Ca(BH_4)_2$	8.6	400	Kim et al. [330]
$Zn(BH_4)_2 = Zn + B_2H_6 + H_2$	$Zn(BH_4)_2$	2.1	115	Jeon el. al. [331], Srinivasan et al. [332, 333]
Ammonia borane and Amido boranes				
$nNH_3BH_3 = (NH_2BH_2)_n + nH_2 = (NHBH)_n + 2nH_2$	NH_3BH_3	12.9	135	Stephens et al. [334], Todd et al. [335]
$LiNH_2BH_3 = LiNBH + 2H_2$	$LiNH_2BH_3$	10.9	85	Xiong et al. [336]
$NaNH_2BH_3 = NaNBH + 2H_2$	$NaNH_2BH_3$	7.5	85	Xiong et al.[336]
$Ca(NH_2BH_3)_2 = Ca(NBH)_2 + 4H_2$	$Ca(NH_2BH_3)_2$	8	167.5	Kim et al. [337]

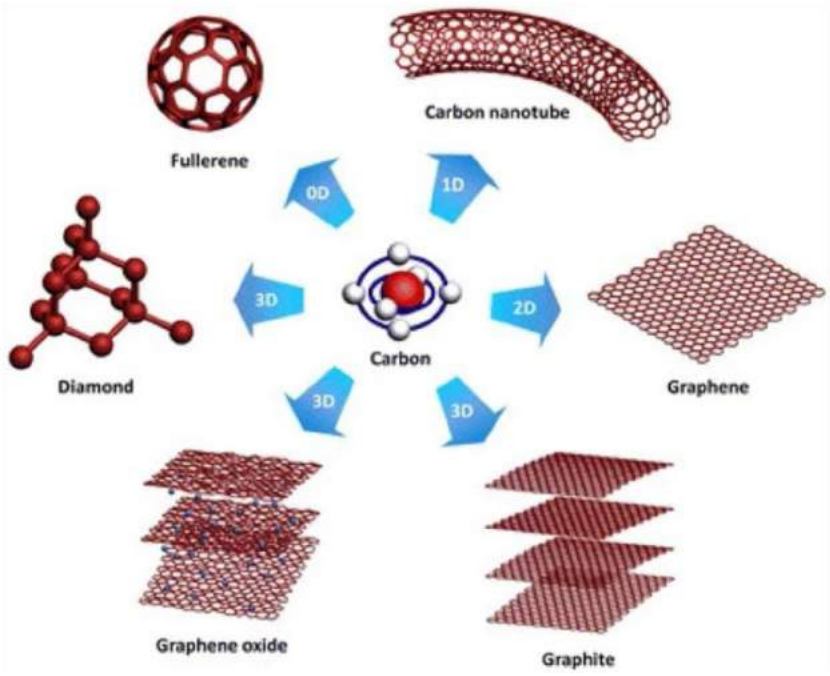

Fig. 10. Different allotropes of carbon that differ in dimensionality. Reprinted from D. Veeman, M.V. Shree, P. Sureshkumar, T. Jagadeesha, L. Natrayan, M. Ravichandran, P. Paramasivam, Sustainable Development of Carbon Nanocomposites: Synthesis and Classification for Environmental Remediation, Journal of Nanomaterials 2021 (2021) 5,840,645, Copyright © 2021, content available under Creative Commons Attribution License [342].

specific surface areas lead to the presence of many adsorption sites. With these desirable properties, carbon nanomaterials present themselves as prospective materials in the field of solid-state hydrogen storage. Fig. 10 depicts the common allotropes of carbon that differ in their dimensionality [342].

9.2. The carbon connection

For solid state hydrogen storage, one requires a good volumetric or gravimetric storage of hydrogen in near-ambient conditions, on-demand desorption at ambient temperatures, quick and reversible storage, and surety of a safe and economical means [300,343–346,347]. The storage can be in the form of molecular or atomic hydrogen. The molecular or atomic form of hydrogen storage depends upon the underlying mechanism of storage. And it is here where the carbon nanomaterials make a difference. Pure carbon nanomaterials are unsuitable for hydrogen storage. However, functionalization of carbon support or decoration of carbon support with nanoparticles can significantly improve the hydrogen storage properties. In case of carbon nanomaterials, the two mechanisms have been reported in literature namely, (a) Kubas interaction and (b) spillover mechanism. The spillover mechanism is a much-debated mechanism in literature where empirical evidence exists both in favor and against it [277,348–352]. The two mechanisms are discussed in sections 5.6 and 5.7 later. It has been discussed above that carbon can form bonds in multiple ways. Thus, when a hydrogen molecule approaches a pure or functionalized carbon network at close atomic distances, the hydrogen molecule's bonding configuration gets affected resulting in physisorption/chemisorption of molecular H_2 or atomic H_2, respectively. In all these approaches, the activation energy is reduced to facilitate either formation of atomic hydrogen from molecular hydrogen or formation of covalent bonds with the carbon support. Because this interaction is tunable by either using different carbon nanoforms, functionalization or nanoparticle dispersion over the carbon support, supports the interaction energies, carbon-based hydrogen storage is a promising field.

9.3. Hydrogen uptake capacity of various carbon materials

A recent review of hydrogen storage by different carbon forms by Mohan et al. reports the highest values reported [349]. At room temperature, the highest reported uptake capacities for activated carbon (5.5 wt.% H_2), graphite (4.48 wt.% H_2), carbon nanotubes (4.5 wt.% single tubes and 6.3 wt.% H_2 multiwalled tubes), and nanofibers (6.5 wt.% H_2) were reported. However, these are the best reported values and many research groups have reported lower hydrogen uptake capacities than these values. Hence, a pure carbon network (combination of sp^3, sp^2, sp^1) cannot serve as a hydrogen storage material. The carbon materials can be functionalized using various schemes as shown in Fig. 11 [350]. Functionalized or doped carbon materials are promising materials in this regard [346,347,351–358].

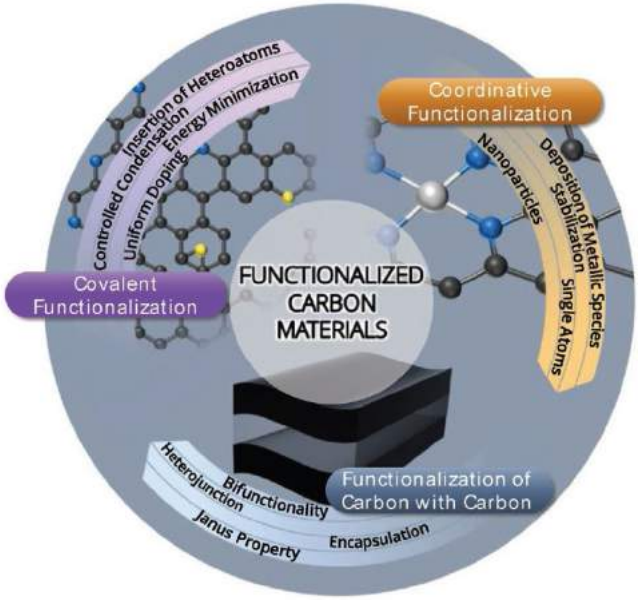

Fig. 11. Some of the ways to functionalize carbon nanomaterials. This figure is reproduced from M. Perovic, Q. Qin, M. Oschatz, From Molecular Precursors to Nanoparticles—Tailoring the Adsorption Properties of Porous Carbon Materials by Controlled Chemical Functionalization, 30 (2020) 1,908,371 available under the Creative Commons CC-BY-NC license [350].

Nitrogen-doped activated carbon has been evaluated for H_2 uptake capacity. The activated carbon after treatment in the presence of ammonia gas was successfully doped with nitrogen and then subsequently decorated by metal nanoparticles. The average size of the nanoparticles used for decorating the nitrogen doped carbon network ranged from 35 nm for Ru to 64 nm Ni nanoparticles. The hydrogen uptake profiles were different at cryogenic temperatures as compared to room temperature uptake profiles. While at cryogenic temperatures a sequential filling of pores (micro- followed by meso- and macro-pores) takes place, and an overlap of Type I and Type IV Langmuir adsorption isotherm is seen suggesting a gradual transition from mono-to-multilayer adsorption. During the filling of micropores alone, the hydrogen molecules present at the surface cause an excess Gibbs energy which is seen to increase the uptake capacity as pressure is increased. Whereas at room temperature, the adsorption in all levels of pores was seen to occur. For nitrogen doped activated carbon, 57% increase was recorded for nitrogen doped activated carbon at 100 MPa pressure and 298 K. For other systems, the maximum uptake capacity was observed to increase by 42% for Pt-decorated nitrogen-doped activated carbon. For Ni and Ru, the improvement in uptake capacity was relatively low at 10% and 8%, respectively [347]. Doping of nitrogen within the carbon network to form g-C_3N_4 and then using Pd nanoparticles over g-C_3N_4 support resulted in a hydrogen uptake capacity of 1.8 wt.% and 2.5 wt.%, respectively at room temperature and 3 MPa hydrogen pressure. The uptake capacity could be improved to 2.6 wt.% and 3.8 wt.%, respectively at lower temperatures of 0 °C [356]. In another study, Ni nanoparticles dispersed over graphite network demonstrated 4.48 wt.% hydrogen uptake at 298 K and hydrogen pressure up to 10 MPa [357]. A dipole induced hydrogen uptake mechanism was proposed for achieving this relatively higher gravimetric storage. However, high pressure conditions like 10 MPa make the material commercially less attractive.

9.4. Ordered mesoporous carbons

Ordered mesoporous carbons have also been studied for hydrogen storage properties after treating them in ammonia atmosphere. Hard template method was used by Giraudet et al. to synthesize nitrogen-doped mesoporous carbon. One of the important conclusions of the study was that nitrogen doping was more influential for electrochemical H_2 storage indicating that nitrogen doping participated in redox reactions directly and that the effect on van der Waal's types of forces was not significant. However, the porosity of the mesoporous carbons played a role at lower temperatures [358]. Other means to store hydrogen have also been reported. For instance, metal hydrides are known to suffer from great thermodynamic stabilities thereby resulting in slow desorption kinetics and high temperatures of adsorption. However, improved thermodynamic properties, better desorption kinetics and the better reversibility by $LiBH_4$_MgH_2 nanocomposites was demonstrated by making use of a porous carbon aerogel scaffold by Nielsen and coworkers [359]. The carbon aerogel scaffold with pores of maximum size of ~ 21 nm served as a nano-sized confined system where the reversible reaction could take place. Composites of Ni, Co and Ni-Co were dispersed over nitrogen doped graphene and tested for hydrogen storage. The authors reported a 1 wt% release of hydrogen at 226 °C and with Ni nanoparticles, 6.5 wt% H_2 release was recorded at 325 °C. Thus, the above studies show that hydrides alone may not be useful for hydrogen storage while their composites with carbon support materials can be useful.

Other systems containing carbon have also been proposed in the recent past. Here, the subset of Liquid Organic Hydrogen Carriers (LOHCs) is promising as it is very easy to transport liquid fuel through the infrastructure supporting the storage and distribution of petroleum-based fuels. LOHCs store hydrogen in liquid state. These are organic in nature and can attach to hydrogen atoms in liquid state and de-hydrogenate. Such systems that include cyclohexane, decalin, etc. are seen as easy substitutes for the present diesel/ petrol liquid fuels. Hydrogenation processes are well understood and can be carried out at large scale. However, efficient, fast, and safe dehydrogenation needs to be achieved. In this regard, some catalysts (Pt, Pd, Rh, etc.) have been used for improving the kinetics of dehydrogenation. However, the goal is to use non-noble metal catalysts (Fig. 12).

Some theoretical studies too are pertinent for discussion. First principles study on fullerenes have shown a theoretical capacity of 7.5 wt.%, which can be increased to 10.5 wt.% for Ti-doped fullerene in the temperature range from 100 to 300 K. The study showed that 56 H_2 molecules could be stored on the fullerene balls. The desorption of H_2 molecules was shown to occur in the temperature range of 245–256 K [361]. Multiwalled carbon nanotubes of varying diameters were also investigated for hydrogen storage properties. A meager uptake of 0.01–0.6 wt.% of hydrogen could be successfully stored reaching 0.6–0.87 wt.% [362]. Doping the carbon nanotubes improved the uptake capacity marginally for Pd-MWNTs and the maximum reported value was 0.87 wt.% [363,364].

The next-generation graphene materials have been explored theoretically [365,366]. Graphdiyne (GDY) is a two-dimensional carbon allotrope which has two stable di-acetylenic groups [367]. Theoretically, the GDY can store hydrogen storage via the van der Waals forces and the interaction strength of about 60–70 meV per molecule. To enhance the interaction strength, GDY was doped with boron and later decorated with Ni to improve the hydrogen bonding. The theoretical study shows that a significant enhancement of about 1.2 eV/H2 molecule is predicted by exploring Ni-GDY in comparison to undoped or B-GDY. However, Ni-GDY is unsuitable for room temperature adsorption/desorption of H2 due to high binding energy. Boron doping proved beneficial as it facilitates charge transfer from Ni to GDY resulting in better synergy between the Ni atoms and the supporting GDY network. An improvement in the binding energy values was predicted when B-GDY was used, and Ni atoms added suitably. The desorption temperature was also predicted to be in the 300 K to 500 K range (Fig. 13). Thus, co-doping of GDY network with B and Ni gives better options for hydrogen storage. Few other theoretical reports also discuss the utility of next-gen graphene derivates in hydrogen storage. A lithium-doped graphene system was studied theoretically by Hussain et al. which was doped by replacing two hydrogen atoms by Li atoms [368]. The positive charges on Li atoms influenced the polarization of approaching hydrogen molecules and resulted in van der Waals bond formation between incoming hydrogen and the substrate. A value of 9.37 wt.% and 12.12 wt.% were reported for zero and non-zero lattice strain, respectively. The binding energy was calculated as falling in the range 0.15 to 0.20 eV [369,370].

9.5. The mechanisms of hydrogen storage with carbonaceous materials

A carbon network (combination of sp^3, sp^2, sp^1) purely cannot serve as a hydrogen storage material. Upon hydrogenation, a carbon network will get passivated soon and then not offer adequate and favorable adsorption sites. Thus, there are no means to increase adsorption on these materials. The interaction strength of adsorbed H_2 molecule is feeble and may lead to undesirable desorption at ambient conditions. For room temperature storage, a range of 20–40 kJ/mol binding enthalpies has been suggested. Cases where physisorption is the primary interaction between H_2 molecules and the adsorbate, the binding enthalpies fall below the suggested range. Examples include pure carbon-based nanomaterials, zeolites, or some metal organic frameworks. Cases where chemisorption is the primary interaction between hydrogen atoms and adsorbate, the binding enthalpies are quite high resulting in stronger covalent bonds. Therefore, even if the adsorption events are favorable, their rates, high heat of adsorption and desorption processes pose a problem for room temperature storage. Therefore, routes that favor binding energies from 20 to 40 kJ/mol need to be explored. Studies indicate that either functionalized carbon supports, or nanoparticle dispersed carbon supports are promising candidates. Depending upon the type of func-

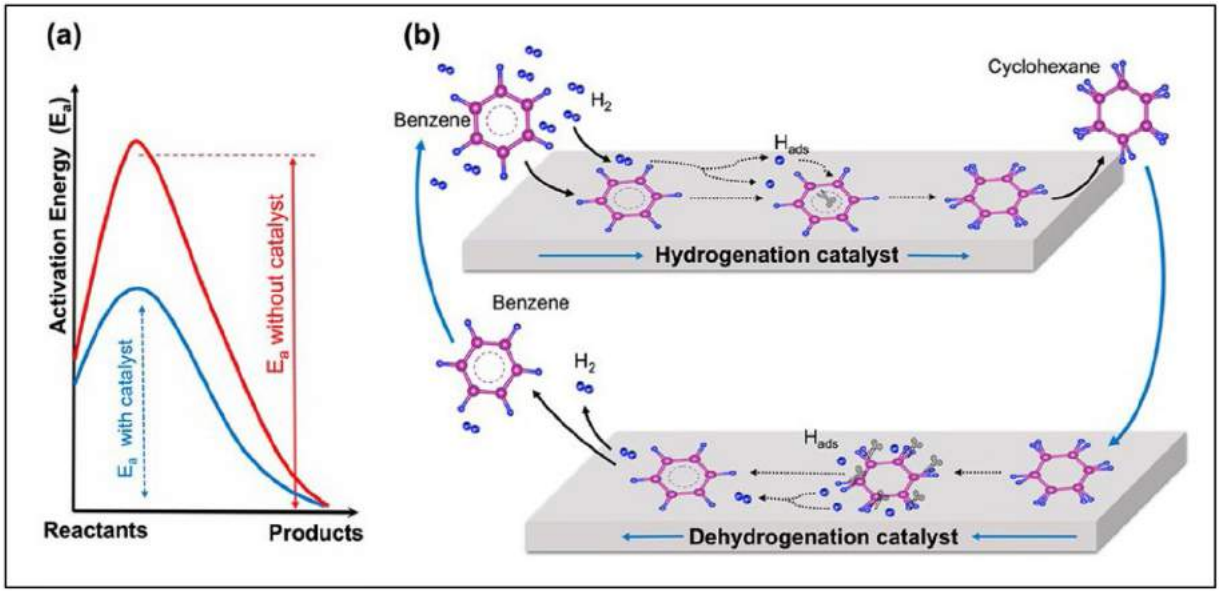

Fig. 12. General principles for adjusting the kinetics of hydrogenation and dehydrogenation reactions with catalysis. (b) Illustration showing the catalytic hydrogenation/dehydrogenation mechanism for the capital CBH cycle. Reprinted with permission from M.S. Salman, N. Rambhujun, C. Pratthana, K. Srivastava, K.-F. Aguey-Zinsou, Catalysis in Liquid Organic Hydrogen Storage: Recent Advances, Challenges, and Perspectives, Industrial & Engineering Chemistry Research 61 (2022) 6067–6105 [360]. Copyright 2022 American Chemical Society [360].

tionalization and nanoparticles, primarily two mechanisms are reported which are discussed now.

9.6. Kubas interaction

Kubas interaction deals with the interaction of hydrogen molecules in the presence of transition-metal (TM) nanoparticles. Studies show that the H–H bond loosens from the 0.74 Å bond length of free hydrogen molecule to more than 0.84 Å for Kubas-type interaction. This loosening of H–H bond occurs due to the interaction of hydrogen bonding electrons that are donated to empty 3d orbitals of TM nanoparticles and then back donated to the anti-bonding of hydrogen. In the whole process, the H–H molecules get oriented towards the metal bonds as shown in Fig. 14. This coordinated molecule can bind hydrogen to the metal and hence improve the hydrogen storage.

9.7. Spillover mechanism

Spillover mechanism addresses the bonding of hydrogen over the carbon support. In this type of mechanism, the support influences the H–H bond strength, which loosens and two dissociated hydrogen atoms form. The energy required for this dissociation is lowered by using nanoparticles as catalysts over the carbon support. Dissociation of H_2 molecules into H atoms is now discussed. In the presence of nanoparticles, the polarizability of the H_2 molecule is affected and hydrogen atoms get chemisorbed on the nanoparticles, which are usually metallic in nature. As the H-atoms chemisorb on metal nanoparticles, their H–H bond loses strength and ultimately breaks. If surface diffusion is favorable on the support material (graphene, functionalized graphene, nanoparticle-decorated graphene, etc. two-dimensional material), then the H-atoms first saturate the nanoparticles, and then diffuse on the underlying support. As H-atoms migrate from the catalyst nanoparticles and *spill* onto the support, the catalyst can dissociate subsequent incoming H_2 molecules and further dissociate them. Thus, a good synergy between the catalyst nanoparticles and carbon support can result in higher storage of hydrogen. Fig. 15 depicts the role of functionalized graphene that favors spilling of the hydrogen atom over the graphene support [348]. Further, if the carbon support is functionalized, then it can bond with the metal nanoparticles and the spilled-over hydrogen atoms resulting in higher uptake capacities [356,359,373]. In both the above mechanisms, nanoparticles act as catalysts. Smaller the size of the nanoparticles, better are their catalytic properties. However, smaller nanoparticles have high cohesive energies. Thus, they tend to agglomerate resulting in reduction of the loss of improved catalytic activity due to smaller-sized nanoparticles. Functionalized carbon support has shown tremendous improvement in this regard [348].

9.8. The future of carbon nanomaterials in hydrogen storage

The benefits of carbon nanomaterials have been discussed in detail in the earlier sections. Functionalized carbon nanomaterials also provide the right binding energy via the physico-chemical bonding options. As it is very easy to handle carbon nanomaterials and functionalize them, their popularity as potential storage materials will always exist. Hence, their use as hydrogen storage materials is promising. With predictions of newer two-dimensional graphene derivatives, it is likely that the new generation of carbon nanomaterials picks up research efforts in the field of hydrogen storage and meets the DOE targets.

10. Metal organic frameworks (MOFs) and related systems

Hydrogen storage is an emerging field of study for future transportation. After low-cost MOF-5 discovery, it was selected to be evaluated in hydrogen storage. MOFs are organometallic materials or coordination polymers that contain a metallic center and organic ligands interconnected with each other. They have been studied mainly in catalysis, adsorption, and gas separation. Recent reviews are available in the literature [371–374]. Some important conclusions emerge: i) Gaining a deeper understanding of the interaction between gas and MOFs materials will be possible through the computational and machine learning techniques, it will promote the design and development of ideal MOFs [374]. ii) Total hydrogen storage lies on 6–15 wt% at 77 K and high pressure, which is good since the US DOE target is 5.5 wt%; but storing at room temperature, typically in 0.5–1wt%, is still a challenge. Important factors are shown in Fig. 16 [371]. iii) There are still challenges to obtain MOFs modified with nanoparticles [372], and iv) MOF modifi-

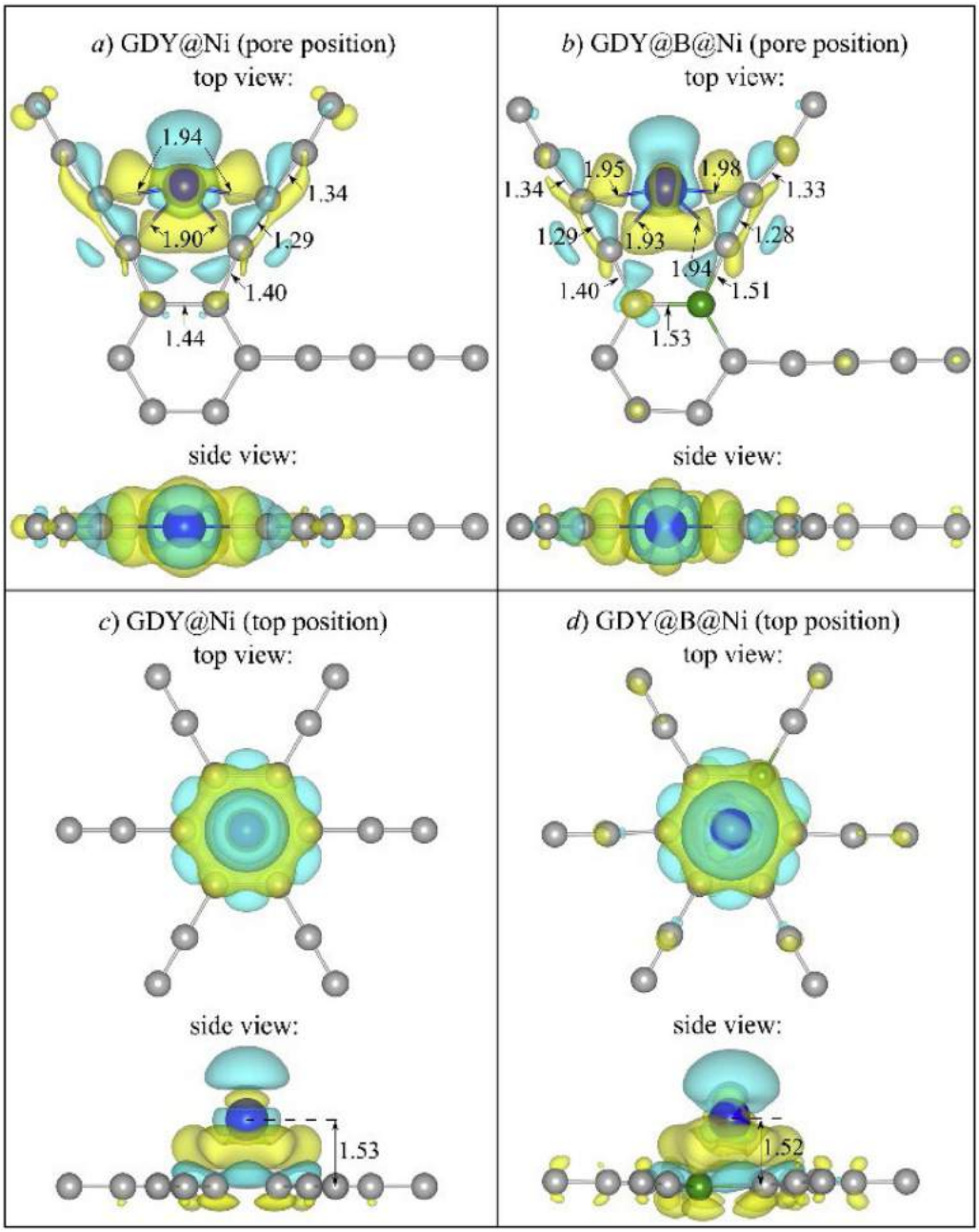

Fig. 13. "Relaxed structures of pristine and B-doped GDY with Ni a) and b) inside the big pore; c) and d) on top of the small pore. Ni, C, and B atoms are blue, gray, and green, respectively. All bond lengths and distances are in Å. Cyan and yellow isosurfaces (0.0025 e) show charge depletion and accumulation, respectively." Reprinted from Materials Today Energy, 16, E.V. Anikina, A. Banerjee, V. P. Beskachko, R. Ahuja, Influence of Kubas-type interaction of B–Ni codoped Graphdiyne with hydrogen molecules on desorption temperature and storage efficiency, 100,421, Copyright (2020), with permission from Elsevier [367].

cations such as doping with metal ions, nanoparticles or formation of composites could favor hydrogen storage [375].

MOFs were discovered in 1999 [375]; they have been researched as hydrogen storage material with a capacity of 5.2 wt% at 77 K and 50 atm. [376]. Table 5 summarize the hydrogen storage capacity of recent literature with a better potential than the former reference. Among materials, MgH_2 occupies high hydrogen capacity of 7.6% w/w together with good reversibility and low cost, but high operating temperature (>300 °C) and slow dehydrogenation kinetics seriously hinder its practical application [281], however modification with Nobium oxide decreased the temperature (Table 5, entry 2). A MOF-derived bimetallic Co@NiO catalyst was synthesized and doped with MgH_2 to enhance the capacity hydrogen desorption, and resorption kinetics. Doped Co@NiO catalyst decreased dehydrogenation temperature since the beginning by 160 °C, compared with un-doped MgH_2 (Table 5, entry 2).

In the other hand, through computational evaluation of near 7444 MOF database H_2 storage capacities were among 8.044 and 12.191 wt% at 77 K and 100 atm., this is the highest value of that was reported by the authors (Table 4, entry 5). Jia et al. have recently reviewed the use of MOF for hydrogen storage showing important facts prior to commercial scale of MOF [374]; the most representative for hydrogen storage are illustrated in Table 5, entries 6 to 8. Also, by computational calculations Heterofullerene $C_{48}B_{12}$-impregnated MOF-5 and IRMOF-10 have been evaluated in hydrogen storage showing adsorption up to 7.1 wt% (Table 5, entry 3). Several MOFs modified with copper were evaluated by computational calculations with the best results in Table 5,

Table 5
Storage capacity of MOFs.

Entry	MOF	Storage capacity (wt%)	Ref.
1	MgH_2 + 9% (mass) Co@NiO composite	5.4 at 165 °C and 30 atm.	Zhang et al. [281]
2	7 wt% Nb_2O_5@MOF doped MgH_2	6.5 at 175 °C and 32 atm.	Zhang et al. [378]
3	Heterofullerene $C_{48}B_{12}$-impregnated IRMOF-10	7.1 at 77 K and 12 atm. (verified with computational calculation)	Yu et al. [379]
4	Cu-MOF-399	8.3 at 77 K and 50 atm. 0.46 t 298 K and 140 atm. (Computational calculations)	Srivastava et al. [380]
5	BOQQAD	12.191 at 77 K and 100 atm. (Computational calculation)	Lu et al. [381]
6	MOF-210	17.6 at 77 K and 80 atm.	Furukawa et al. [382]
7	NPF-200	13.1 at 77 K and 100 atm.	Zhang et al. [383]
8	NU-100	16.4 at 77 K and 70 atm.	Sen Wang et al. [384]
9	BP-COF-5	8.57 at 77 K and 100 atm. (Computational calculation)	Bian et al. [377]
10	she-MOF-1	12.6 at 77 K and 100 atm.	Gomez-Gualdron et al. [385]
11	DUT-32	14.21 at 77 K and 80 atm.	Grunker et al. [386]
12	NU 1501-Al	14.5 at 77 K and 100 atm.	Chen et al. [387]
13	MOF-519	16 at 77 K and 100 atm. (Computational calculation)	Rahali et al. [388]
14	Li- MOF-C30	6.6 at 300 K and 100 atm. (Computational calculation)	Volkova et al. [389]
15	Zn BTC Rb^+	0.15 at 77 K and 1 atm	Almasi et al. [390]
16	$C_4H_{18}B_2Na_2O_{14}$	0.108 at 77 K and 1 atm.	Ozer et al. [391]

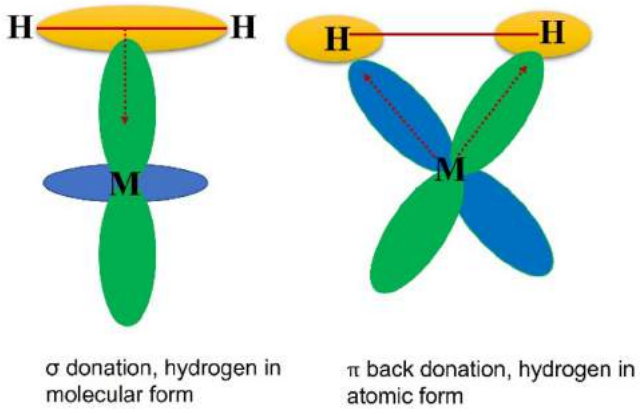

Fig. 14. Kubas interaction depicting sigma donation and pi-back-donation.

entry 4. Bian et al. reported also by computational calculations boron-phosphorus cube based covalent organic frameworks (BP-COFs), being the best storage 8.57 wt% (Table 5, entry 9) [377]. Shet et al. have reviewed MOF for hydrogen storage [373], the most representative materials are in Table 5, entries 10 and 11. NU-1501-Al exhibits a high BET surface area equal to 7310 $m^2\ g^{-1}$ that contributes to hydrogen storage capacity (Table 5, entry 12). Through computational calculations MOF-19 conformed by octahedral Al and modified with ligands (octametallic inorganic secondary building units exhibited a high hydrogen storage capacity (Table 5, entry 13). It is shown in Table 5, entries 15 and 16, typical values of storage a low pressure, furthermore, increasing temperature strongly reduce the adsorption capacity (Table 5, entry 14).

The literature review indicates that computational could accelerate the finding of the best MOFs for hydrogen storage, but it is still an open field in the production of selected structures based on MOFs. It is preferred materials with high surface areas, but factors such as composition, adding ligands, or confinement effects are important to promote hydro-

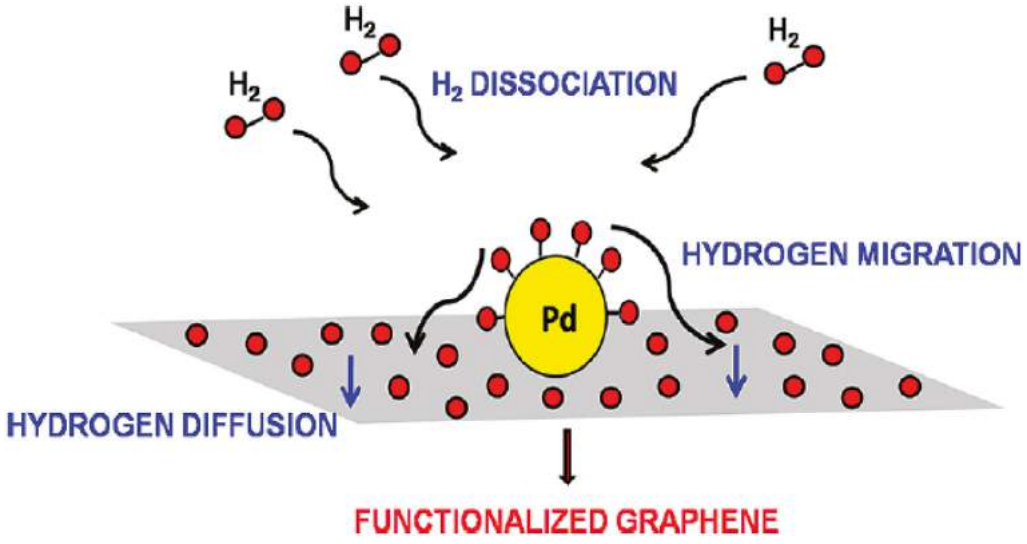

Fig. 15. Schematic of hydrogen spillover on functionalized graphene [348].

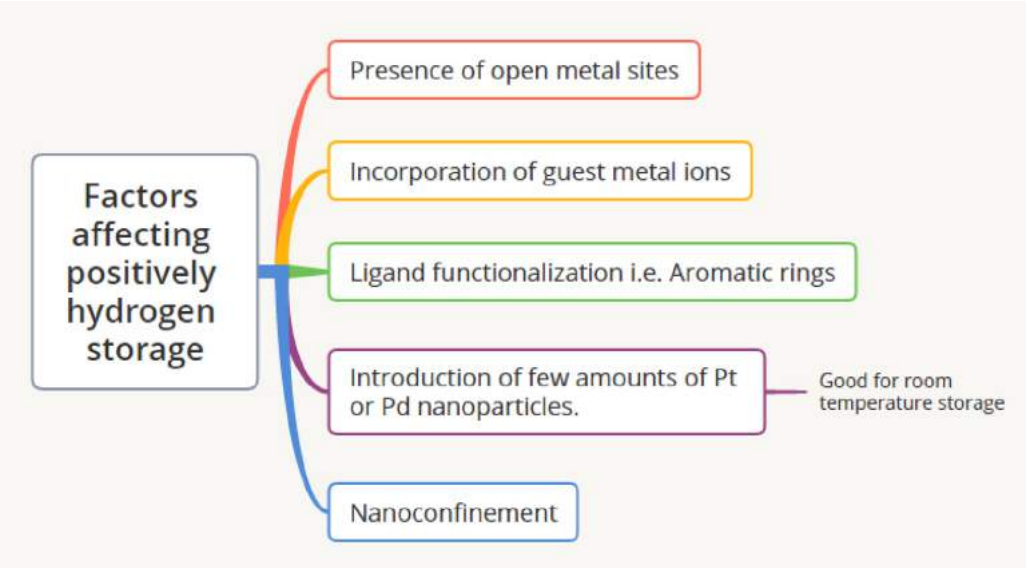

Fig. 16. Factors affecting hydrogen storage.

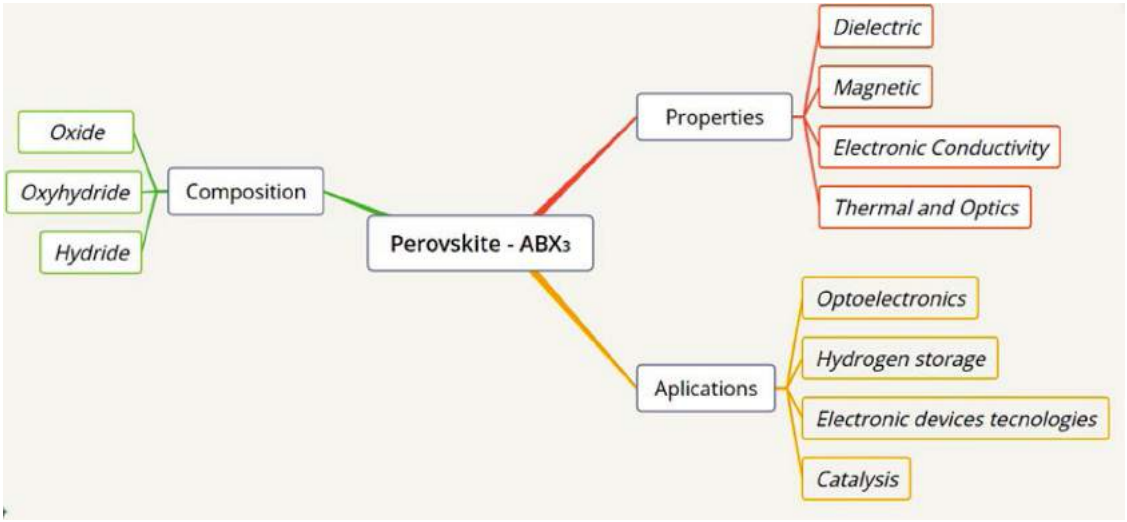

Fig. 17. Important issues about perovskites.

gen storage capacity. The most reported methods of synthesis are based on precipitation (either hydrothermal treatment or not).

11. Perovskites and related systems

Another type of materials researched for hydrogen applications are perovskites [392–395]. The first perovskite was discovered in 1839 by the Prussian mineralogist Gustav Rose in mineral deposits in the Ural Mountains with formula $CaTiO_3$ [396]. Subsequently, synthetic perovskites were obtained by different preparation routes. The crystal structure of this compound, initially thought to be cubic, was later shown to be orthorhombic. The general formula is derived from the composition ABX_3. To some extent the multiplicity of phases that belong to the perovskite family can be rationalized by assuming that perovskites are simple ionic compounds, where A and B are metal cations, and X is non-metal anion [396]. Depending on the composition, perovskite can have quite different structures, such as oxides, oxyhydrides and hydrides; with several applications as shown in Fig. 17, where oxyhydrides and hydrides have also been investigated to measure hydrogen storage capacity. Gencer et al. approached their study on $XNiH_3$ perovskite type hydrides (being X atoms of Li, Na or K) perovskite type hydrides and reported that $LiNiH_3$ had better results related to hydrogen storage capacity and desorption temperature (4.40 wt%, 446.3 K) while $KNiH_3$ had the lowest ones (3.30 wt%, 367.5 K). Among the conclusions mentioned by the authors is the influence of X atom type from Li to K, due to the hydrogen storage capacity decreases with the increasing of the mass of the element in the perovskite; and they also found in this study, that these compounds are energetically, mechanically and dynamically stable and synthesizable [392]. Another study, $NaXH_3$ perovskite (being X atoms of Mn, Fe, Co) have also been investigated and the results of the structural optimizations showed that all these compounds have negative formation energy implying the thermodynamic stability and synthesizability. Regarding the investigation on hydrogen storage characteristics of $NaXH_3$ compounds resulted in hydrogen storage capacities of 3.74, 3.70 and 3.57 wt% for X equal to Mn, Fe and Co, respectively. The authors indicated that their study is the first investigation of $NaXH_3$ perovskite type hydrides as known up to date and may provide remarkable contributions to the future research in hydrogen storage applications [394]. Garara et al. [395] focused their research on hydrogen storage properties using the $MgCoH_3$ perovskite were found a structure mechanically stable, for-

mation energy equal to −71.30 kJ.mol^{-1}.H_2, comparable value with the theoretical value −73.32 kJ.mol^{-1}.H_2, desorption temperature equal to 545.52 K, and storage capacity equal to 3.505 wt%. Hayat et al. published in their work perovskites type hydrides with composition $XCuH_3$, (being X atoms of Co, Ni, or Zn); and their effect in the properties of each material.

The results showed that $NiCuH_3$ is more appropriate for hydrogen storage. The gravimetric ratio of hydrogen storage capacities was determined as 2.8 wt.%, 3.0 wt.%, and 2.7 wt.% for $CoCuH_3$, $NiCuH_3$ and $ZnCuH_3$, respectively. Anti-ferromagnetism was reported for $NiCuH_3$ and $ZnCuH_3$ while magnetism has been observed for $CoCuH_3$. According to the authors, the current study is the first computational attempt of $XCuH_3$, which may contribute outstanding amelioration for future investigations in hydrogen storage applications [397]. Besides, they indicate that regarding hydrogen storage capacity is consistent with the values reported in the literature for different materials and concluded that hydride perovskites $XCuH_3$ are suitable materials for hydrogen storage devices due to occurrence of sufficient value of hydrogen storage capacity, and large values of negative formation energy produce energetically stable and synthesizable materials [397].

Regarding perovskite type oxyhydride, Gencer et al. [393] reported the gravimetric hydrogen storage capacity of $CaTiO_3H_6$ equal to 4.27 wt.% and the hydrogen desorption temperature is equal to 827.1 K. They compared with other materials as $MgTiO_3H_x$ and $CaTiO_3H_x$ perovskite compounds and their hydrogen storage application that provides some insights for the future theoretical and experimental studies. And they conclude that this type of research is crucial to promote usage of hydrogen technology especially for on-board applications. In this sense, $MgTiO_3$ and $CaTiO_3$ perovskite compounds are investigated for hydrogen storage in terms of structural, mechanical, electronic and hydrogen storage properties systematically by using first-principle calculations. Another material, $BaYO_3H_3$ was reported with a gravimetric hydrogen storage capacity equal to 1.09 wt%. And they found that the composition based in $BaYO_3H_9$, the structure is unstable, and it is not suitable for hydrogen storage purposes [398]. The authors conclude in this study that the perovskites for solid state hydrogen storage method could be useful in the future theoretical.

12. Hydrogen storage for mobility and energy applications

The rising demand for energy production with lesser resource depletion and environmental damage leads to the development of high-performance, inexpensive, and environmentally friendly energy production and storage technologies. The main factor in lowering greenhouse gas emissions is the dependence on fossil fuels. In this regard, we are compelled to investigate new environmentally friendly energy sources for the expanding population and rising demand for electricity. In a future energy economy built on sources and carriers that are ecologically friendly, hydrogen is anticipated to play a significant role. Its advantages as a preferred fuel are lightweight, high-energy density, and the absence of dangerous chemicals by-products from combustion. In addition, hydrogen is regarded as green energy because it can be produced using renewable resources and is non-polluting. However, the lack of a secure and convenient means of storage continues to be a significant obstacle to the widespread use of hydrogen as the preferred fuel in mobile transportation [399]. To improve the performance of energy storage devices like supercapacitors, Li-ion batteries, fuel cells and hydrogen storage systems, researchers focus on using hydrogen as an energy carrier for the anticipated hydrogen economy.

Fuel cell electric vehicles (FCEVs) would become more widely available and more quickly commercialized with a low-cost, lightweight, and small hydrogen storage system, which could help cut net carbon emissions if hydrogen fuel is developed using low-carbon techniques. An in-depth understanding of the hydrogen storage technologies pertinent to transportation applications is needed. The desirable characteristics of an ideal storage medium are high volumetric and gravimetric energy densities, quick fuel uptake and release, operation at standard room temperature, and atmospheric pressure [400]. These characteristics should be optimized to produce a safe and balanced, cost-effective product. There are numerous problems with the present hydrogen storage solutions, including complicated heat management systems, boil-off, low efficiency, costly catalysts, stability problems, sluggish response times, high working pressures, low energy densities, and dangers of violent and uncontrolled spontaneous reactions. Even though it is far from ideal, the leading industry standard for compressed hydrogen now on the market offers a workable solution and shows that, in contrast to other technologies, it can provide a storage alternative for mobility.

In this regard, we must assess the hydrogen storage possibilities for transportation-related applications. Refueling for transportation needs to be quick, safety must come first, and the storage system's size and weight should be as small as feasible. It is essential to take the system into account to develop a viable solution that the industry can accept. Given present battery technology, it is critical to discuss whether hydrogen storage is required for mobility applications.

Evaluation of hydrogen storage system-related parts, including the tank, valves, piping, insulation, and reactants, while material-based value solely considers reactants or materials that contain hydrogen is needed [401]. In addition to gravimetric and volumetric requirements, the US Department of Energy has also addressed the difficulties in achieving other important system performance objectives, including cost, charge and discharge kinetics, and durability. Each method has benefits and drawbacks, and no technology is now available that can satisfy every need. Although there is still room for many advancements and fresh discoveries, hydrogen production, storage, and conversion have reached a technological level. The hydrogen storage is frequently viewed as the bottleneck of the hydrogen-based renewable energy industry. Numerous hydrogen storage techniques and materials have already been discussed; further research is required.

13. Conclusions

Research efforts are underway globally to address the energy and environment challenges that the world faces. With growing awareness and government initiatives all over the world, attempts and intentions are being converted into actions. While alternatives like nuclear, solar, wind, geothermal, electrochemical, etc. energies are also being looked into, no one energy technology would be sufficient to meet the demands. In this regard, hydrogen energy presents a very good and competitive alternative for vehicular energy demands. Hydrogen production, storage and distribution are the three main concerns, of which safe and reversible storage of hydrogen is seen as the biggest bottleneck. This article presents an overview of potential materials, the solid-state storage journey of hydrogen in different materials, existing challenges, their processing, and design strategies. While alloying, nanostructuring, scaffolding, hierarchical designs, 2-D materials, newer derivatives of existing materials have shown a positive and upward trend in the storage capacity of solid materials, the world still awaits its alternate commercial prototype that meets the DOE targets. Combination of chemi-physisorption mechanism may be the answer to the longstanding storage challenge that provides the pathway for tackling both the thermodynamic and kinetic constraints.

Declaration of Competing Interest

There is no conflict of interest found.

Acknowledgements

The authors acknowledge their respective institutions for the support to accomplish this review study. SSS and SLA would like to acknowledge the support of Fulbright Foundation (Project # FSP: P005908) of USA and Colombia for the exchange visit and collaborative discussions.

VK and SS[7] acknowledges the support from the National Convergence Research of Scientific Challenges through the NRF (National Research Foundation of Korea) funded by the Ministry of Science and ICT (No. 2021M3F7A1017476). In memory of Padma Shri Professor O.N.S Srivastava ("The Hydrogen Man of India"). Authors, SSS, VK, SS[2], SLH and RA gratefully dedicate this review paper for his extraordinary guidance and introduction to the field of Hydrogen Energy Technology, specifically Hydrogen Storage research during their Ph.D. and Post-Doctoral careers.

References

[1] Morrison, P., The discovery of global warming, 57 (2004) 60–61. 10.1063/1.1784277.
[2] Lelieveld, J., Klingmüller, K., Pozzer, A., Burnett, R.T., Haines, A.,Ramanathan, V., Effects of fossil fuel and total anthropogenic emission removal on public health and climate, 116 (2019) 7192–7197. doi:10.1073/pnas.1819989116.
[3] R. York, Do alternative energy sources displace fossil fuels? Nat. Clim. Chang. 2 (2012) 441–443, doi:10.1038/nclimate1451.
[4] A. Sulaiman, F. Inambao, G. Bright, Solar energy as an alternative energy source to power mobile robots, in: J.-H. Kim, E.T. Matson, H. Myung, P. Xu, F. Karray (Eds.), Robot Intelligence Technology and Applications 2: Results from the 2nd International Conference on Robot Intelligence Technology and Applications, Springer International Publishing, Cham, 2014, pp. 957–969.
[5] Felseghi, R.-A., Carcadea, E., Raboaca, M.S., Trufin, C.N.,Filote, C., Hydrogen Fuel Cell Technology for the Sustainable Future of Stationary Applications, 12 (2019) 4593.
[6] M. Balat, Potential importance of hydrogen as a future solution to environmental and transportation problems, Int. J. Hydrogen Energy 33 (2008) 4013–4029, doi:10.1016/j.ijhydene.2008.05.047.
[7] F. Gutiérrez-Martín, J.M. García-De María, A. Baïri, N. Laraqi, Management strategies for surplus electricity loads using electrolytic hydrogen, Int. J. Hydrogen Energy 34 (2009) 8468–8475, doi:10.1016/j.ijhydene.2009.08.018.
[8] A. Pareek, R. Dom, J. Gupta, J. Chandran, V. Adepu, P.H. Borse, Insights into renewable hydrogen energy: recent advances and prospects, Mater. Sci. Energy Technol. 3 (2020) 319–327, doi:10.1016/j.mset.2019.12.002.
[9] Mazloomi, K., Sulaiman, N.B.,Moayedi, H., Electrical efficiency of electrolytic hydrogen production, 2012.
[10] R.H. Jones, G.J. Thomas, Materials For the Hydrogen Economy, Taylor & Francis Group, Boca Raton, Florida, USA, 2007.
[11] M. Dresselhaus, G. Crabtree, M. Buchanan, T. Mallouk, L. Mets, K. Taylor, P. Jena, F. DiSalvo, T. Zawodzinski, H. Kung, I.S. Anderson, P. Britt, L. Curtiss, J. Keller, R. Kumar, W. Kwok, J. Taylor, J. Allgood, B. Campbell, K. Talamini, Basic Research Needs for the Hydrogen Economy, in: Report of the Basic Energy Sciences Workshop on Hydrogen Production, Storage and Use, 2003, p. 2004. May 13-15.
[12] L. Schlapbach, Hydrogen as a Fuel and Its storage for mobility and transport, MRS Bull. 27 (2002) 675–679, doi:10.1557/mrs2002.220.
[13] Broom, D.P.,Complementary characterisation techniques. In D. P. Broom (Ed.), Hydrogen Storage Materials: The Characterisation of Their Storage Properties (pp. 141–181). London: Springer London, 2011.
[14] Granholm, J.M. AMR 2022: opening Remarks from the U.S. Department of Energy. DOE Hydrogen Program 2022 Annual Merit Review and Peer Evaluation Meeting, ENERGY.GOV Hydrogen Program, 2022 Retrieved 18.01.2023, 2023, from https://www.energy.gov/eere/fuelcells/amr-2022-opening-remarks-us-department-energy-text-version.
[15] Satyapal, S. AMR 2022: DOE Hydrogen Program Update. DOE Hydrogen Program 2022 Annual Merit Review and Peer Evaluation Meeting, ENERGY.GOV Hydrogen Program, 2022 Retrieved 18.01.2023, 2023
[16] Commission, E. A hydrogen strategy for a climate-neutral Europe. Communication From The Commission To The European Parliament, The Council, The European Economic And Social Committee And The Committee Of The Regions, 2020 Retrieved 18.01.2023, 2023, from https://eur-lex.europa.eu/legal-content/EN/TXT/HTML/?uri=CELEX:52020DC0301™from=EN.
[17] Commission, E. EU-Africa: global Gateway Investment Package - Africa-EU Green Energy Initiative. 2022 Retrieved 18.01.2023, 2023, from https://ec.europa.eu/commission/presscorner/detail/en/fs_22_1120.
[18] Bhargava, P.L., Sam, Methodology for Determining the Greenhouse Gas Emissions Associated with the Production of Hydrogen, 2021.
[19] China maps 2021-2035 plan on hydrogen energy development. Korea Hydrogen Economy Roadmap 2040 2022.
[20] Focus On Hydrogen: japan's Energy Strategy For Hydrogen And Ammonia, White Paper On Building A Green Hydrogen Economy And Policy Roadmap For India. International Energy Agency. Data and Statistics.
[21] H.J. Schellnhuber, S. Rahmstorf, R. Winkelmann, Why the right climate target was agreed in Paris, Nat. Clim. Chang. 6 (2016) 649–653, doi:10.1038/nclimate3013.
[22] U. Eberle, B. Müller, R. von Helmolt, Fuel cell electric vehicles and hydrogen infrastructure: status 2012, Energy Environ. Sci. 5 (2012) 8780–8798, doi:10.1039/C2EE22596D.
[23] G.J. Offer, D. Howey, M. Contestabile, R. Clague, N.P. Brandon, Comparative analysis of battery electric, hydrogen fuel cell and hybrid vehicles in a future sustainable road transport system, Energy Policy 38 (2010) 24–29, doi:10.1016/j.enpol.2009.08.040.
[24] G.W. Crabtree, M.S. Dresselhaus, M.V. Buchanan, The hydrogen economy, Phys. Today 57 (2004) 39–44, doi:10.1063/1.1878333.
[25] M. Khodayari, A. Aslani, Analysis of the energy storage technology using Hype Cycle approach, Sustain. Energy Technol. Assess. 25 (2018) 60–74, doi:10.1016/j.seta.2017.12.002.
[26] B. Heid, M. Linder, A. Orthofer, M. Wilthaner, Hydrogen: The next Wave For Electric vehicles?, McKinsey & Company, 2017.
[27] Uddenfeldt, F., Hype Doesn't Change the World. Scale Does, 2022
[28] The Annual Energy Outlook explores long-term energy trends in the United States, 2022
[29] M. Wieliczko, N. Stetson, Hydrogen technologies for energy storage: a perspective, MRS Energy Sustain. 7 (2020) E41. 10.1557/mre.2020.43.
[30] Verma, H., Gambhir, J.,Goyal, S., Energy storage: a review, 2013.
[31] L. Trahey, F.R. Brushett, N.P. Balsara, G. Ceder, L. Cheng, Y.-.M. Chiang, N.T. Hahn, B.J. Ingram, S.D. Minteer, J.S. Moore, K.T. Mueller, L.F. Nazar, K.A. Persson, D.J. Siegel, K. Xu, K.R. Zavadil, V. Srinivasan, G.W. Crabtree, Energy storage emerging: a perspective from the Joint Center for Energy Storage Research, Proc. Natl. Acad. Sci. 117 (2020) 12550–12557, doi:10.1073/pnas.1821672117.
[32] Hydrogen Storage. Office of Energy Efficiency & Renewable Energy, from https://www.energy.gov/eere/fuelcells/hydrogen-storage. 2022
[33] G. Valenti, 2 - Hydrogen liquefaction and liquid hydrogen storage, in: R.B. Gupta, A. Basile, T.N. Veziroğlu (Eds.), Compendium of Hydrogen Energy, Woodhead Publishing, 2016, pp. 27–51.
[34] L. Eric, Thermophysical Properties of Fluids, CRC, CO, 2009 CRC.
[35] Superjumbo Tube Trailers, 2022
[36] Materials-Based Hydrogen Storage, 2022
[37] M. Simanullang, L. Prost, Nanomaterials for on-board solid-state hydrogen storage applications, Int. J. Hydrogen Energy 47 (2022) 29808–29846, doi:10.1016/j.ijhydene.2022.06.301.
[38] S. Sonkaria, V. Khare, Exploring the landscape between synthetic and biosynthetic materials discovery: important considerations via systems connectivity, cooperation and scale-driven convergence in biomanufacturing, Biomanuf. Rev. 5 (1) (2020), doi:10.1007/s40898-020-0007-7.
[39] A.W. Thornton, C.M. Simon, J. Kim, O. Kwon, K.S. Deeg, K. Konstas, S.J. Pas, M.R. Hill, D.A. Winkler, M. Haranczyk, B. Smit, Materials genome in action: identifying the performance limits of physical hydrogen storage, Chem. Mater. 29 (2017) 2844–2854, doi:10.1021/acs.chemmater.6b04933.
[40] M.O.J. Jäger, E.V. Morooka, F. Federici Canova, L. Himanen, A.S. Foster, Machine learning hydrogen adsorption on nanoclusters through structural descriptors, NPJ Comput. Mater. 4 (2018) 37, doi:10.1038/s41524-018-0096-5.
[41] A. Rahnama, G. Zepon, S. Sridhar, Machine learning based prediction of metal hydrides for hydrogen storage, part II: prediction of material class, Int. J. Hydrogen Energy 44 (2019) 7345–7353, doi:10.1016/j.ijhydene.2019.01.264.
[42] A. Rahnama, G. Zepon, S. Sridhar, Machine learning based prediction of metal hydrides for hydrogen storage, part I: prediction of hydrogen weight percent, Int. J. Hydrogen Energy 44 (2019) 7337–7344, doi:10.1016/j.ijhydene.2019.01.261.
[43] S.K. Dewangan, M. Mohan, V. Kumar, A. Sharma, B. Ahn, A comprehensive review of the prospects for future hydrogen storage in materials-application and outstanding issues, Int. J. Energy Res. 46 (2022) 16150–16177, doi:10.1002/er.8322.
[44] A. Pasturel, C. Chatillon, A. Percheron-Guegan, J.C. Achard, Thermodynamic properties of $LaNi_4M$ compounds and their hydrides, in: G.J. McCarthy, H.B. Silber, J.J. Rhyne, F.M. Kalina (Eds.), The Rare Earths in Modern Science and Technology: Volume 3, Springer US, Boston, MA, 1982, pp. 489–492.
[45] G.V. Raynor, The relative stabilities and structural characteristics of intermediate phases of the CaCu5 structure, J. Less Common Metals 53 (1977) 167–176, doi:10.1016/0022-5088(77)90101-1.
[46] C.B. Magee, J. Liu, C.E. Lundin, Relationships between intermetallic compound structure and hydride formation, J. Less Common Metals 78 (1981) 119–138, doi:10.1016/0022-5088(81)90120-X.
[47] J.J.G. Willems, K.H.J. Buschow, From permanent magnets to rechargeable hydride electrodes, J. Less Common Metals 129 (1987) 13–30, doi:10.1016/0022-5088(87)90029-4.
[48] Vucht, J.H.N.v., Kuijpers, F.A.,Bruning, H., Reversible Room-Temperature Absorption of Large Quantities of Hydrogen by Intermetallic Compounds, 1970.
[49] Reilly, J.J.B.W.J., Richard H. (1974). USA Patent No.: U. S. P. Office.
[50] G.D. Sandrock, A new family of hydrogen storage alloys based on the system nickel-mischmetal-calcium, Paper Presented At the 12th International Energy Conversion Engineering Conference (IECEC), Washington, D.C., 2022.
[51] G. Sandrock, The metallurgy and production of rechargeable hydrides, in: A.F. Andresen, A.J. Maeland (Eds.), Hydrides For Energy Storage, Pergamon, 1978, pp. 353–393.
[52] G. Sandrock, G. Thomas, The IEA/DOE/SNL on-line hydride databases, J. Appl. Phys. A 72 (2001) 153–155.
[53] G. Sandrock, State-of-the-art Review of Hydrogen Storage in Reversible Metal Hydrides for Military Fuel Cell Application (Report No. Final 11/5/96-7/24/97), Office of Naval Research, Arlington, VA 22217-5660, USA, 1997.
[54] Y. Osumi, H. Suzuki, A. Kato, M. Nakane, Y. Miyake, Absorption-desorption characteristics of hydrogen for mischmetal based alloys, Nippon Kagaku Kaishi (1978) 1472–1477 1978, doi:10.1246/nikkashi.1978.1472.
[55] Y. Osumi, A. Kato, H. Suzuki, M. Nakane, Y. Miyake, Hydrogen absorption-desorption characteristics of mischmetal-nickel-aluminum alloys, J. Less Common Metals 66 (1979) 67–75, doi:10.1016/0022-5088(79)90196-6.
[56] Y. Osumi, H. Suzuki, A. Kato, M. Nakane, Y. Miyake, Absorption-desorption characteristics of hydrogen for mischmetal-nickel-manganese alloys, Nippon Kagaku Kaishi 1979 (1979) 45–48, doi:10.1246/nikkashi.1979.45.
[57] Y. Osumi, H. Suzuki, A. Kato, M. Nakane, Y. Miyake, Absorption-desorption char-

acteristics of hydrogen for mischmetal-nickel-cobalt alloys, Nippon Kagaku Kaishi 1979 (1979) 722–726, doi:10.1246/nikkashi.1979.722.
[58] V.K. Sharma, E. Anil Kumar, Effect of measurement parameters on thermodynamic properties of La-based metal hydrides, Int. J. Hydrogen Energy 39 (2014) 5888–5898, doi:10.1016/j.ijhydene.2014.01.174.
[59] V.K. Sharma, E. Anil Kumar, M. Prakash Maiya, S. Srinivasa Murthy, Experimental and theoretical studies on static and dynamic pressure–concentration isotherms of MmNi5−xAlx (x = 0, 0.3, 0.5 and 0.8) hydrides, Int. J. Hydrogen Energy 39 (2014) 18940–18951, doi:10.1016/j.ijhydene.2014.09.028.
[60] S.L. Li, P. Wang, W. Chen, G. Luo, X.B. Han, D.M. Chen, K. Yang, Study on hydrogen storage properties of LaNi3.8Al1.2−xMnx alloys, Int. J. Hydrogen Energy 35 (2010) 12391–12397, doi:10.1016/j.ijhydene.2010.08.049.
[61] S.L. Li, W. Chen, G. Luo, X.B. Han, D.M. Chen, K. Yang, W.P. Chen, Effect of hydrogen absorption/desorption cycling on hydrogen storage properties of a LaNi3.8Al1.0Mn0.2 alloy, Int. J. Hydrogen Energy 37 (2012) 3268–3275, doi:10.1016/j.ijhydene.2011.10.106.
[62] W. Zhou, Z. Ma, C. Wu, D. Zhu, L. Huang, Y. Chen, The mechanism of suppressing capacity degradation of high-Al AB5-type hydrogen storage alloys at 60 °C, Int. J. Hydrogen Energy 41 (2016) 1801–1810, doi:10.1016/j.ijhydene.2015.10.070.
[63] H. Falahati, D.P.J. Barz, Evaluation of hydrogen sorption models for AB5-type metal alloys by employing a gravimetric technique, Int. J. Hydrogen Energy 38 (2013) 8838–8851, doi:10.1016/j.ijhydene.2013.04.148.
[64] M. Anik, N.B. Hatirnaz, A.B. Aybar, Molten salt synthesis of La(Ni1−xCox)5 (x = 0, 0.1, 0.2, 0.3) type hydrogen storage alloys, Int. J. Hydrogen Energy 41 (2016) 361–368, doi:10.1016/j.ijhydene.2015.11.060.
[65] S. Srivastava, O.N. Srivastava, Investigations of synthesis and characterization of MmNi4.3Al0.3Mn0.4 AND MmNi4.0Al0.3Mn0.4Si0.3, hydrogen storage materials through thermal and spin melting processes, Int. J. Hydrogen Energy 23 (1998) 7–13, doi:10.1016/S0360-3199(97)00019-0.
[66] S. Srivastava, O.N. Srivastava, Investigations on synthesis, characterization and hydrogenation behaviour of the spin- and thermal-melted versions of LaNi5−xSix (x=0.1, 0.3, 0.5) hydrogen storage materials, J. Alloys Compd. 267 (1998) 240–245, doi:10.1016/S0925-8388(97)00479-9.
[67] S. Srivastava, S.S.S. Raman, B.K. Singh, O.N. Srivastava, On the synthesis and characterization of some new AB5 type MmNi4.3Al0.3Mn0.4, LaNi5-xSix (x=0.1, 0.3, 0.5) and Mg−x wt% CFMmNi5−y wt% Si hydrogen storage materials, Int. J. Hydrogen Energy 25 (2000) 431–440, doi:10.1016/S0360-3199(99)00055-5.
[68] V.V. Sarma, S.S.S. Raman, D.J. Davidson, O.N. Srivastava, On the mechanically pulverized MmNi4.6Fe0.4 as a viable hydrogen storage material, Int. J. Hydrogen Energy 26 (2001) 231–236, doi:10.1016/S0360-3199(00)00060-4.
[69] S. Chumphongphan, M. Paskevicius, D.A. Sheppard, C.E. Buckley, Effect of Al and Mo substitution on the structural and hydrogen storage properties of CaNi5, Int. J. Hydrogen Energy 38 (2013) 2325–2331, doi:10.1016/j.ijhydene.2012.11.107.
[70] S. Srivastava, R.K. Upadhyaya, Investigations of AB5-type hydrogen storage materials with enhanced hydrogen storage capacity, Int. J. Hydrogen Energy 36 (2011) 7114–7121, doi:10.1016/j.ijhydene.2011.02.111.
[71] S. Srivastava, R.K. Upadhyay, Investigations on synthesis, characterization and hydrogenation behavior of hydrogen storage alloys, Mm1-xCaxNi5-yzAlyFez(x=0,0.05,0.1,0.2,0.3;y=0,0.1;z=0,0.1), Int. J. Hydrogen Energy 32 (2007) 4195–4201, doi:10.1016/j.ijhydene.2007.06.011.
[72] S. Srivastava, O.N. Srivastava, Hydrogenation behaviour with regard to storage capacity, kinetics, stability and thermodynamic behaviour of hydrogen storage composite alloys, LaNi5/La2Ni7, LaNi3, J. Alloys Compd. 290 (1999) 250–256, doi:10.1016/S0925-8388(99)00196-6.
[73] S. Srivastava, O.N. Srivastava, Synthesis, characterization and hydrogenation behaviour of composite hydrogen storage alloys, LaNi5/La2Ni7, LaNi3, J. Alloys Compd. 282 (1999) 197–205, doi:10.1016/S0925-8388(98)00741-5.
[74] H. Miyamura, T. Sakai, K. Oguro, A. Kato, H. Ishikawa, Hydrogen absorption and phase transitions in rapidly quenched LaNi alloys, J. Less Common Metals 146 (1989) 197–203, doi:10.1016/0022-5088(89)90376-7.
[75] A. Kaabi, C. Khaldi, J. Lamloumi, Thermodynamic and kinetic parameters and high rate discharge-ability of the AB5-type metal hydride anode, Int. J. Hydrogen Energy 41 (2016) 9914–9923, doi:10.1016/j.ijhydene.2016.03.128.
[76] I. Kunce, M. Polański, T. Czujko, Microstructures and hydrogen storage properties of LaNiFeVMn alloys, Int. J. Hydrogen Energy 42 (2017) 27154–27164, doi:10.1016/j.ijhydene.2017.09.039.
[77] C. Briki, M. Bouzid, M.H. Dhaou, A. Jemni, A.B. Lamine, Experimental and theoretical study of hydrogen absorption by LaNi3.6Mn0.3Al0.4Co0.7 alloy using statistical physics modeling, Int. J. Hydrogen Energy 43 (2018) 9722–9732, doi:10.1016/j.ijhydene.2018.02.201.
[78] A. Satheesh, P. Muthukumar, Performance investigations of a single-stage metal hydride heat pump, Int. J. Hydrogen Energy 35 (2010) 6950–6958, doi:10.1016/j.ijhydene.2010.04.043.
[79] S. Srivastava, R.K. Upadhyay, Investigations of AB5-type negative electrode for nickel-metal hydride cell with regard to electrochemical and microstructural characteristics, J. Power Sources 195 (2010) 2996–3001, doi:10.1016/j.jpowsour.2009.11.070.
[80] S. Srivastava, R.K. Upadhyaya, Iron-substituted AB5-type MH electrode, Bull. Mater. Sci. 36 (2013) 1267–1274, doi:10.1007/s12034-013-0608-3.
[81] C. Dongliang, Z. Chenglin, M. Zhewen, Y. Fei, W. Yucheng, Z. Ding, W. Chaoling, C. Yungui, Improvement in high-temperature performance of Co-free high-Fe AB5-type hydrogen storage alloys, Int. J. Hydrogen Energy 37 (2012) 12375–12383, doi:10.1016/j.ijhydene.2012.05.147.
[82] H. Drulis, A. Hackemer, P. Głuchowski, K. Giza, L. Adamczyk, H. Bala, Gas phase hydrogen absorption and electrochemical performance of La2(Ni,Co,Mg,M)10 based alloys, Int. J. Hydrogen Energy 39 (2014) 2423–2429, doi:10.1016/j.ijhydene.2013.11.092.
[83] L.A. Benavides, D.J. Cuscueta, A.A. Ghilarducci, MWCNT as mechanical support during ball milling of an AB5 alloy used as negative electrode of a Ni–MH battery, Int. J. Hydrogen Energy 40 (2015) 4925–4930, doi:10.1016/j.ijhydene.2015.01.164.
[84] R.C. Cui, C.C. Yang, M.M. Li, B. Jin, X.D. Ding, Q. Jiang, Enhanced high-rate performance of ball-milled MmNi3.55Co0.75Mn0.4Al0.3 hydrogen storage alloys with graphene nanoplatelets, J. Alloys Compd. 693 (2017) 126–131, doi:10.1016/j.jallcom.2016.09.157.
[85] K.D. Modibane, M. Lototskyy, M.W. Davids, M. Williams, M.J. Hato, K.M. Molapo, Influence of co-milling with palladium black on hydrogen sorption performance and poisoning tolerance of surface modified AB5-type hydrogen storage alloy, J. Alloys Compd. 750 (2018) 523–529, doi:10.1016/j.jallcom.2018.04.003.
[86] M.R. Esquivel, G. Meyer, A comparison of the evolution during the mechanical alloying of both a MmNi5–Ni and a Mm–Ni mixtures: stages of milling and microstructural characterization, J. Alloys Compd. (2007) 212–217 446-447, doi:10.1016/j.jallcom.2007.01.111.
[87] S. Srivastava, K. Panwar, Investigations on microstructures of ball–milled MmNi5 hydrogen storage alloy, Mater. Res. Bull. 73 (2016) 284–289, doi:10.1016/j.materresbull.2015.09.021.
[88] X. Shan, J.H. Payer, W.D. Jennings, Mechanism of increased performance and durability of Pd-treated metal hydriding alloys, Int. J. Hydrogen Energy 34 (2009) 363–369, doi:10.1016/j.ijhydene.2008.09.040.
[89] S. Srivastava, K. Panwar, Effect of transition metals on ball-milled MmNi5 hydrogen storage alloy, Mater. Renew. Sustain. Energy 4 (19) (2015), doi:10.1007/s40243-015-0062-9.
[90] K. Panwar, S. Srivastava, Enhancement in hydrogenation properties of ball-milled AB5-type hydrogen storage alloy through catalyst, J. Phys. 2267 (2022) 012052, doi:10.1088/1742-6596/2267/1/012052.
[91] A.V. Ledovskikh, D.L. Danilov, M. Vliex, P.H.L. Notten, Modeling and experimental verification of the thermodynamic properties of hydrogen storage materials, Int. J. Hydrogen Energy 41 (2016) 3904–3918, doi:10.1016/j.ijhydene.2015.11.038.
[92] G. Liu, D. Chen, Y. Wang, K. Yang, First-principles calculations of crystal and electronic structures and thermodynamic stabilities of La–Ni–H, La–Ni–Al–H and La–Ni–Al–Mn–H hydrogen storage compounds, Int. J. Hydrogen Energy 41 (2016) 12194–12204, doi:10.1016/j.ijhydene.2016.05.172.
[93] S.V. Mitrokhin, A.A. Tepanov, V.N. Verbetsky, Hydrogen interaction with alloys of NdNi5−xAlx system, Int. J. Hydrogen Energy 42 (2017) 22353–22357, doi:10.1016/j.ijhydene.2017.05.098.
[94] P. Canjura Rodriguez, N. Gallandat, A. Züttel, Accurate measurement of pressure-composition isotherms and determination of thermodynamic and kinetic parameters of metal hydrides, Int. J. Hydrogen Energy 44 (2019) 13583–13591, doi:10.1016/j.ijhydene.2019.03.224.
[95] K. Panwar, S. Srivastava, Investigations on calculation of heat of formation for multi-element AB5-type hydrogen storage alloy, Int. J. Hydrogen Energy 43 (2018) 11079–11084, doi:10.1016/j.ijhydene.2018.04.213.
[96] K. Panwar, S. Srivastava, On structural model of AB5-type multi-element hydrogen storage alloy, Int. J. Hydrogen Energy 44 (2019) 30208–30217, doi:10.1016/j.ijhydene.2019.09.138.
[97] K. Panwar, S. Srivastava, Theoretical model on the electronic properties of multi-element AB5-type metal hydride, Int. J. Hydrogen Energy 46 (2021) 10819–10829, doi:10.1016/j.ijhydene.2020.12.170.
[98] N. Garkoti, K. Panwar, S. Srivastava, Correlation of Structural properties with Thermodynamic Properties for Multi-Element AB 5-Type Hydrogen Storage Alloy, Stud. J. Phys. 8 (2019) 33–39.
[99] K.P. Sapna Prajapati, S. Sumita, Effects of structural properties on Hydrogen Storage capacity of multi-element AB 5-type Hydrogen Storage alloy, Stud. J. Phys. 8 (2020) 70–77.
[100] D.F. Wong, K. Young, K.Y.S. Ng, First-principles study of structure, initial lattice expansion, and pressure-composition-temperature hysteresis for substituted LaNi5 and TiMn2 alloys, Model. Simul. Mater. Sci. Eng. 24 (2016) 085007, doi:10.1088/0965-0393/24/8/085007.
[101] K. Malleswararao, N. Aswin, P. Kumar, P. Dutta, S. Srinivasa Murthy, Experiments on a novel metal hydride cartridge for hydrogen storage and low temperature thermal storage, Int. J. Hydrogen Energy 47 (2022) 16144–16155, doi:10.1016/j.ijhydene.2022.03.097.
[102] P.V. Jithu, G. Mohan, Performance simulation of metal hydride based helical spring actuators during hydrogen sorption, Int. J. Hydrogen Energy 47 (2022) 14942–14951, doi:10.1016/j.ijhydene.2022.02.234.
[103] A.K. Aadhithiyan, R. Sreeraj, S. Anbarasu, Thermal modelling and performance evaluation of LmNi4.91Sn0.15 hydride bed configurations for space-constrained thermal applications, Appl. Therm. Eng. 216 (2022) 119116, doi:10.1016/j.applthermaleng.2022.119116.
[104] G.R. de Almeida Neto, C.A. Gonçalves Beatrice, L.A. Pessan, Spray-dried composite microparticles of polyetherimide and LaNi5 as a versatile material for hydrogen storage applications, Int. J. Hydrogen Energy 47 (2022) 16996–17009, doi:10.1016/j.ijhydene.2022.03.193.
[105] L. Liang, Q. Yang, S. Zhao, L. Wang, F. Liang, Excellent catalytic effect of LaNi5 on hydrogen storage properties for aluminium hydride at mild temperature, Int. J. Hydrogen Energy 46 (2021) 38733–38740, doi:10.1016/j.ijhydene.2021.09.130.
[106] S. Chandra, P. Sharma, P. Muthukumar, S.S.V. Tatiparti, Modeling and numerical simulation of a 5 kg LaNi5-based hydrogen storage reactor with internal conical fins, Int. J. Hydrogen Energy 45 (2020) 8794–8809, doi:10.1016/j.ijhydene.2020.01.115.
[107] X. Chen, J. Xu, W. Zhang, S. Zhu, N. Zhang, D. Ke, J. Liu, K. Yan, H. Cheng, Effect of Mn on the long-term cycling performance of AB5-type hydrogen storage alloy, Int. J. Hydrogen Energy 46 (2021) 21973–21983, doi:10.1016/j.ijhydene.2021.04.021.

[108] J.H. Wernick, Topologically Close-Packed Structures, in: E.J.H. Westbrook (Ed.), in : Intermetallic Compounds, John Wiley, 1967, pp. 197–216. John Wiley.
[109] K. Yvon, P. Fischer, Crystal and magnetic structures of ternary metal hydrides: a comprehensive review, in: L. Schlapbach (Ed.), Hydrogen in Intermetallic Compounds I: Electronic, Thermodynamic, and Crystallographic Properties, Preparation, Heidelberg: Springer Berlin Heidelberg, Berlin, 1988, pp. 87–138.
[110] Beck, R.,Mueller, W.M., Investigation of hydriding characteristics of intermetallic compounds, 1962.
[111] D. Shaltiel, I. Jacob, D. Davidov, Hydrogen absorption and desorption properties of AB2 laves-phase pseudobinary compounds, J. Less Common Metals 53 (1977) 117–131, doi:10.1016/0022-5088(77)90162-X.
[112] A. Pebler, E.A. Gulbransen, Equilibrium Studies On the Systems ZrCr2-H2, ZrV2-H2, and ZrMo2-H2 Between 0 and 900 C, Trans. TMS AIME 239 (1967) 1593–1596.
[113] Trzeciak, M.J., Dilthey, D.F.,Mallett, M.W., Study of hydrides. Rept. BMI-1112, 1956.
[114] A.J. Maeland, G.G. Libowitz, Hydrides of beryllium-based intermetallic compounds, J. Less Common Metals 89 (1983) 197–200, doi:10.1016/0022-5088(83)90266-7.
[115] O. Bernauer, J. Töpler, D. Noréus, R. Hempelmann, D. Richter, Fundamentals and properties of some Ti/Mn based Laves phase hydrides, Int. J. Hydrogen Energy 14 (1989) 187–200, doi:10.1016/0360-3199(89)90053-0.
[116] T. Gamo, Y. Moriwaki, N. Yanagihara, T. Yamashita, T. Iwaki, Formation and properties of titanium-manganese alloy hydrides, Int. J. Hydrogen Energy 10 (1985) 39–47, doi:10.1016/0360-3199(85)90134-X.
[117] Y. Moriwaki, T. Gamo, H. Seri, T. Iwaki, Electrode characteristics of C15-type laves phasealloys, J. Less Common Metals 172-174 (1991) 1211–1218, doi:10.1016/S0022-5088(06)80029-9.
[118] G. Xueping, S. Deying, Z. Yunshi, W. Genshi, S. Panwen, Characteristics of the stoichiometric and non-stoichiometric Laves phase alloys and their hydride electrodes, J. Alloys Compd. 223 (1995) 77–80, doi:10.1016/0925-8388(94)01423-X.
[119] G. Sandrock, Hydrogen-metal systems, in: Y. Yurum (Ed.), in : Hydrogen energy System - production and Utilization of Hydrogen and Future Aspects, Kluwer Academic, Dordrecht, 1995, pp. 135–166. (Ed.).
[120] S.K. Zhang, Q.D. Wang, Y.Q. Lei, G.L. Lü, L.X. Chen, F. Wu, The phase structure and electrochemical properties of the melt-spun alloy Zr0.7Ti0.3Mn0.4V0.4Ni1.2, J. Alloys Compd. 330-332 (2002) 855–860, doi:10.1016/S0925-8388(01)01482-7.
[121] S. Semboshi, N. Masahashi, T.J. Konno, M. Sakurai, S. Hanada, Composition dependence of hydrogen absorbing properties in melt quenched and annealed TiMn2 based alloys, J. Alloys Compd. 379 (2004) 290–297, doi:10.1016/j.jallcom.2004.02.045.
[122] M.A. Fetcenko, S.R. Ovshinsky, K. Young, B. Reichman, C. Fierro, J. Koch, F. Martin, W. Mays, T. Ouchi, B. Sommers, A. Zallen, High catalytic activity disordered VTiZrNiCrCoMnAlSn hydrogen storage alloys for nickel–metal hydride batteries, J. Alloys Compd. 330-332 (2002) 752–759, doi:10.1016/S0925-8388(01)01460-8.
[123] S. Semboshi, M. Sakurai, N. Masahashi, T.J. Konno, S. Hanada, Effect of structural changes on degradation of hydrogen absorbing capacity in cyclically hydrogenated TiMn2 based alloys, J. Alloys Compd. 376 (2004) 232–240, doi:10.1016/j.jallcom.2003.12.044.
[124] K. Young, J. Koch, T. Ouchi, A. Banik, M.A. Fetcenko, Study of AB2 alloy electrodes for Ni/MH battery prepared by centrifugal casting and gas atomization, J. Alloys Compd. 496 (2010) 669–677, doi:10.1016/j.jallcom.2010.02.161.
[125] K. Young, J. Nei, T. Ouchi, M.A. Fetcenko, Phase abundances in AB2 metal hydride alloys and their correlations to various properties, J. Alloys Compd. 509 (2011) 2277–2284, doi:10.1016/j.jallcom.2010.11.005.
[126] X.W. Yang, J.S. Li, T.B. Zhang, R. Hu, X.Y. Xue, H.Z. Fu, Role of defect structure on hydrogenation properties of Zr0.9Ti0.1V2 alloy, Int. J. Hydrogen Energy 36 (2011) 9318–9323, doi:10.1016/j.ijhydene.2011.05.009.
[127] K. Young, T. Ouchi, J. Yang, M.A. Fetcenko, Studies of off-stoichiometric AB2 metal hydride alloy: part 1. Structural characteristics, Int. J. Hydrogen Energy 36 (2011) 11137–11145, doi:10.1016/j.ijhydene.2011.05.057.
[128] M. Kazemipour, H. Salimijazi, A. Saidi, A. Saatchi, A. Aref arjmand, Hydrogen storage properties of Ti0.72Zr0.28Mn1.6V0.4 alloy prepared by mechanical alloying and copper boat induction melting, Int. J. Hydrogen Energy 39 (2014) 12784–12788, doi:10.1016/j.ijhydene.2014.06.085.
[129] A.R. Merlino, C.R. Luna, A. Juan, M.E. Pronsato, A DFT study of hydrogen storage in Zr(Cr0.5Ni0.5)2 Laves phase, Int. J. Hydrogen Energy 41 (2016) 2700–2710, doi:10.1016/j.ijhydene.2015.10.077.
[130] M.S. El-Eskandarany, F. Al-Ajmi, M. Banyan, A. Al-Duweesh, Synergetic effect of reactive ball milling and cold pressing on enhancing the hydrogen storage behavior of nanocomposite MgH2/10 wt% TiMn2 binary system, Int. J. Hydrogen Energy 44 (2019) 26428–26443, doi:10.1016/j.ijhydene.2019.08.093.
[131] I.D. Wijayanti, L. Mølmen, R.V. Denys, J. Nei, S. Gorsse, K. Young, M.N. Guzik, V. Yartys, The electrochemical performance of melt-spun C14-Laves type TiZr-based alloy, Int. J. Hydrogen Energy 45 (2020) 1297–1303, doi:10.1016/j.ijhydene.2019.02.093.
[132] Z. Cao, P. Zhou, X. Xiao, L. Zhan, Z. Li, S. Wang, L. Chen, Investigation on Ti–Zr–Cr–Fe–V based alloys for metal hydride hydrogen compressor at moderate working temperatures, Int. J. Hydrogen Energy 46 (2021) 21580–21589, doi:10.1016/j.ijhydene.2021.03.247.
[133] P. Edalati, A. Mohammadi, Y. Li, H.-W. Li, R. Floriano, M. Fuji, K. Edalati, High-entropy alloys as anode materials of nickel - metal hydride batteries, Scr. Mater. 209 (2022) 114387, doi:10.1016/j.scriptamat.2021.114387.
[134] C. Qin, H. Wang, W. Jiang, J. Liu, L. Ouyang, M. Zhu, Comparative study of Ga and Al alloying with ZrFe2 for high-pressure hydrogen storage, Int. J. Hydrogen Energy 47 (2022) 13409–13417, doi:10.1016/j.ijhydene.2021.12.110.
[135] S. Suwarno, G. Dicky, A. Suyuthi, M. Effendi, W. Witantyo, L. Noerochim, M. Ismail, Machine learning analysis of alloying element effects on hydrogen storage properties of AB2 metal hydrides, Int. J. Hydrogen Energy 47 (2022) 11938–11947, doi:10.1016/j.ijhydene.2022.01.210.
[136] K. Miwa, R. Asahi, Path integral study on C15-type Laves TiCr2 hydride, Int. J. Hydrogen Energy 44 (2019) 23708–23715, doi:10.1016/j.ijhydene.2019.07.086.
[137] J.J. Reilly Jr., R.H. Wiswall Jr., Reaction of hydrogen with alloys of magnesium and nickel and the formation of Mg2NiH4, Inorg. Chem. 7 (1968) 2254–2256, doi:10.1021/ic50069a016.
[138] Noréus, D., Properties of Formal Low-Valence Transition Metal — Hydrogen Complexes in Mg2NiH4 and Na2PdH2*, 163 (1989) 575–578. doi:10.1524/zpch.1989.163.Part_2.0575.
[139] J.C. Bolcich, A.A. Yawny, H.L. Corso, H.A. Peretti, C.O. Ayala, Hydrogen storage employing Mg-10 wt% Ni alloy, Int. J. Hydrogen Energy 19 (1994) 605–609, doi:10.1016/0360-3199(94)90219-4.
[140] A. Seiler, L. Schlapbach, T. Von Waldkirch, D. Shaltiel, F. Stucki, Surface analysis of Mg2NiMg, Mg2Ni and Mg2Cu, J. Less Common Metals 73 (1980) 193–199, doi:10.1016/0022-5088(80)90360-4.
[141] F. Stucki, L. Schlapbach, Magnetic properties of LaNi5, FeTi, Mg2Ni and their hydrides, J. Less Common Metals 74 (1980) 143–151, doi:10.1016/0022-5088(80)90084-3.
[142] J.P. Darnaudery, B. Darriet, M. Pezat, The Mg2Ni0.75M0.25 alloys (M = 3d element): their application to hydrogen storage, Int. J. Hydrogen Energy 8 (1983) 705–708, doi:10.1016/0360-3199(83)90179-9.
[143] S.N. Klyamkin, K.N. Semenenko, I.A. Kinas, New hydride formation of MoSi2-type intermetallic compounds at hydrogen pressures up to 2000 atm, J. Alloys Compd. 204 (1994) 65–69, doi:10.1016/0925-8388(94)90072-8.
[144] A.J. Maeland, G.G. Libowitz, Hydrogen absorption in some A2B intermetallic compounds with the MoSi2-type structure (C11b), J. Less Common Metals 74 (1980) 295–300, doi:10.1016/0022-5088(80)90165-4.
[145] A.K. Singh, A.K. Singh, O.N. Srivastava, On the synthesis of the Mg2Ni alloy by mechanical alloying, J. Alloys Compd. 227 (1995) 63–68, doi:10.1016/0925-8388(95)01625-2.
[146] Thomas, G.J., Guthrie, S.E., Bauer, W., Yang, N.Y.C.,Sandrock, G., Hydride Development For Hydrogen Storage, United States, 2022.
[147] L. Zaluski, A. Zaluska, J.O. Ström-Olsen, Hydrogen absorption in nanocrystalline Mg2Ni formed by mechanical alloying, J. Alloys Compd. 217 (1995) 245–249, doi:10.1016/0925-8388(94)01348-9.
[148] M.Y. Song, B. Darriet, M. Pezat, P. Hagenmuller, Dehydriding kinetics of a mechanically alloyed mixture with a composition Mg2Ni, Int. J. Hydrogen Energy 12 (1987) 27–30, doi:10.1016/0360-3199(87)90123-6.
[149] H.Y. Lee, N.H. Goo, W.T. Jeong, K.S. Lee, The surface state of nanocrystalline and amorphous Mg2Ni alloys prepared by mechanical alloying, J. Alloys Compd. 313 (2000) 258–262, doi:10.1016/S0925-8388(00)01205-6.
[150] H. Yang, H. Yuan, J. Ji, H. Sun, Z. Zhou, Y. Zhang, Characteristics of Mg2Ni0.75M0.25 (M=Ti, Cr, Mn, Fe, Co, Ni, Cu and Zn) alloys after surface treatment, in: J. Alloys Compd., 330-332, 2002, pp. 640–644, doi:10.1016/S0925-8388(01)01535-3.
[151] J. Cermak, B. David, Catalytic effect of Ni, Mg2Ni and Mg2NiH4 upon hydrogen desorption from MgH2, Int. J. Hydrogen Energy 36 (2011) 13614–13620, doi:10.1016/j.ijhydene.2011.07.133.
[152] Y.T. Wang, C.B. Wan, R.L. Wang, X.H. Meng, M.F. Huang, X. Ju, Effect of Cr substitution by Ni on the cycling stability of Mg2Ni alloy using EXAFS, Int. J. Hydrogen Energy 39 (2014) 14858–14867, doi:10.1016/j.ijhydene.2014.07.032.
[153] X. Hou, R. Hu, T. Zhang, H. Kou, W. Song, J. Li, Hydrogen desorption performance of high-energy ball milled Mg2NiH4 catalyzed by multi-walled carbon nanotubes coupling with TiF3, Int. J. Hydrogen Energy 39 (2014) 19672–19681, doi:10.1016/j.ijhydene.2014.09.170.
[154] G.-.X. Li, Z.-.Q. Lan, Y.-.S. Tseng, W.-.Z. Zhou, J. Guo, S.L.I. Chan, Penetration and diffusion of hydrogen in Mg2Ni: a first-principles investigation, Int. J. Hydrogen Energy 42 (2017) 3097–3105, doi:10.1016/j.ijhydene.2016.09.218.
[155] T. Káňa, J. Čermák, L. Král, Substitution of nickel in Mg2Ni and its hydride with elements from groups XIII and XIV: an ab initio study, Int. J. Hydrogen Energy 46 (2021) 15691–15701, doi:10.1016/j.ijhydene.2021.02.011.
[156] S. Varnagiris, M. Urbonavicius, Hydrogen generation kinetics via hydrolysis of Mg2Ni and Mg2NiH4 powders, Int. J. Hydrogen Energy 46 (2021) 36323–36335, doi:10.1016/j.ijhydene.2021.08.139.
[157] S. Kumar, H. Miyaoka, T. Ichikawa, G.K. Dey, Y. Kojima, Micro-alloyed Mg2Ni for better performance as negative electrode of Ni-MH battery and hydrogen storage, Int. J. Hydrogen Energy 42 (2017) 5220–5226, doi:10.1016/j.ijhydene.2016.10.128.
[158] H. Hu, C. Ma, Q. Chen, Improved hydrogen storage properties of Ti2CrV alloy by Mo substitutional doping, Int. J. Hydrogen Energy 47 (2022) 11929–11937, doi:10.1016/j.ijhydene.2022.01.212.
[159] K. Xiao, L. Zhou, X. Kong, D. Luo, J. Song, Hydrogen interaction with Mn-doped Zr2Fe (101) surface: a DFT study, Int. J. Hydrogen Energy 47 (2022) 20932–20941, doi:10.1016/j.ijhydene.2022.04.203.
[160] S. Hai, X. Liu, W. Wang, Y. Liu, J. Li, Microstructure and electrochemical performance of Zn-doped of Mg2Ni1-xZnx hydrogen storage alloys, Int. J. Hydrogen Energy 47 (2022) 20604–20616, doi:10.1016/j.ijhydene.2022.04.167.
[161] J.J. Reilly, G.D. Sandrock, Hydrogen storage in metal hydrides, Sci. Am. 242 (1980) 118–131.
[162] G.G. Libowitz, H.F. Hayes, T.R.P. Gibb Jr, The system zirconium–nickel and hydrogen, J. Phys. Chem. 62 (1958) 76–79, doi:10.1021/j150559a019.

[163] Hoffman, K.C., Winsche, W.E., Wiswall, R.H., Reilly, J.J., Sheehan, T.V.,Waide, C.H., Metal Hydrides as a Source of Fuel for Vehicular Propulsion, 1969. Retrieved from https://doi.org/10.4271/690232.
[164] J.J. Reilly, R.H. Wiswall, Formation and properties of iron titanium hydride, Inorg. Chem. 13 (1974) 218–222, doi:10.1021/ic50131a042.
[165] R. Burch, N.B. Mason, Absorption of hydrogen by titanium–cobalt and titanium–nickel intermetallic alloys. Part 1.—Experimental results, J. Chem. Soc., Faraday Trans. 1 75 (1979) 561–577, doi:10.1039/F19797500561.
[166] Reilly, J.J.,Johnson, J.R., Titanium alloy hydrides - Their properties and applications, 2022.
[167] K. Oguro, Y. Osumi, H. Suzuki, A. Kato, Y. Imamura, H. Tanaka, Hydrogen storage properties of TiFe1−xNiyMz alloys, J. Less Common Metals 89 (1983) 275–279, doi:10.1016/0022-5088(83)90280-1.
[168] Mitrokhin, S.V., Verbetsky, V.N., Cunmao, H., Yufen, Z.J.Z.f.P.C., Hydriding characteristics of FeTi-based Ti-Fe-V-Mn alloy*, 181 (1993) 283–287.
[169] C.H. Chiang, Z.H. Chin, T.P. Perng, Hydrogenation of TiFe by high-energy ball milling, J. Alloys Compd. 307 (2000) 259–265, doi:10.1016/S0925-8388(00)00827-6.
[170] M.W. Davids, M. Lototskyy, A. Nechaev, Q. Naidoo, M. Williams, Y. Klochko, Surface modification of TiFe hydrogen storage alloy by metal-organic chemical vapour deposition of palladium, Int. J. Hydrogen Energy 36 (2011) 9743–9750, doi:10.1016/j.ijhydene.2011.05.036.
[171] K. Benyelloul, Y. Bouhadda, M. Bououdina, H.I. Faraoun, H. Aourag, L. Seddik, The effect of hydrogen on the mechanical properties of FeTi for hydrogen storage applications, Int. J. Hydrogen Energy 39 (2014) 12667–12675, doi:10.1016/j.ijhydene.2014.05.190.
[172] K. Edalati, J. Matsuda, A. Yanagida, E. Akiba, Z. Horita, Activation of TiFe for hydrogen storage by plastic deformation using groove rolling and high-pressure torsion: similarities and differences, Int. J. Hydrogen Energy 39 (2014) 15589–15594, doi:10.1016/j.ijhydene.2014.07.124.
[173] W. Ali, M. Li, P. Gao, C. Wu, Q. Li, X. Lu, C. Li, Hydrogenation properties of Ti-Fe-Mn alloy with Cu and Y as additives, Int. J. Hydrogen Energy 42 (2017) 2229–2238, doi:10.1016/j.ijhydene.2016.09.037.
[174] N. Endo, S. Suzuki, K. Goshome, T. Maeda, Operation of a bench-scale TiFe-based alloy tank under mild conditions for low-cost stationary hydrogen storage, Int. J. Hydrogen Energy 42 (2017) 5246–5251, doi:10.1016/j.ijhydene.2016.11.088.
[175] R.A. Silva, R.M. Leal Neto, D.R. Leiva, T.T. Ishikawa, C.S. Kiminami, A.M. Jorge, W.J. Botta, Room temperature hydrogen absorption by Mg and MgTiFe nanocomposites processed by high-energy ball milling, Int. J. Hydrogen Energy 43 (2018) 12251–12259, doi:10.1016/j.ijhydene.2018.04.174.
[176] R.B. Falcão, E.D.C.C. Dammann, C.J. Rocha, M. Durazzo, R.U. Ichikawa, L.G. Martinez, W.J. Botta, R.M. Leal Neto, An alternative route to produce easily activated nanocrystalline TiFe powder, Int. J. Hydrogen Energy 43 (2018) 16107–16116, doi:10.1016/j.ijhydene.2018.07.027.
[177] P. Lv, Z. Liu, V. Dixit, Improved hydrogen storage properties of TiFe alloy by doping (Zr+2V) additive and using mechanical deformation, Int. J. Hydrogen Energy 44 (2019) 27843–27852, doi:10.1016/j.ijhydene.2019.08.249.
[178] J. Manna, B. Tougas, J. Huot, First hydrogenation kinetics of Zr and Mn doped TiFe alloy after air exposure and reactivation by mechanical treatment, Int. J. Hydrogen Energy 45 (2020) 11625–11631, doi:10.1016/j.ijhydene.2020.02.043.
[179] H. Shang, Y. Li, Y. Zhang, D. Zhao, Y. Qi, X. Xu, Investigations on hydrogen storage performances and mechanisms of as-cast TiFe0.8-mNi0.2Com (m=0, 0.03, 0.05 and 0.1) alloys, Int. J. Hydrogen Energy 46 (2021) 17840–17852, doi:10.1016/j.ijhydene.2021.02.179.
[180] A. Zeaiter, D. Chapelle, F. Cuevas, A. Maynadier, M. Latroche, Milling effect on the microstructural and hydrogenation properties of TiFe0.9Mn0.1 alloy, Powder Technol. 339 (2018) 903–910, doi:10.1016/j.powtec.2018.08.085.
[181] S. Pati, S. Trimbake, M. Vashistha, P. Sharma, Tailoring the activation behaviour and oxide resistant properties of TiFe alloys by doping with Mn, Int. J. Hydrogen Energy 46 (2021) 34830–34838, doi:10.1016/j.ijhydene.2021.08.041.
[182] A.K. Patel, D. Siemiaszko, J. Dworecka-Wójcik, M. Polański, Just shake or stir. About the simplest solution for the activation and hydrogenation of an FeTi hydrogen storage alloy, Int. J. Hydrogen Energy 47 (2022) 5361–5371, doi:10.1016/j.ijhydene.2021.11.136.
[183] M. Bedrunka, N. Bornemann, G. Steinebach, D. Reith, A metal hydride system for a forklift: feasibility study on on-board chemical storage of hydrogen using numerical simulation, Int. J. Hydrogen Energy 47 (2022) 12240–12250, doi:10.1016/j.ijhydene.2021.05.179.
[184] V. Kumar, P. Kumar, K. Takahashi, P. Sharma, Hydrogen adsorption studies of TiFe surfaces via 3-d transition metal substitution, Int. J. Hydrogen Energy 47 (2022) 16156–16164, doi:10.1016/j.ijhydene.2022.03.138.
[185] J.O. Fadonougbo, K.B. Park, T.-.W. Na, C.-.S. Park, H.-.K. Park, W.-.S. Ko, An integrated computational and experimental method for predicting hydrogen plateau pressures of TiFe1-xMx-based room temperature hydrides, Int. J. Hydrogen Energy 47 (2022) 17673–17682, doi:10.1016/j.ijhydene.2022.03.240.
[186] J. Barale, E.M. Dematteis, G. Capurso, B. Neuman, S. Deledda, P. Rizzi, F. Cuevas, M. Baricco, TiFe0.85Mn0.05 alloy produced at industrial level for a hydrogen storage plant, Int. J. Hydrogen Energy 47 (2022) 29866–29880, doi:10.1016/j.ijhydene.2022.06.295.
[187] Reilly, J.J.,Wiswall, R.H., The effect of minor constituents on the properties of vanadium and niobium hydrides, 2022.
[188] Lynch, J.F., Maeland, A.J.,Libowitz, G.G.J.Z.f.P.C., Lattice parameter variation and thermodynamics of dihydride formation in the Vanadium-Rich V—Ti—Fe/H2 System*, 145 (1985) 51–59.
[189] I.G. Konstanchuk, E.Y. Ivanov, B.B. Bokhonov, V.V. Boldyrev, Hydriding properties of mechanically alloyed icosahedral phase Ti45Zr38Ni17, J. Alloys Compd. 319 (2001) 290–295, doi:10.1016/S0925-8388(01)00911-2.
[190] M. Gao, S. Zhang, H. Miao, Y. Liu, H. Pan, Pulverization mechanism of the multiphase Ti–V-based hydrogen storage electrode alloy during charge/discharge cycling, J. Alloys Compd. 489 (2010) 552–557, doi:10.1016/j.jallcom.2009.09.107.
[191] M. Aoki, T. Noritake, A. Ito, M. Ishikiriyama, S.-i. Towata, Improvement of cyclic durability of Ti–Cr–V alloy by Fe substitution, Int. J. Hydrogen Energy 36 (2011) 12329–12332, doi:10.1016/j.ijhydene.2011.07.019.
[192] A. Kamble, P. Sharma, J. Huot, Effect of doping and particle size on hydrogen absorption properties of BCC solid solution 52Ti-12V-36Cr, Int. J. Hydrogen Energy 42 (2017) 11523–11527, doi:10.1016/j.ijhydene.2017.02.137.
[193] M. Novelli, K. Edalati, S. Itano, H.-.W. Li, E. Akiba, Z. Horita, T. Grosdidier, Microstructural details of hydrogen diffusion and storage in Ti–V–Cr alloys activated through surface and bulk severe plastic deformation, Int. J. Hydrogen Energy 45 (2020) 5326–5336, doi:10.1016/j.ijhydene.2019.07.058.
[194] J. Liu, J. Xu, S. Sleiman, X. Chen, S. Zhu, H. Cheng, J. Huot, Microstructure and hydrogen storage properties of Ti–V–Cr based BCC-type high entropy alloys, Int. J. Hydrogen Energy 46 (2021) 28709–28718, doi:10.1016/j.ijhydene.2021.06.137.
[195] S.-i. Towata, T. Noritake, A. Itoh, M. Aoki, K. Miwa, Cycle durability of Ti–Cr–V alloys partially substituted by Nb or Fe, J. Alloys Compd. 580 (2013) S226–S228, doi:10.1016/j.jallcom.2013.03.163.
[196] S. Sleiman, J. Huot, Effect of particle size, pressure and temperature on the activation process of hydrogen absorption in TiVZrHfNb high entropy alloy, J. Alloys Compd. 861 (2021) 158615, doi:10.1016/j.jallcom.2021.158615.
[197] Z. Hang, L. Chen, X. Xiao, Z. Yao, L. Shi, Y. Feng, L. Yang, Microstructure and hydrogen storage properties of Ti10+xV80-xFe6Zr4 (x=0∼15) alloys, Int. J. Hydrogen Energy 46 (2021) 27622–27630, doi:10.1016/j.ijhydene.2021.06.019.
[198] A. Kumar, T.P. Yadav, N.K. Mukhopadhyay, Notable hydrogen storage in Ti–Zr–V–Cr–Ni high entropy alloy, Int. J. Hydrogen Energy 47 (2022) 22893–22900, doi:10.1016/j.ijhydene.2022.05.107.
[199] J. Cermak, L. Kral, P. Roupcova, Hydrogen storage in TiVCrMo and TiZrNbHf multiprinciple-element alloys and their catalytic effect upon hydrogen storage in Mg, Renew. Energy 188 (2022) 411–424, doi:10.1016/j.renene.2022.02.
[200] Sustainability, U. D. R. a. I. f. V. E. a. E., MAy 2017). Target Explanation Document: onboard Hydrogen Storage for Light-Duty Fuel Cell Vehicles. 2014 Retrieved 19.01.2023, 2023, from https://www.energy.gov/sites/default/files/2017/05/f34/fcto_targets_onboard_hydro_storage_explanation.pdf.
[201] B. Vigeholm, J. Kjøller, B. Larsen, A.S. Pedersen, Formation and decomposition of magnesium hydride, J. Less Common Metals 89 (1983) 135–144, doi:10.1016/0022-5088(83)90259-X.
[202] Noritake, T., Aoki, M., Towata, S., Seno, Y., Hirose, Y., Nishibori, E., Takata, M.,Sakata, M., Chemical bonding of hydrogen in MgH2, 81 (2002) 2008–2010. 10.1063/1.1506007.
[203] Z. Wu, J. Fang, N. Liu, J. Wu, L. Kong, The improvement in hydrogen storage performance of MgH2 enabled by multilayer Ti3C2, Micromachines (Basel) 12 (2021) 1190.
[204] W. Liu, E.J. Setijadi, K.-.F. Aguey-Zinsou, Tuning the thermodynamic properties of MgH2 at the nanoscale via a catalyst or destabilizing element coating strategy, J. Phys. Chem. C 118 (2014) 27781–27792, doi:10.1021/jp5097663.
[205] X.L. Zhang, Y.F. Liu, X. Zhang, J.J. Hu, M.X. Gao, H.G. Pan, Empowering hydrogen storage performance of MgH2 by nanoengineering and nanocatalysis, Mater. Today Nano 9 (2020) 100064, doi:10.1016/j.mtnano.2019.100064.
[206] C. Zhou, Z.Z. Fang, J. Lu, X. Zhang, Thermodynamic and kinetic destabilization of magnesium hydride using Mg–In solid solution alloys, J. Am. Chem. Soc. 135 (2013) 10982–10985, doi:10.1021/ja4058794.
[207] T.T. Le, C. Pistidda, V.H. Nguyen, P. Singh, P. Raizada, T. Klassen, M. Dornheim, Nanoconfinement effects on hydrogen storage properties of MgH2 and LiBH4, Int. J. Hydrogen Energy 46 (2021) 23723–23736, doi:10.1016/j.ijhydene.2021.04.150.
[208] Y. Wang, Y. Wang, Recent advances in additive-enhanced magnesium hydride for hydrogen storage, Progress Nat. Sci. 27 (2017) 41–49, doi:10.1016/j.pnsc.2016.12.016.
[209] J. Zhang, Z. Li, Y. Wu, X. Guo, J. Ye, B. Yuan, S. Wang, L. Jiang, Recent advances on the thermal destabilization of Mg-based hydrogen storage materials, RSC Adv. 9 (2019) 408–428, doi:10.1039/C8RA05596C.
[210] T.K. Nielsen, F. Besenbacher, T.R. Jensen, Nanoconfined hydrides for energy storage, Nanoscale 3 (2011) 2086–2098, doi:10.1039/C0NR00725K.
[211] H. Gleiter, Nanostructured materials: basic concepts and microstructure, Acta Mater. 48 (2000) 1–29, doi:10.1016/S1359-6454(99)00285-2.
[212] A. Schneemann, J.L. White, S. Kang, S. Jeong, L.F. Wan, E.S. Cho, T.W. Heo, D. Prendergast, J.J. Urban, B.C. Wood, M.D. Allendorf, V. Stavila, Nanostructured metal hydrides for hydrogen storage, Chem. Rev. 118 (2018) 10775–10839, doi:10.1021/acs.chemrev.8b00313.
[213] M. Paskevicius, D.A. Sheppard, C.E. Buckley, Thermodynamic changes in mechanochemically synthesized magnesium hydride nanoparticles, J. Am. Chem. Soc. 132 (2010) 5077–5083, doi:10.1021/ja908398u.
[214] Q. Zhang, Y. Huang, L. Xu, L. Zang, H. Guo, L. Jiao, H. Yuan, Y. Wang, Highly dispersed MgH2 nanoparticle–graphene nanosheet composites for hydrogen storage, ACS Appl. Nano Mater. 2 (2019) 3828–3835, doi:10.1021/acsanm.9b00694.
[215] N. Rambhujun, K.-F. Aguey-Zinsou, Halide-free Grignard reagents for the synthesis of superior MgH2 nanostructures, Int. J. Hydrogen Energy 46 (2021) 28675–28685, doi:10.1016/j.ijhydene.2021.06.095.
[216] A.R. Tanna, H.H. Joshi, Effect of high energy mechanical milling on hysteresis and dielectric properties of CaxBa1−xZrxTi1−xO3 (x = 0 and 0.1) ferroelectric materials, Mater. Res. Express 5 (2018) 096302, doi:10.1088/2053-1591/aad610.
[217] T. Czujko, E.E. Oleszek, M. Szot, New Aspects of MgH(2) morphological and structural changes during high-energy ball milling, Materials (Basel, Switzerland) (2020) 13, doi:10.3390/ma13204550.

[218] A. Zaluska, L. Zaluski, J.O. Ström–Olsen, Nanocrystalline magnesium for hydrogen storage, J. Alloys Compd. 288 (1999) 217–225, doi:10.1016/S0925-8388(99)00073-0.

[219] A. Zaluska, L. Zaluski, J.O. Ström-Olsen, Synergy of hydrogen sorption in ball-milled hydrides of Mg and Mg2Ni, J. Alloys Compd. 289 (1999) 197–206, doi:10.1016/S0166-0462(99)00013-7.

[220] R.A. Varin, T. Czujko, C. Chiu, Z. Wronski, Particle size effects on the desorption properties of nanostructured magnesium dihydride (MgH2) synthesized by controlled reactive mechanical milling (CRMM), J. Alloys Compd. 424 (2006) 356–364, doi:10.1016/j.jallcom.2005.12.087.

[221] C. Shen, K.-.F. Aguey-Zinsou, Can γ-MgH2 improve the hydrogen storage properties of magnesium? J. Mater. Chem. A 5 (2017) 8644–8652, doi:10.1039/C7TA01724C.

[222] M. Lototskyy, J. Goh, M.W. Davids, V. Linkov, L. Khotseng, B. Ntsendwana, R. Denys, V.A. Yartys, Nanostructured hydrogen storage materials prepared by high-energy reactive ball milling of magnesium and ferrovanadium, Int. J. Hydrogen Energy 44 (2019) 6687–6701, doi:10.1016/j.ijhydene.2019.01.135.

[223] A. Baran, M. Knioła, T. Rogala, M. Polanski, New horizon in mechanochemistry—High-temperature, high-pressure mechanical synthesis in a planetary ball mill—With magnesium hydride synthesis as an example, Int. J. Hydrogen Energy 47 (2022) 35003–35016, doi:10.1016/j.ijhydene.2022.08.080.

[224] Y. Huang, G. Xia, J. Chen, B. Zhang, Q. Li, X. Yu, One-step uniform growth of magnesium hydride nanoparticles on graphene, Progress Nat. Sci. 27 (2017) 81–87, doi:10.1016/j.pnsc.2016.12.015.

[225] L.J. Huang, S.T. Shi, J. Cui, J.W. Liu, L.Z. Ouyang, H. Wang, Thermally-assisted milling and hydrogenolysis for synthesizing ultrafine MgH2 with destabilized thermodynamics, Nanotechnology 32 (2021) 285402, doi:10.1088/1361-6528/abf20e.

[226] K.-.J. Jeon, H.R. Moon, A.M. Ruminski, B. Jiang, C. Kisielowski, R. Bardhan, J.J. Urban, Air-stable magnesium nanocomposites provide rapid and high-capacity hydrogen storage without using heavy-metal catalysts, Nat. Mater. 10 (2011) 286–290, doi:10.1038/nmat2978.

[227] M.S.L. Hudson, K. Takahashi, A. Ramesh, S. Awasthi, A.K. Ghosh, P. Ravindran, O.N. Srivastava, Graphene decorated with Fe nanoclusters for improving the hydrogen sorption kinetics of MgH2 – experimental and theoretical evidence, Catal. Sci. Technol. 6 (2016) 261–268, doi:10.1039/C5CY01016K.

[228] F. Guo, T. Zhang, L. Shi, L. Song, Hydrogen absorption/desorption cycling performance of Mg-based alloys with in-situ formed Mg2Ni and LaHx (x = 2, 3) nanocrystallines, J. Magnes. Alloys (2021), doi:10.1016/j.jma.2021.06.013.

[229] J. Zhang, S. Yan, H. Qu, Recent progress in magnesium hydride modified through catalysis and nanoconfinement, Int. J. Hydrogen Energy 43 (2018) 1545–1565, doi:10.1016/j.ijhydene.2017.11.135.

[230] C. Comanescu, Recent Development in Nanoconfined Hydrides for Energy Storage, Int. J. Mol. Sci. 23 (13) (2022) Retrieved from, doi:10.3390/ijms23137111.

[231] R. Gosalawit–Utke, T.K. Nielsen, K. Pranzas, I. Saldan, C. Pistidda, F. Karimi, D. Laipple, J. Skibsted, T.R. Jensen, T. Klassen, M. Dornheim, 2LiBH4–MgH2 in a resorcinol–furfural carbon aerogel scaffold for reversible hydrogen storage, J. Phys. Chem. C 116 (2012) 1526–1534, doi:10.1021/jp2088127.

[232] D. Pukazhselvan, G. Capurso, A. Maddalena, S. Lo Russo, D.P. Fagg, Hydrogen storage characteristics of magnesium impregnated on the porous channels of activated charcoal scaffold, Int. J. Hydrogen Energy 39 (2014) 20045–20053, doi:10.1016/j.ijhydene.2014.10.038.

[233] Zhang, Z., Wang, Y., Wang, H., Xue, X.,Lin, Q., Metal-Organic Frameworks Promoted Hydrogen Storage Properties of Magnesium Hydride for In-Situ Resource Utilization (ISRU) on Mars, 8 (2021). 10.3389/fmats.2021.766288.

[234] P. Jani, H. Desai, B.S. Madhukar, A. Tanna, Investigations of calcium ferrite nanoparticles synthesized by sol-gel auto combustion and solution mixture methods, Mater. Res. Innovat. 26 (2022) 189–195, doi:10.1080/14328917.2021.1932318.

[235] P.E. de Jongh, T.M. Eggenhuisen, Melt infiltration: an emerging technique for the preparation of novel functional nanostructured materials, Adv. Mater. 25 (2013) 6672–6690, doi:10.1002/adma.201301912.

[236] A.F. Gross, C.C. Ahn, S.L. Van Atta, P. Liu, J.J. Vajo, Fabrication and hydrogen sorption behaviour of nanoparticulate MgH2 incorporated in a porous carbon host, Nanotechnology 20 (2009) 204005, doi:10.1088/0957-4484/20/20/204005.

[237] Y. Liu, J. Zou, X. Zeng, X. Wu, H. Tian, W. Ding, J. Wang, A. Walter, Study on hydrogen storage properties of Mg nanoparticles confined in carbon aerogels, Int. J. Hydrogen Energy 38 (2013) 5302–5308, doi:10.1016/j.ijhydene.2013.02.012.

[238] Z. Ma, S. Panda, Q. Zhang, F. Sun, D. Khan, W. Ding, J. Zou, Improving hydrogen sorption performances of MgH2 through nanoconfinement in a mesoporous CoS nano-boxes scaffold, Chem. Eng. J. 406 (2021) 126790, doi:10.1016/j.cej.2020.126790.

[239] L. Ren, W. Zhu, Y. Li, X. Lin, H. Xu, F. Sun, C. Lu, J. Zou, Oxygen vacancy-rich 2D TiO2 nanosheets: a bridge toward high stability and rapid hydrogen storage kinetics of nano-confined MgH2, Nano-Micro Lett. 14 (2022) 144, doi:10.1007/s40820-022-00891-9.

[240] W. Zhu, L. Ren, C. Lu, H. Xu, F. Sun, Z. Ma, J. Zou, Nanoconfined and in Situ Catalyzed MgH2 Self-Assembled on 3D Ti3C2 MXene Folded Nanosheets with Enhanced Hydrogen Sorption Performances, ACS Nano 15 (2021) 18494–18504 10.1021/acsnano.1c08343.

[241] L. Ren, W. Zhu, Q. Zhang, C. Lu, F. Sun, X. Lin, J. Zou, MgH2 confinement in MOF-derived N-doped porous carbon nanofibers for enhanced hydrogen storage, Chem. Eng. J. 434 (2022) 134701, doi:10.1016/j.cej.2022.134701.

[242] J. Zhang, S. Yan, G. Xia, X. Zhou, X. Lu, L. Yu, X. Yu, P. Peng, Stabilization of low-valence transition metal towards advanced catalytic effects on the hydrogen storage performance of magnesium hydride, J. Magnes. Alloys 9 (2021) 647–657, doi:10.1016/j.jma.2020.02.029.

[243] N. Hanada, T. Ichikawa, H. Fujii, Catalytic effect of nanoparticle 3d-transition metals on hydrogen storage properties in magnesium hydride MgH2 prepared by mechanical milling, J. Phys. Chem. B 109 (2005) 7188–7194, doi:10.1021/jp044576c.

[244] W. Oelerich, T. Klassen, R. Bormann, Metal oxides as catalysts for improved hydrogen sorption in nanocrystalline Mg-based materials, J. Alloys Compd. 315 (2001) 237–242, doi:10.1016/S0925-8388(00)01284-6.

[245] S.T. Sabitu, A.J. Goudy, Dehydrogenation kinetics and modeling studies of MgH2 enhanced by transition metal oxide catalysts using constant pressure thermodynamic driving forces, Metals (Basel) 2 (3) (2012) 219–228 Retrieved from, doi:10.3390/met2030219.

[246] T. Sadhasivam, M. Sterlin Leo Hudson, S.K. Pandey, A. Bhatnagar, M.K. Singh, K. Gurunathan, O.N. Srivastava, Effects of nano size mischmetal and its oxide on improving the hydrogen sorption behaviour of MgH2, Int. J. Hydrogen Energy 38 (2013) 7353–7362, doi:10.1016/j.ijhydene.2013.04.040.

[247] R. Kesarwani, V. Shukla, M.S.L. Hudson, M.A. Shaz, Improved hydrogen storage characteristics of magnesium hydride using dual auto catalysts (MgF2+CsH), Int. J. Hydrogen Energy 47 (2022) 27049–27058, doi:10.1016/j.ijhydene.2022.06.035.

[248] M. Jangir, A. Jain, S. Yamaguchi, T. Ichikawa, C. Lal, I.P. Jain, Catalytic effect of TiF4 in improving hydrogen storage properties of MgH2, Int. J. Hydrogen Energy 41 (2016) 14178–14183, doi:10.1016/j.ijhydene.2016.06.238.

[249] L.P. Ma, X.D. Kang, H.B. Dai, Y. Liang, Z.Z. Fang, P.J. Wang, P. Wang, H.M. Cheng, Superior catalytic effect of TiF3 over TiCl3 in improving the hydrogen sorption kinetics of MgH2: catalytic role of fluorine anion, Acta Mater. 57 (2009) 2250–2258, doi:10.1016/j.actamat.2009.01.025.

[250] I.E. Malka, M. Pisarek, T. Czujko, J. Bystrzycki, A study of the ZrF4, NbF5, TaF5, and TiCl3 influences on the MgH2 sorption properties, Int. J. Hydrogen Energy 36 (2011) 12909–12917, doi:10.1016/j.ijhydene.2011.07.020.

[251] Z. Tian, Z. Wang, P. Yao, C. Xia, T. Yang, Q. Li, Hydrogen storage behaviors of magnesium hydride catalyzed by transition metal carbides, Int. J. Hydrogen Energy 46 (2021) 40203–40216, doi:10.1016/j.ijhydene.2021.09.212.

[252] S.K. Verma, M.A. Shaz, T.P. Yadav, Enhanced hydrogen absorption and desorption properties of MgH2 with graphene and vanadium disulfide, Int. J. Hydrogen Energy (2022), doi:10.1016/j.ijhydene.2021.12.269.

[253] P. Wang, Z. Tian, Z. Wang, C. Xia, T. Yang, X. Ou, Improved hydrogen storage properties of MgH2 using transition metal sulfides as catalyst, Int. J. Hydrogen Energy 46 (2021) 27107–27118, doi:10.1016/j.ijhydene.2021.05.172.

[254] K.C. Tome, S. Xi, Y. Fu, C. Lu, N. Lu, M. Guan, S. Zhou, H. Yu, Remarkable catalytic effect of Ni and ZrO2 nanoparticles on the hydrogen sorption properties of MgH2, Int. J. Hydrogen Energy 47 (2022) 4716–4724, doi:10.1016/j.ijhydene.2021.11.102.

[255] L. Zhang, Z. Sun, Z. Yao, L. Yang, N. Yan, X. Lu, B. Xiao, X. Zhu, L. Chen, Excellent catalysis of Mn3O4 nanoparticles on the hydrogen storage properties of MgH2: an experimental and theoretical study, Nanoscale Adv. 2 (2020) 1666–1675, doi:10.1039/D0NA00137F.

[256] Z. Wang, Z. Ren, N. Jian, M. Gao, J. Hu, F. Du, H. Pan, Y. Liu, Vanadium oxide nanoparticles supported on cubic carbon nanoboxes as highly active catalyst precursors for hydrogen storage in MgH_2, J. Mater. Chem. A 6 (2018) 16177–16185, doi:10.1039/C8TA05437A.

[257] S.K. Pandey, A. Bhatnagar, R.R. Shahi, M.S. Hudson, M.K. Singh, O.N. Srivastava, Effect of TiO2 nanoparticles on the hydrogen sorption characteristics of magnesium hydride, J. Nanosci. Nanotechnol. 13 (2013) 5493–5499, doi:10.1166/jnn.2013.7516.

[258] H. Yu, S. Bennici, A. Auroux, Hydrogen storage and release: kinetic and thermodynamic studies of MgH2 activated by transition metal nanoparticles, Int. J. Hydrogen Energy 39 (2014) 11633–11641, doi:10.1016/j.ijhydene.2014.05.069.

[259] Q. Hou, J. Zhang, G. XinTao, G. Xu, X. Yang, Synthesis of low-cost biomass charcoal-based Ni nanocatalyst and evaluation of their kinetic enhancement of MgH2, Int. J. Hydrogen Energy 47 (2022) 15209–15223, doi:10.1016/j.ijhydene.2022.03.040.

[260] A. Jubair, M.A. Rahman, M.M.R. Khan, M.W. Rahman, Catalytic role of binary oxides (CuO and Al2O3) on hydrogen storage in MgH2, Environ. Prog. Sustain. Energy 42 (2023) e13940, doi:10.1002/ep.13940.

[261] S.K. Pandey, A. Bhatnagar, V. Shukla, R. Kesarwani, U. Deshpandey, T.P. Yadav, Catalytic mechanism of TiO2 quantum dots on the de/re-hydrogenation characteristics of magnesium hydride, Int. J. Hydrogen Energy 46 (2021) 37340–37350, doi:10.1016/j.ijhydene.2021.09.006.

[262] Y. Jia, J. Zou, X. Yao, Catalytically enhanced dehydrogenation of MgH2 by activated carbon supported Pd–VOx (x=2.38) nanocatalyst, Int. J. Hydrogen Energy 37 (2012) 13393–13399, doi:10.1016/j.ijhydene.2012.06.063.

[263] H. Cheng, G. Chen, Y. Zhang, Y. Zhu, L. Li, Boosting low-temperature de/re-hydrogenation performances of MgH2 with Pd-Ni bimetallic nanoparticles supported by mesoporous carbon, Int. J. Hydrogen Energy 44 (2019) 10777–10787, doi:10.1016/j.ijhydene.2019.02.218.

[264] B. Ding, X. Wu, Transition metal oxides anchored on graphene/carbon nanotubes conductive network as both the negative and positive electrodes for asymmetric supercapacitor, J. Alloys Compd. 842 (2020) 155838 155838-, doi:10.1016/j.jallcom.2020.155838.

[265] M.A. Lillo-Ródenas, K.F. Aguey-Zinsou, D. Cazorla-Amorós, A. Linares-Solano, Z.X. Guo, Effects of carbon-supported nickel catalysts on MgH2 decomposition, J. Phys. Chem. C 112 (2008) 5984–5992, doi:10.1021/jp711749h.

[266] Zeng, L., Qing, P., Cai, F., Huang, X., Liu, H., Lan, Z.,Guo, J., Enhanced hydrogen storage properties of MgH2 using a Ni and TiO2 Co-doped reduced graphene oxide nanocomposite as a catalyst, 8 (2020). 10.3389/fchem.2020.00207.

[267] G. Chen, Y. Zhang, J. Chen, X. Guo, Y. Zhu, L. Li, Enhancing hydrogen storage performances of MgH2 by Ni nano-particles over mesoporous carbon CMK-3, Nanotechnology 29 (2018) 265705, doi:10.1088/1361-6528/aabcf3.

[268] K. Kajiwara, H. Sugime, S. Noda, N. Hanada, Fast and stable hydrogen storage in the porous composite of MgH2 with Nb2O5 catalyst and carbon nanotube, J. Alloys Compd. 893 (2022) 162206, doi:10.1016/j.jallcom.2021.162206.
[269] Sun, Z., Lu, X., Nyahuma, F.M., Yan, N., Xiao, J., Su, S.,Zhang, L., Enhancing hydrogen storage properties of MgH2 by transition metals and carbon materials: a brief review, 8 (2020). 10.3389/fchem.2020.00552.
[270] H. Gi, K. Shinzato, R. Balgis, T. Ogi, M. Sadakane, Y. Wang, S. Isobe, H. Miyaoka, T. Ichikawa, Effective factor on catalysis of niobium oxide for magnesium, ACS Omega 5 (2020) 21906–21912, doi:10.1021/acsomega.0c03101.
[271] K. Shinzato, H. Gi, T. Murayama, M. Sadakane, Y. Wang, S. Isobe, T. Ichikawa, H. Miyaoka, Catalytic activities of various niobium oxides for hydrogen absorption/desorption reactions of magnesium, ACS Omega 6 (2021) 23564–23569, doi:10.1021/acsomega.1c03687.
[272] M. Zhang, X. Xiao, Z. Hang, M. Chen, X. Wang, N. Zhang, L. Chen, Superior catalysis of NbN nanoparticles with intrinsic multiple valence on reversible hydrogen storage properties of magnesium hydride, Int. J. Hydrogen Energy 46 (2021) 814–822, doi:10.1016/j.ijhydene.2020.09.173.
[273] Z. Lan, H. Fu, R. Zhao, H. Liu, W. Zhou, H. Ning, J. Guo, Roles of in situ-formed NbN and Nb2O5 from N-doped Nb2C MXene in regulating the re/hydrogenation and cycling performance of magnesium hydride, Chem. Eng. J. 431 (2022) 133985, doi:10.1016/j.cej.2021.133985.
[274] H. Shen, H. Li, Z. Yang, C. Li, Magic of hydrogen spillover: understanding and application, Green Energy Environ. 7 (2022) 1161–1198, doi:10.1016/j.gee.2022.01.013.
[275] Q. Hou, X. Yang, J. Zhang, W. Yang, E. Lv, Catalytic effect of NiO/C derived from Ni-UMOFNs on the hydrogen storage performance of magnesium hydride, J. Alloys Compd. 899 (2022) 163314, doi:10.1016/j.jallcom.2021.163314.
[276] Y. Shao, H. Gao, Q. Tang, Y. Liu, J. Liu, Y. Zhu, J. Zhang, L. Li, X. Hu, Z. Ba, Ultrafine TiO2 nanoparticles supported on three-dimensionally ordered macroporous structure for improving the hydrogen storage performance of MgH2, Appl. Surf. Sci. 585 (2022) 152561, doi:10.1016/j.apsusc.2022.152561.
[277] H. Gao, R. Shi, Y. Liu, Y. Zhu, J. Zhang, L. Li, X. Hu, Facet-dependent catalytic activity of two-dimensional Ti3C2Tx MXene on hydrogen storage performance of MgH2, J. Magnes. Alloys (2022), doi:10.1016/j.jma.2022.02.006.
[278] H. Gao, R. Shi, Y. Shao, Y. Liu, Y. Zhu, J. Zhang, L. Li, Catalysis derived from flower-like Ni MOF towards the hydrogen storage performance of magnesium hydride, Int. J. Hydrogen Energy 47 (2022) 9346–9356, doi:10.1016/j.ijhydene.2022.01.020.
[279] J. Yang, K. Zhang, Z. Ma, X. Zhang, T. Huang, S. Panda, J. Zou, Trimesic acid-Ni based metal organic framework derivative as an effective destabilizer to improve hydrogen storage properties of MgH2, Int. J. Hydrogen Energy 46 (2021) 28134–28143, doi:10.1016/j.ijhydene.2021.06.083.
[280] A.M. Lakhnik, I.M. Kirian, A.D. Rud, The Mg/MAX-phase composite for hydrogen storage, Int. J. Hydrogen Energy 47 (2022) 7274–7280, doi:10.1016/j.ijhydene.2021.02.081.
[281] Y. Zhang, J. Zheng, Z. Lu, M. Song, J. He, F. Wu, L. Zhang, Boosting the hydrogen storage performance of magnesium hydride with metal organic framework-derived Cobalt@Nickel oxide bimetallic catalyst, Chin. J. Chem. Eng. 52 (2022) 161–171, doi:10.1016/j.cjche.2022.06.026.
[282] H. Gao, R. Shi, Y. Shao, Y. Liu, Y. Zhu, J. Zhang, X. Hu, L. Li, Z. Ba, One-step self-assembly of TiO2/MXene heterostructures for improving the hydrogen storage performance of magnesium hydride, J. Alloys Compd. 895 (2022) 162635, doi:10.1016/j.jallcom.2021.162635.
[283] X. Huang, X. Xiao, W. Zhang, X. Fan, L. Zhang, C. Cheng, S. Li, H. Ge, Q. Wang, L. Chen, Transition metal (Co, Ni) nanoparticles wrapped with carbon and their superior catalytic activities for the reversible hydrogen storage of magnesium hydride, Phys. Chem. Chem. Phys. 19 (2017) 4019–4029, doi:10.1039/C6CP07852D.
[284] Z. Ma, J. Zhang, Y. Zhu, H. Lin, Y. Liu, Y. Zhang, D. Zhu, L. Li, Facile synthesis of carbon supported nano-ni particles with superior catalytic effect on hydrogen storage kinetics of MgH_2, ACS Appl. Energy Mater. 1 (2018) 1158–1165, doi:10.1021/acsaem.7b00266.
[285] M. Chen, X. Xiao, X. Wang, Y. Lu, M. Zhang, J. Zheng, L. Chen, Self-templated carbon enhancing catalytic effect of ZrO_2 nanoparticles on the excellent dehydrogenation kinetics of MgH_2, Carbon N Y 166 (2020) 46–55, doi:10.1016/j.carbon.2020.05.025.
[286] S. Wang, M. Gao, Z. Yao, K. Xian, M. Wu, Y. Liu, W. Sun, H. Pan, High-loading, ultrafine Ni nanoparticles dispersed on porous hollow carbon nanospheres for fast (de)hydrogenation kinetics of MgH_2, J. Magnes. Alloys 10 (2022) 3354–3366, doi:10.1016/j.jma.2021.05.004.
[287] Z. Lan, X. Wen, L. Zeng, Z. Luo, H. Liang, W. Shi, F. Hong, H. Liu, H. Ning, W. Zhou, J. Guo, In situ incorporation of highly dispersed nickel and vanadium trioxide nanoparticles in nanoporous carbon for the hydrogen storage performance enhancement of magnesium hydride, Chem. Eng. J. 446 (2022) 137261, doi:10.1016/j.cej.2022.137261.
[288] Y. Zhao, Y. Zhu, J. Liu, Z. Ma, J. Zhang, Y. Liu, Y. Li, L. Li, Enhancing hydrogen storage properties of MgH_2 by core-shell CoNi@C, J. Alloys Compd. 862 (2021) 158004, doi:10.1016/j.jallcom.2020.158004.
[289] S. Ren, Y. Fu, L. Zhang, L. Cong, Y. Xie, H. Yu, W. Wang, Y. Li, L. Jian, Y. Wang, S. Han, An improved hydrogen storage performance of MgH_2 enabled by core-shell structure Ni/Fe_3O_4@MIL, J. Alloys Compd. 892 (2022) 162048, doi:10.1016/j.jallcom.2021.162048.
[290] Z. Ding, Y. Fu, L. Zhang, I.A. Rodríguez-Pérez, H. Zhang, W. Wang, Y. Li, S. Han, Improve hydrogen sorption kinetics of MgH_2 by doping carbon-encapsulated iron-nickel nanoparticles, J. Alloys Compd. 843 (2020) 156035, doi:10.1016/j.jallcom.2020.156035.
[291] H.C. Zhong, H. Wang, L.Z. Ouyang, Improving the hydrogen storage properties of MgH_2 by reversibly forming Mg–Al solid solution alloys, Int. J. Hydrogen Energy 39 (2014) 3320–3326, doi:10.1016/j.ijhydene.2013.12.074.
[292] J. Cermak, L. Kral, P. Roupcova, Significantly decreased stability of MgH_2 in the Mg-In-C alloy system: long-period-stacking-ordering as a new way how to improve performance of hydrogen storage alloys? Renew. Energy 150 (2020) 204–212, doi:10.1016/j.renene.2019.12.107.
[293] O. Ershova, V. Dobrovolsky, Y. Solonin, Mechanical alloys Mg-Me (Me: Ti, Fe, Ni, Al) & Mg-Me1-Me2(Me1:Al, Me2: Ti, Fe, Ni) with low resistance and improved kinetics of hydrogenation/dehydrogenation for hydrogen storage applications, Fr.-Ukr. J. Chem. 6 (2018) 31–55.
[294] X. Lu, L. Zhang, J. Zheng, X. Yu, Construction of carbon covered Mg2NiH4 nanocrystalline for hydrogen storage, J. Alloys Compd. 905 (2022) 164169, doi:10.1016/j.jallcom.2022.164169.
[295] A. Züttel, Materials for hydrogen storage, Mater. Today 6 (2003) 24–33, doi:10.1016/S1369-7021(03)00922-2.
[296] R. Schulz, S. Boily, L. Zaluski, A. Zaluka, P. Tessier, J.O. Strom-Olsen, Nanocrystalline materials for hydrogen storage, Innovat. Metal. Mater. (1995) 529–535.
[297] S. Srinivasan, D.E. Demirocak, A. Kaushik, M. Sharma, G.R. Chaudhary, N. Hickman, E. Stefanakos, Reversible Hydrogen Storage Using Nanocomposites, Appl. Sci. 10 (13) (2020) Retrieved from, doi:10.3390/app10134618.
[298] B. Bogdanović, M. Schwickardi, in: Ti-doped alkali metal aluminium hydrides as potential novel reversible hydrogen storage materials1Invited paper presented at the International Symposium on Metal–Hydrogen Systems, Les Diablerets, 253-254, 1996, pp. 1–9, doi:10.1016/S0925-8388(96)03049-6. 1997.
[299] S. Sesha, R. Luis, E. Diego, S. Elias, Light weight complex metal hydrides for reversible hydrogen storage, in: C. Luigi, A. Muhammad (Eds.), Advanced Applications of Hydrogen and Engineering Systems in the Automotive Industry (pp. Ch. 6), IntechOpen, Rijeka, 2021.
[300] Bogdanović, B., Felderhoff, M., Pommerin, A., Schüth, F.,Spielkamp, N., Advanced Hydrogen-Storage Materials Based on Sc-, Ce-, and Pr-Doped NaAlH4, 18 (2006) 1198–1201. https://doi.org/10.1002/adma.200501367.
[301] S.S. Srinivasan, H.W. Brinks, B.C. Hauback, D. Sun, C.M. Jensen, Long term cycling behavior of titanium doped $NaAlH_4$ prepared through solvent mediated milling of NaH and Al with titanium dopant precursors, J. Alloys Compd. 377 (2004) 283–289, doi:10.1016/j.jallcom.2004.01.044.
[302] A.W. Vittetoe, M.U. Niemann, S.S. Srinivasan, K. McGrath, A. Kumar, D.Y. Goswami, E.K. Stefanakos, S. Thomas, Destabilization of $LiAlH_4$ by nanocrystalline MgH_2, Int. J. Hydrogen Energy 34 (2009) 2333–2339, doi:10.1016/j.ijhydene.2009.01.025.
[303] E.M. Dematteis, M.B. Amdisen, T. Autrey, J. Barale, M.E. Bowden, C.E. Buckley, Y.W. Cho, S. Deledda, M. Dornheim, P. de Jongh, J.B. Grinderslev, G. Gizer, V. Gulino, B.C. Hauback, M. Heere, T.W. Heo, T.D. Humphries, T.R. Jensen, S.Y. Kang, Y.-.S. Lee, H.-.W. Li, S. Li, K.T. Møller, P. Ngene, S.-i. Orimo, M. Paskevicius, M. Polanski, S. Takagi, L. Wan, B.C. Wood, M. Hirscher, M. Baricco, Hydrogen storage in complex hydrides: past activities and new trends, Prog. Energy 4 (2022) 032009, doi:10.1088/2516-1083/ac7499.
[304] Su, W., Zhao, F., Ma, L., Tang, R., Dong, Y., Kong, G., Zhang, Y., Niu, S., Tang, G., Wang, Y., Pang, A., Li, W.,Wei, L., Synthesis and stability of hydrogen storage material aluminum hydride, 14 (2021) 2898.
[305] H.I. Schlesinger, H.C. Brown, E.K. Hyde, The Preparation of other borohydrides by metathetical reactions utilizing the alkali metal borohydrides1, J. Am. Chem. Soc. 75 (1953) 209–213, doi:10.1021/ja01097a055.
[306] B.R.S. Hansen, M. Paskevicius, H.-.W. Li, E. Akiba, T.R. Jensen, Metal boranes: progress and applications, Coord. Chem. Rev. 323 (2016) 60–70, doi:10.1016/j.ccr.2015.12.003.
[307] Srinivasan, S.S., Demirocak, D.E., Goswami, Y.,Stefanakos, E., Investigation of catalytic effects and compositional variations in desorption characteristics of LiNH2-nanoMgH2, 7 (2017) 701.
[308] J.R. Hattrick-Simpers, J.E. Maslar, M.U. Niemann, C. Chiu, S.S. Srinivasan, E.K. Stefanakos, L.A. Bendersky, Raman spectroscopic observation of dehydrogenation in ball-milled LiNH2–LiBH4–MgH2 nanoparticles, Int. J. Hydrogen Energy 35 (2010) 6323–6331, doi:10.1016/j.ijhydene.2010.02.101.
[309] S.X. Tao, P.H.L. Notten, R.A. van Santen, A.P.J. Jansen, First-principles predictions of potential hydrogen storage materials: nanosized Ti(core)/Mg(shell) hydrides, Phys. Rev. B 83 (2011) 195403, doi:10.1103/PhysRevB.83.195403.
[310] T. Ichikawa, S. Isobe, N. Hanada, H. Fujii, Lithium nitride for reversible hydrogen storage, J. Alloys Compd. 365 (2004) 271–276, doi:10.1016/S0925-8388(03)00637-6.
[311] Diyabalanage, H.V.K., Shrestha, R.P., Semelsberger, T.A., Scott, B.L., Bowden, M.E., Davis, B.L.,Burrell, A.K., Calcium Amidotrihydroborate: a Hydrogen Storage Material, 46 (2007) 8995–8997. https://doi.org/10.1002/anie.200702240.
[312] P. Chen, Z. Xiong, J. Luo, J. Lin, K.L. Tan, Interaction of hydrogen with metal nitrides and imides, Nature 420 (2002) 302–304, doi:10.1038/nature01210.
[313] Y. Chen, P. Wang, C. Liu, H.-.M. Cheng, Improved hydrogen storage performance of Li–Mg–N–H materials by optimizing composition and adding single-walled carbon nanotubes, Int. J. Hydrogen Energy 32 (2007) 1262–1268, doi:10.1016/j.ijhydene.2006.07.019.
[314] M. Aoki, K. Miwa, T. Noritake, G. Kitahara, Y. Nakamori, S. Orimo, S. Towata, Destabilization of LiBH4 by mixing with LiNH2, Appl. Phys. A 80 (2005) 1409–1412, doi:10.1007/s00339-004-3194-9.
[315] H.Y. Leng, T. Ichikawa, S. Hino, N. Hanada, S. Isobe, H. Fujii, New Metal–N–H system composed of Mg(NH2)2 and LiH for hydrogen storage, J. Phys. Chem. B 108 (2004) 8763–8765, doi:10.1021/jp048002j.
[316] F.E. Pinkerton, G.P. Meisner, M.S. Meyer, M.P. Balogh, M.D. Kundrat, Hydrogen desorption exceeding ten weight percent from the new quaternary hydride Li3BN2H8, J. Phys. Chem. B 109 (2005) 6–8, doi:10.1021/jp0455475.
[317] J. Hu, G. Wu, Y. Liu, Z. Xiong, P. Chen, K. Murata, K. Sakata, G. Wolf, Hydrogen release from Mg(NH2)2−MgH2 through mechanochemical reaction, J. Phys. Chem. B 110 (2006) 14688–14692, doi:10.1021/jp061279u.

[318] Xiong, Z., Wu, G., Hu, J., Liu, Y., Chen, P., Luo, W.,Wang, J., Reversible hydrogen storage by a Li–Al–N–H complex, 17 (2007) 1137–1142. https://doi.org/10.1002/adfm.200600759.
[319] Z.T. Xiong, J.J. Hu, G.T. Wu, Y.F. Liu, P. Chen, Large amount of hydrogen desorption and stepwise phase transition in the chemical reaction of NaNH2 and LiAlH4, Catal. Today 120 (2007) 287–291, doi:10.1016/j.cattod.2006.09.006.
[320] Liu, Y., Liu, T., Xiong, Z., Hu, J., Wu, G., Chen, P., Wee, A.T.S., Yang, P., Murata, K.,Sakata, K., Synthesis and structural characterization of a new alkaline earth imide: MgCa(NH)2, 2006 (2006) 4368–4373. https://doi.org/10.1002/ejic.200600492.
[321] Y.S. Chua, G. Wu, Z. Xiong, P. Chen, Investigations on the solid state interaction between LiAlH4 and NaNH2, J. Solid State Chem. 183 (2010) 2040–2044, doi:10.1016/j.jssc.2010.07.014.
[322] G. Wu, Z. Xiong, T. Liu, Y. Liu, J. Hu, P. Chen, Y. Feng, A.T.S. Wee, Synthesis and characterization of a new ternary ImideLi2Ca(NH)2, Inorg. Chem. 46 (2007) 517–521, doi:10.1021/ic060769y.
[323] Y. Kojima, M. Matsumoto, Y. Kawai, T. Haga, N. Ohba, K. Miwa, S.-i. Towata, Y. Nakamori, S.-i. Orimo, Hydrogen absorption and desorption by the Li–Al–N–H system, J. Phys. Chem. B 110 (2006) 9632–9636, doi:10.1021/jp060525z.
[324] M.U. Niemann, S.S. Srinivasan, A. Kumar, E.K. Stefanakos, D.Y. Goswami, K. McGrath, Processing analysis of the ternary LiNH2–MgH2–LiBH4 system for hydrogen storage, Int. J. Hydrogen Energy 34 (2009) 8086–8093, doi:10.1016/j.ijhydene.2009.07.065.
[325] A. Züttel, S. Rentsch, P. Fischer, P. Wenger, P. Sudan, P. Mauron, C. Emmenegger, Hydrogen storage properties of LiBH4, J. Alloys Compd. 356-357 (2003) 515–520, doi:10.1016/S0925-8388(02)01253-7.
[326] J.P. Soulié, G. Renaudin, R. Černý, K. Yvon, Lithium boro-hydride LiBH4: I. Crystal structure, J. Alloys Compd. 346 (2002) 200–205, doi:10.1016/S0925-8388(02)00521-2.
[327] Y. Nakamori, H. Li, K. Miwa, S.-i. Towata, S.-i. Orimo, Syntheses and Hydrogen Desorption Properties of Metal-Borohydrides M(BH₄)<I>n</I> (M=Mg, Sc, Zr, Ti, and Zn; <I>n</I>=2–4) as advanced hydrogen storage materials, Mater. Trans. 47 (2006) 1898–1901, doi:10.2320/matertrans.47.1898.
[328] Y. Nakamori, S.-i. Orimo, Destabilization of Li-based complex hydrides, J. Alloys Compd. 370 (2004) 271–275, doi:10.1016/j.jallcom.2003.08.089.
[329] G. Soloveichik, J.-.H. Her, P.W. Stephens, Y. Gao, J. Rijssenbeek, M. Andrus, J.C. Zhao, Ammine Magnesium Borohydride Complex as a New Material for Hydrogen Storage: structure and Properties of Mg(BH4)2·2NH3, Inorg. Chem. 47 (2008) 4290–4298, doi:10.1021/ic7023633.
[330] J.-.H. Kim, S.-.A. Jin, J.-.H. Shim, Y.W. Cho, Thermal decomposition behavior of calcium borohydride Ca(BH4)2, J. Alloys Compd. 461 (2008) L20–L22, doi:10.1016/j.jallcom.2007.07.097.
[331] E. Jeon, Y. Cho, Mechanochemical synthesis and thermal decomposition of zinc borohydride, J. Alloys Compd. 422 (2006) 273–275, doi:10.1016/j.jallcom.2005.11.045.
[332] S. Srinivasan, D. Escobar, Y. Goswami, E. Stefanakos, Effects of catalysts doping on the thermal decomposition behavior of Zn(BH4)2, Int. J. Hydrogen Energy 33 (2008) 2268–2272, doi:10.1016/j.ijhydene.2008.02.062.
[333] S. Srinivasan, D. Escobar, M. Jurczyk, Y. Goswami, E. Stefanakos, Nanocatalyst doping of Zn(BH4)2 for on-board hydrogen storage, J. Alloys Compd. 462 (2008) 294–302, doi:10.1016/j.jallcom.2007.08.028.
[334] F.H. Stephens, V. Pons, R. Tom Baker, Ammonia–borane: the hydrogen source par excellence? Dalton Trans. (2007) 2613–2626, doi:10.1039/B703053C.
[335] T.B. Marder, Will we soon be fueling our automobiles with Ammonia–Borane? Angew. Chem. Int. Ed. 46 (2007) 8116–8118, doi:10.1002/anie.200703150.
[336] Z. Xiong, C.K. Yong, G. Wu, P. Chen, W. Shaw, A. Karkamkar, T. Autrey, M.O. Jones, S.R. Johnson, P.P. Edwards, W.I.F. David, High-capacity hydrogen storage in lithium and sodium amidoboranes, Nat. Mater. 7 (2008) 138–141, doi:10.1038/nmat2081.
[337] J.-.H. Kim, S.-.A. Jin, J.-.H. Shim, Y.W. Cho, Reversible hydrogen storage in calcium borohydride Ca(BH4)2, Scr. Mater. 58 (2008) 481–483, doi:10.1016/j.scriptamat.2007.10.042.
[338] Thakur, A.K., Kurtyka, K., Majumder, M., Yang, X., Ta, H.Q., Bachmatiuk, A., Liu, L., Trzebicka, B.,Rummeli, M.H., Recent advances in boron- and nitrogen-doped carbon-based materials and their various applications, 9 (2022) 2101964. https://doi.org/10.1002/admi.202101964.
[339] S.V. Sawant, A.W. Patwardhan, J.B. Joshi, K. Dasgupta, Boron doped carbon nanotubes: synthesis, characterization and emerging applications – A review, Chem. Eng. J. 427 (2022) 131616, doi:10.1016/j.cej.2021.131616.
[340] L.S. Panchakarla, A. Govindaraj, C.N.R. Rao, Boron- and nitrogen-doped carbon nanotubes and graphene, Inorg. Chim. Acta 363 (2010) 4163–4174, doi:10.1016/j.ica.2010.07.057.
[341] J.P. Paraknowitsch, A. Thomas, Doping carbons beyond nitrogen: an overview of advanced heteroatom doped carbons with boron, sulphur and phosphorus for energy applications, Energy Environ. Sci. 6 (2013) 2839–2855, doi:10.1039/C3EE41444B.
[342] D. Veeman, M.V. Shree, P. Sureshkumar, T. Jagadeesha, L. Natrayan, M. Ravichandran, P. Paramasivam, Sustainable development of carbon nanocomposites: synthesis and classification for environmental remediation, J. Nanomater. 2021 (2021) 5840645, doi:10.1155/2021/5840645.
[343] R. Nagar, B.P. Vinayan, S.S. Samantaray, S. Ramaprabhu, Recent advances in hydrogen storage using catalytically and chemically modified graphene nanocomposites, J. Mater. Chem. A 5 (2017) 22897–22912, doi:10.1039/C7TA05068B.
[344] M. Sterlin Leo Hudson, H. Raghubanshi, S. Awasthi, T. Sadhasivam, A. Bhatnager, S. Simizu, S.G. Sankar, O.N. Srivastava, Hydrogen uptake of reduced graphene oxide and graphene sheets decorated with Fe nanoclusters, Int. J. Hydrogen Energy 39 (2014) 8311–8320, doi:10.1016/j.ijhydene.2014.03.118.
[345] C.-.C. Huang, N.-.W. Pu, C.-.A. Wang, J.-.C. Huang, Y. Sung, M.-.D. Ger, Hydrogen storage in graphene decorated with Pd and Pt nano-particles using an electroless deposition technique, Sep. Purif. Technol. 82 (2011) 210–215, doi:10.1016/j.seppur.2011.09.020.
[346] Chen, J.-.W., Hsieh, S.-.H., Wong, S.-.S., Chiu, Y.-.C., Shiu, H.-.W., Wang, C.-.H., Yang, Y.-.W., Hsu, Y.-.J., Convertino, D., Coletti, C., Heun, S., Chen, C.-.H.,Wu, C.-L.J.a.e.-p., Hydrogen spillover and storage on graphene with single-site Ti catalysts. arXiv:2206.06638, 2022. Retrieved from https://ui.adsabs.harvard.edu/abs/2022arXiv220606638C
[347] M.F.A. Aboud, Z.A. Alothman, A.A. Bagabas, Hydrogen Storage in Untreated/Ammonia-Treated and Transition Metal-Decorated (Pt, Pd, Ni, Rh, Ir and Ru) Activated Carbons, Appl. Sci. 11 (14) (2021) Retrieved from, doi:10.3390/app11146604.
[348] V.B. Parambhath, R. Nagar, K. Sethupathi, S. Ramaprabhu, Investigation of spillover mechanism in palladium decorated hydrogen exfoliated functionalized graphene, J. Phys. Chem. C 115 (2011) 15679–15685, doi:10.1021/jp202797q.
[349] S.K. Konda, A. Chen, Palladium based nanomaterials for enhanced hydrogen spillover and storage, Mater. Today 19 (2016) 100–108, doi:10.1016/j.mattod.2015.08.002.
[350] Perovic, M., Qin, Q.,Oschatz, M., From molecular precursors to nanoparticles—tailoring the adsorption properties of porous carbon materials by controlled chemical functionalization, 30 (2020) 1908371. https://doi.org/10.1002/adfm.201908371.
[351] K.-.Y. Lin, W.-.T. Tsai, J.-.K. Chang, Decorating carbon nanotubes with Ni particles using an electroless deposition technique for hydrogen storage applications, Int. J. Hydrogen Energy 35 (2010) 7555–7562, doi:10.1016/j.ijhydene.2010.04.145.
[352] M. Sahoo, K.P. Sreena, B.P. Vinayan, S. Ramaprabhu, Green synthesis of boron doped graphene and its application as high performance anode material in Li ion battery, Mater. Res. Bull. 61 (2015) 383–390, doi:10.1016/j.materresbull.2014.10.049.
[353] V.B. Parambhath, R. Nagar, S. Ramaprabhu, Effect of nitrogen doping on hydrogen storage capacity of palladium decorated graphene, Langmuir 28 (2012) 7826–7833, doi:10.1021/la301232r.
[354] B.P. Vinayan, R. Nagar, V. Raman, N. Rajalakshmi, K.S. Dhathathreyan, S. Ramaprabhu, Synthesis of graphene-multiwalled carbon nanotubes hybrid nanostructure by strengthened electrostatic interaction and its lithium ion battery application, J. Mater. Chem. 22 (2012) 9949–9956, doi:10.1039/C2JM16294F.
[355] C. Chang, P. Gao, D. Bao, L. Wang, Y. Wang, Y. Chen, X. Zhou, S. Sun, G. Li, P. Yang, Ball-milling preparation of one-dimensional Co–carbon nanotube and Co–carbon nanofiber core/shell nanocomposites with high electrochemical hydrogen storage ability, J. Power Sources 255 (2014) 318–324, doi:10.1016/j.jpowsour.2014.01.034.
[356] A.A.S. Nair, R. Sundara, N. Anitha, Hydrogen storage performance of palladium nanoparticles decorated graphitic carbon nitride, Int. J. Hydrogen Energy 40 (2015) 3259–3267, doi:10.1016/j.ijhydene.2014.12.065.
[357] B.-.J. Kim, S.-.J. Park, Optimization of the pore structure of nickel/graphite hybrid materials for hydrogen storage, Int. J. Hydrogen Energy 36 (2011) 648–653, doi:10.1016/j.ijhydene.2010.09.097.
[358] S. Giraudet, Z. Zhu, X. Yao, G. Lu, Ordered mesoporous carbons enriched with nitrogen: application to hydrogen storage, J. Phys. Chem. C 114 (2010) 8639–8645, doi:10.1021/jp101119r.
[359] T.K. Nielsen, U. Bösenberg, R. Gosalawit, M. Dornheim, Y. Cerenius, F. Besenbacher, T.R. Jensen, A reversible nanoconfined chemical reaction, ACS Nano 4 (2010) 3903–3908, doi:10.1021/nn1006946.
[360] M.S. Salman, N. Rambhujun, C. Pratthana, K. Srivastava, K.-F. Aguey-Zinsou, Catalysis in liquid organic hydrogen storage: recent advances, challenges, and perspectives, Ind. Eng. Chem. Res. 61 (2022) 6067–6105, doi:10.1021/acs.iecr.1c03970.
[361] R.Y. Sathe, H. Bae, H. Lee, T.J. Dhilip Kumar, Hydrogen storage capacity of low-lying isomer of C_{24} functionalized with Ti, Int. J. Hydrogen Energy 45 (2020) 9936–9945, doi:10.1016/j.ijhydene.2020.02.016.
[362] Rimza, T., Saha, S., Dhand, C., Dwivedi, N., Patel, S.S., Singh, S.,Kumar, P., Carbon-based sorbents for hydrogen storage: challenges and sustainability at operating conditions for renewable energy, 15 (2022) e202200281. https://doi.org/10.1002/cssc.202200281.
[363] T. Das, S. Banerjee, K. Dasgupta, J.B. Joshi, V. Sudarsan, Nature of the Pd–CNT interaction in Pd nanoparticles dispersed on multi-walled carbon nanotubes and its implications in hydrogen storage properties, RSC Adv. 5 (2015) 41468–41474, doi:10.1039/C5RA03508B.
[364] K. Wenelska, B. Michalkiewicz, X. Chen, E. Mijowska, Pd nanoparticles with tunable diameter deposited on carbon nanotubes with enhanced hydrogen storage capacity, Energy 75 (2014) 549–554, doi:10.1016/j.energy.2014.08.016.
[365] O.K. Alekseeva, I.V. Pushkareva, A.S. Pushkarev, V.N. Fateev, Graphene and graphene-like materials for hydrogen energy, Nanotechnol. Russ. 15 (2020) 273–300, doi:10.1134/S1995078020030027.
[366] V. Jain, B. Kandasubramanian, Functionalized graphene materials for hydrogen storage, J. Mater. Sci. 55 (2020) 1865–1903, doi:10.1007/s10853-019-04150-y.
[367] E.V. Anikina, A. Banerjee, V.P. Beskachko, R. Ahuja, Influence of Kubas-type interaction of B–Ni codoped graphdiyne with hydrogen molecules on desorption temperature and storage efficiency, Mater. Today Energy 16 (2020) 100421, doi:10.1016/j.mtener.2020.100421.
[368] T. Hussain, A. De Sarkar, R. Ahuja, Strain induced lithium functionalized graphane as a high capacity hydrogen storage material, Appl. Phys. Lett. 101 (2012) 103907, doi:10.1063/1.4751249.

[369] Q. Peng, A.K. Dearden, J. Crean, L. Han, S. Liu, X. Wen, S. De, New materials graphyne, graphdiyne, graphone, and graphane: review of properties, synthesis, and application in nanotechnology, Nanotechnol. Sci. Appl. 7 (2014) 1–29, doi:10.2147/nsa.S40324.
[370] S.S. Samantaray, P. Anees, V.,S, R. Bhaghavathi Parambath, Graphene supported MgNi alloy nanocomposite as a room temperature hydrogen storage material – Experiments and theoretical insights, Acta Mater. 215 (2021) 117040, doi:10.1016/j.actamat.2021.117040.
[371] H.W. Langmi, J. Ren, B. North, M. Mathe, D. Bessarabov, Hydrogen storage in metal-organic frameworks: a review, Electrochim. Acta 128 (2014) 368–392, doi:10.1016/j.electacta.2013.10.190.
[372] P. Railey, Y. Song, T. Liu, Y. Li, Metal organic frameworks with immobilized nanoparticles: synthesis and applications in photocatalytic hydrogen generation and energy storage, Mater. Res. Bull. 96 (2017) 385–394, doi:10.1016/j.materresbull.2017.04.020.
[373] S.P. Shet, S. Shanmuga Priya, K. Sudhakar, M. Tahir, A review on current trends in potential use of metal-organic framework for hydrogen storage, Int. J. Hydrogen Energy 46 (2021) 11782–11803, doi:10.1016/j.ijhydene.2021.01.020.
[374] T. Jia, Y. Gu, F. Li, Progress and potential of metal-organic frameworks (MOFs) for gas storage and separation: a review, J. Environ. Chem. Eng. 10 (2022) 108300, doi:10.1016/j.jece.2022.108300.
[375] H. Li, M. Eddaoudi, M. O'Keeffe, O.M. Yaghi, Design and synthesis of an exceptionally stable and highly porous metal-organic framework, Nature 402 (1999) 276–279, doi:10.1038/46248.
[376] M. El Kassaoui, M. Lakhal, A. Benyoussef, A. El Kenz, M. Loulidi, Enhancement of hydrogen storage properties of metal-organic framework-5 by substitution (Zn, Cd and Mg) and decoration (Li, Be and Na), Int. J. Hydrogen Energy 46 (2021) 26426–26436, doi:10.1016/j.ijhydene.2021.05.107.
[377] L.-.Y. Bian, X.-.D. Li, X.-.Y. Huang, P.-h. Yang, Y.-.D. Wang, X.-Y. Liu, Z. Chen, Molecular simulation on hydrogen storage properties of five novel covalent organic frameworks with the higher valency, Int. J. Hydrogen Energy 47 (2022) 29390–29398, doi:10.1016/j.ijhydene.2022.06.285.
[378] L. Zhang, F.M. Nyahuma, H. Zhang, C. Cheng, J. Zheng, F. Wu, L. Chen, Metal organic framework supported niobium pentoxide nanoparticles with exceptional catalytic effect on hydrogen storage behavior of MgH2, Green Energy Environ. (2021), doi:10.1016/j.gee.2021.09.004.
[379] S. Yu, X. Meng, Z. Li, W. Zhang, X. Ju, Heterofullerene C48B12-impregnated MOF-5 and IRMOF-10 for hydrogen storage: a combined DFT and GCMC simulations study, Int. J. Hydrogen Energy 47 (2022) 39586–39594, doi:10.1016/j.ijhydene.2022.09.123.
[380] S. Srivastava, S.P. Shet, S. Shanmuga Priya, K. Sudhakar, M. Tahir, Molecular simulation of copper based metal-organic framework (Cu-MOF) for hydrogen adsorption, Int. J. Hydrogen Energy 47 (2022) 15820–15831, doi:10.1016/j.ijhydene.2022.03.089.
[381] X. Lu, Z. Xie, X. Wu, M. Li, W. Cai, Hydrogen storage metal-organic framework classification models based on crystal graph convolutional neural networks, Chem. Eng. Sci. 259 (2022) 117813, doi:10.1016/j.ces.2022.117813.
[382] H. Furukawa, N. Ko, Y.B. Go, N. Aratani, S.B. Choi, E. Choi, A.Ö. Yazaydin, R.Q. Snurr, M. O'Keeffe, J. Kim, O.M. Yaghi, Ultrahigh porosity in metal-organic frameworks, Science 329 (2010) 424–428, doi:10.1126/science.1192160.
[383] X. Zhang, R.-.B. Lin, J. Wang, B. Wang, B. Liang, T. Yildirim, J. Zhang, W. Zhou, B. Chen, Optimization of the pore structures of MOFs for record high hydrogen volumetric working capacity, Adv. Mater. 32 (2020) 1907995, doi:10.1002/adma.201907995.
[384] X.-.S. Wang, S. Ma, K. Rauch, J.M. Simmons, D. Yuan, X. Wang, T. Yildirim, W.C. Cole, J.J. López, A.d. Meijere, H.-.C. Zhou, Metal–organic frameworks based on double-bond-coupled di-isophthalate linkers with high hydrogen and methane uptakes, Chem. Mater. 20 (2008) 3145–3152, doi:10.1021/cm800403d.
[385] D.A. Gómez-Gualdrón, Y.J. Colón, X. Zhang, T.C. Wang, Y.-.S. Chen, J.T. Hupp, T. Yildirim, O.K. Farha, J. Zhang, R.Q. Snurr, Evaluating topologically diverse metal–organic frameworks for cryo-adsorbed hydrogen storage, Energy Environ. Sci. 9 (2016) 3279–3289, doi:10.1039/C6EE02104B.
[386] R. Grünker, V. Bon, P. Müller, U. Stoeck, S. Krause, U. Mueller, I. Senkovska, S. Kaskel, A new metal–organic framework with ultra-high surface area, Chem. Commun. 50 (2014) 3450–3452, doi:10.1039/C4CC00113C.
[387] Z. Chen, P. Li, R. Anderson, X. Wang, X. Zhang, L. Robison, L.R. Redfern, S. Moribe, T. Islamoglu, D.A. Gómez-Gualdrón, T. Yildirim, J.F. Stoddart, O.K. Farha, Balancing volumetric and gravimetric uptake in highly porous materials for clean energy, Science 368 (2020) 297–303, doi:10.1126/science.aaz8881.
[388] S. Rahali, Y. Belhocine, M. Seydou, F. Maurel, B. Tangour, Multiscale study of the structure and hydrogen storage capacity of an aluminum metal-organic framework, Int. J. Hydrogen Energy 42 (2017) 15271–15282, doi:10.1016/j.ijhydene.2017.04.258.
[389] E.I. Volkova, A.V. Vakhrushev, M. Suyetin, Improved design of metal-organic frameworks for efficient hydrogen storage at ambient temperature: a multiscale theoretical investigation, Int. J. Hydrogen Energy 39 (2014) 8347–8350, doi:10.1016/j.ijhydene.2014.03.167.
[390] M. Almáši, A. Sharma, T. Zelenka, Anionic zinc(II) metal-organic framework post-synthetically modified by alkali-ion exchange: synthesis, characterization and hydrogen adsorption properties, Inorg. Chim. Acta 526 (2021) 120505, doi:10.1016/j.ica.2021.120505.
[391] D. Ozer, D.A. Köse, O. Sahin, N.A. Oztas, Study of structural, surface and hydrogen storage properties of boric acid mediated metal (sodium)-organic frameworks, J. Mol. Struct. 1157 (2018) 159–164, doi:10.1016/j.molstruc.2017.12.063.
[392] A. Gencer, G. Surucu, Investigation of structural, electronic and lattice dynamical properties of XNiH3 (X = Li, Na and K) perovskite type hydrides and their hydrogen storage applications, Int. J. Hydrogen Energy 44 (2019) 15173–15182, doi:10.1016/j.ijhydene.2019.04.097.
[393] A. Gencer, G. Surucu, S. Al, MgTiO3Hx and CaTiO3Hx perovskite compounds for hydrogen storage applications, Int. J. Hydrogen Energy 44 (2019) 11930–11938, doi:10.1016/j.ijhydene.2019.03.116.
[394] G. Surucu, A. Candan, A. Gencer, M. Isik, First-principle investigation for the hydrogen storage properties of NaXH3 (X= Mn, Fe, Co) perovskite type hydrides, Int. J. Hydrogen Energy 44 (2019) 30218–30225, doi:10.1016/j.ijhydene.2019.09.201.
[395] M. Garara, H. Benzidi, M. Abdellaoui, M. Lakhal, A. El kenz, A. Benyoussef, O. Mounkachi, M. Loulidi, Hydrogen storage properties of perovskite-type $MgCoH_3$ under strain effect, Mater. Chem. Phys. 254 (2020) 123417, doi:10.1016/j.matchemphys.2020.123417.
[396] R.J.D. Tilley, in: Perovskites : Structure-property relationships, First Edition ed., Wiley, Chichester, West Sussex, United Kingdom, 2016, p. 2016.
[397] S. Hayat, R.M.A. Khalil, M.I. Hussain, A.M. Rana, F. Hussain, First-principles investigations of the structural, optoelectronic, magnetic and thermodynamic properties of hydride perovskites XCuH3 (X = Co, Ni, Zn) for hydrogen storage applications, Optik (Stuttg) 228 (2021) 166187, doi:10.1016/j.ijleo.2020.166187.
[398] A. Gencer, G. Surucu, Properties of BaYO3 perovskite and hydrogen storage properties of BaYO3Hx, Int. J. Hydrogen Energy 45 (2020) 10507–10515, doi:10.1016/j.ijhydene.2019.06.198.
[399] M.M. Whiston, I.M. Lima Azevedo, S. Litster, C. Samaras, K.S. Whitefoot, J.F. Whitacre, Hydrogen storage for fuel cell electric vehicles: expert elicitation and a levelized cost of driving model, Environ. Sci. Technol. 55 (2021) 553–562, doi:10.1021/acs.est.0c04145.
[400] D. Mori, K. Hirose, Recent challenges of hydrogen storage technologies for fuel cell vehicles, Int. J. Hydrogen Energy 34 (2009) 4569–4574, doi:10.1016/j.ijhydene.2008.07.115.
[401] E. Rivard, M. Trudeau, K. Zaghib, Hydrogen Storage for Mobility: a Review, Materials 12 (12) (2019) Retrieved from, doi:10.3390/ma12121973.

Enhancement in hydrogenation properties of ball-milled AB_5-type hydrogen storage alloy through catalyst

Enhancement in hydrogenation properties of ball-milled AB_5-type hydrogen storage alloy through catalyst

K Panwar[1] and S Srivastava[2*]
[1]Department of Physics, Pt.L.M.S.Government Post Graduate College, Rishikesh (Autonomous College), India -249201
[2]Government Degree College, Pokhri Quili, Tehri Garhwal, India -249146
Email: sumita_uki1@rediffmail.com

Abstract. Ball-milling of the hydrogen storage alloy has been shown to improve many hydrogenation properties under specific ball-milling parameters. The present investigation is based on further improvement in the hydrogenation properties through the addition of a catalyst. Catalysts are known to increase the rate of reaction. In the present investigation, rigorous studies have been performed on the various factors affecting the hydrogenation reaction through the addition of catalyst during ball-milling. The basic idea of the mechanism of catalyst is the availability of the free valencies behaving like active centres for promoting the reaction rate. Free valencies are more crowded at corners, peaks and cracks on the catalyst. The rough surface of the catalyst and finely dispersed catalyst are more effective in promoting the reaction rate. In the present investigation, various factors like spillover effect; defects introduced to the catalyst and hydrogen storage alloy during ball-milling; elasticity of metal hydride matrix; nature, size, hardness, number of unpaired electrons and variable valency of catalyst; the electronegative difference between catalyst and metal hydride; electron distribution and orbital structure; the ability of the catalyst to transfer stable diatomic hydrogen into the desired ionic configuration; binding between H atoms and catalyst and lowering of activation energy due to catalyst have been discussed in terms of their effect on hydrogenation properties. It has been found that all these factors help in lowering the activation energy for the hydrogenation process and improve the hydrogenation properties.

1. Introduction

The rate of reaction and related properties are known to increase by the use of catalysts. In the context of ball-milling of hydrogen storage alloys, many investigations have been reported to improve activation and hydrogen absorption-desorption kinetics through adding a suitable catalyst, mainly in Mg-based alloys [1-5]. Various catalysts like transition elements [6-13], Pd [14], V_2O_5, VN, VC, V [6], oxides of metal like titanium, vanadium, chromium, manganese, iron, copper, aluminium, silicon, scandium [15], and specially designed catalysts [16] are known to enhance the hydrogenation behaviour of magnesium group of alloys. Many reports are available for the study of catalytic effect on Mg-containing alloys; less attention has been paid on the study of catalytic effect on AB_5-type hydrogen storage alloys. In earlier study, we have reported the effect of transition elements as catalyst on the ball-milled $MmNi_5$-type alloy [17]. The employed transition elements were Co, Ni, Mn and Fe. An improvement has been noticed in the hydrogenation properties like activation, storage capacity, kinetics and cyclic stability by addition of transition elements. The improvement was observed in order of Co>Ni>Mn>Fe. The earlier studies emphasizing the effect of a catalyst on ball-milled alloys have

established the improvement in hydrogenation characteristics, but the reason behind such improvements are not discussed critically.

In the present study, efforts will be focused on discussing all such factors of the catalyst that may affect the hydrogenation properties. It may help the researchers to select the proper catalyst.

2. Methodology

The present investigation is based on the phenomenological approach towards enhancement in hydrogenation characteristics of ball-milled AB_5-type metal hydrides through catalyst. Firstly, the study was made on the basic mechanism of catalyst based on the existing known theory. After that, it was applied to the ball-milling hydrogen storage alloy. In this context, various steps of hydrogenation and dehydrogenation were reviewed. All the factors associated with the catalytic action, which may affect any hydrogenation step were correlated with the hydrogenation mechanism. In this way, the conditions of various factors related to catalytic action were optimized to give an improvement in the hydrogenation properties.

3. Results and discussions

3.1 Mechanism of catalytic reaction

It has been observed that the rate of a chemical reaction may be influenced considerably in the presence of a small amount of a specific substance. Such a substance is called a catalyst and the phenomenon is referred to as catalysis. Catalyst is an additive, which is not consumed in the reaction and remains chemically unchanged at the end of the reaction. However, the addition of catalyst alters the rate of chemical reaction. The catalyst can be recovered at the end of the reaction. A catalyst provides an alternative path with a lower energy barrier. Due to the lowering of the energy barrier, a larger number of molecules of reactants can cross it. Consequently the rate of reaction increases. Thus the main role of a catalyst is to lower the activation energy of the reaction by providing an alternative path with a lower energy barrier.

The general mechanism of improvement in hydrogenation behaviour of hydrogen storage alloys through the addition of catalyst during the ball-milling process can be understood through the theory of adsorption. Adsorption theory has been proposed to explain the mechanism of heterogeneous catalytic reactions (contact catalysis), particularly those involving gaseous reactant and solid catalyst. According to this theory, the surface of a solid catalyst possesses certain free valencies or active centres on its surface due to the presence of unsatisfied valencies and can hold the molecules of gaseous reactant through some sort of loose chemical combination. The action of a catalyst is two-fold in adsorption theory.

3.1.1 Adsorption theory of catalysis. Due to the adsorption, the concentration of reactant molecules on the surface of the catalyst increases. This leads to an increase in the frequency of collisions per unit time. Consequently, the rate of reaction increases by the law of mass action. This enhances the overall rate of reaction. Due to the presence of free valencies on the catalyst surface, the reactant molecules undergo chemisorptions and enter into a loose chemical combination with the catalyst leading to the formation of the intermediate activated compound. The product is obtained by the decomposition of the intermediate compound. The formation of the activated complex provides an alternative path of lower activation energy as compared to the uncatalysed reaction. This facilitates a large number of reactant molecules to cross over the energy barrier and to transform into products. Eventually, the rate of reaction increases.

The steps of the mechanism of catalysed reaction as suggested by the adsorption theory are being described here:

- *Adsorption of reactant molecules:* In the very first step, the catalytic surface absorbs the diffused reactant molecules. In the case of physical adsorption, week van der Waals' forces is operative; while in chemisorptions valence bond forces are present.

- *Formation of the activated intermediate compound:* The heat is released during adsorption due to exothermic nature of the reaction. The bonds within the adsorbed reactant molecules become weak or even break due to absorption of released heat and turning the adsorbed molecules into activated state. Hence, the molecules close to each other form an activated unstable compound.
- *Decomposition of the activated complex:* Due to unstable nature, the activated compound decomposes into the products. The products are attached to the catalyst surface by partial chemical bonds.
- *Desorption of products:* In final step, the products are released from the catalyst surface. The catalyst surface is again free for the adsorption of fresh reactant molecules.

3.1.2 *Free valencies and catalytic activity.* In the bulk of metal, constituent atoms are linked together and all of their valencies are satisfied. But, this is not true for the atoms present on the surface. The atoms present on the surface possess unbalanced chemical bonds, usually referred to as free valencies. The free valencies present at the surface of the catalyst particle are shown in figure 1.

As mentioned above, the free valencies present on the surface of a catalyst are responsible for holding the reactant molecules through chemisorptions. The distribution of free valencies on the catalyst surface is not uniform. They are much more in number at corners, peaks and cracks as shown in figure 2. The catalytic activity of the catalyst is maximum at these spots. Therefore, they are referred to as active centres. The greater the number of active centres, the greater is the catalytic activity of the catalyst. The active centres increase the rate of reaction not only by increasing the concentration of the reactant molecules at the surface of the catalyst but also by increasing the activity of the adsorbed molecules.

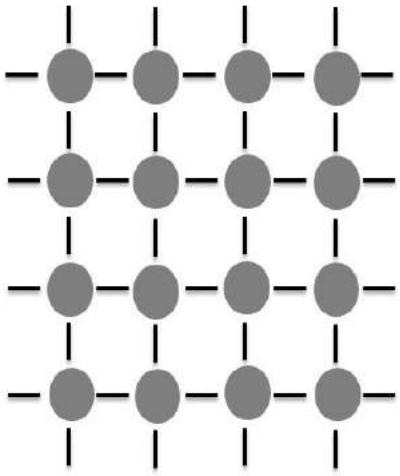

Figure 1. Free valencies at the surface of catalyst particle.

.

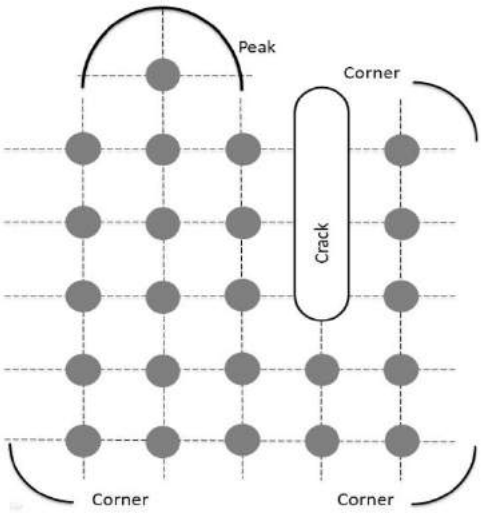

Figure 2. Free valencies are more crowded at corners, peaks and cracks on the catalyst surface.

Since the catalytic activity of a catalyst depends upon the number of active centres present on its surface, the catalytic activity of a catalyst can be increased by increasing the number of active centres. This can be achieved by two ways, as given in the following:

- By sub-division of the catalyst: The sub-division of a solid catalyst increases the number of free valencies as shown in figure 3. Thus, the sub-division of a catalyst increases its catalytic activity. This

is why a catalyst used in the finely divided state or the colloidal form is much more efficient as compared to the one which is in the form of lumps.

- By making the surface of the catalyst rough: Rough surfaces possess several corners, peaks and cracks which are rich in free valencies. They enhance the adsorption and thus increase the activity of the catalyst. This is why a catalyst with a rough surface is more efficient than that possessing a smooth surface.

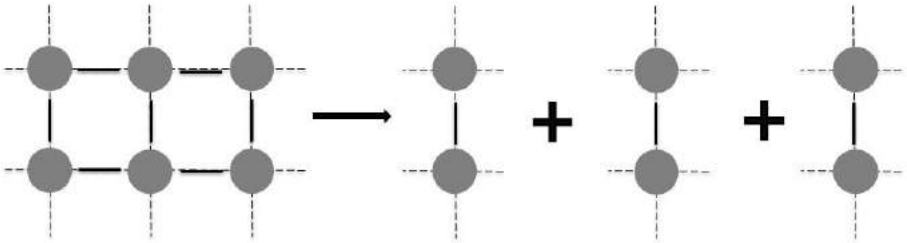

Figure 3. Subdivision of a catalyst increases the number of free valencies on its surface.

3.1.3 Explanation of characteristics of contact catalysis based on the adsorption theory. The various characteristics of contact catalysis (heterogeneous catalysis) can be explained based on the adsorption theory as follows.

- Increase of the reaction rate by the use of the catalyst: A catalyst provides an alternative path of lower activation energy by forming an activated complex as explained earlier. This facilitates a larger number of reactant molecules to cross the energy barrier. Consequently the rate of reaction increases.
- The specificity of a catalyst: According to the adsorption theory, the reactant molecules get attached to the surface of the catalyst through unbalanced chemical bonds (free valencies). The phenomenon involved is thus chemisorption. Chemisorption depends on the chemical nature of both the catalyst and reacting molecules. Thus, a catalyst prefers to chemisorbed on a particular type of reactant. This is why the action of the catalyst is specific and a particular catalyst is suitable for a particular reaction.
- Unchangeability of the catalyst: Desorption of the reactant products from the catalyst surface leaves the catalyst unchanged chemically and quantitatively. Therefore the catalyst remains unchanged chemically and can be obtained as it is at the end of the reaction.
- Effectiveness of small quantity of catalyst: According to the adsorption theory, the reactant molecules continuously adsorbed on the surface of the catalyst combined and get desorbed, leaving the catalyst free. Therefore a small quantity of catalyst is effective in converting a large number of reactants to the products.
- Greater efficiency of finely divided catalyst: As explained earlier, the sub-division of the catalyst increases tremendously its surface area and consequently the number of active centres present on its surface. This increases the efficiency of the catalyst. Hence, the catalyst in the finely divided state is more efficient than in the form of the lump or coarse powder.
- The action of promoter: A promoter increases the number of unbalanced chemical bonds by changing the crystal lattice of the catalyst. This increases the number of active centres and hence increases the catalytic activity of the catalyst.
- The action of poison: Catalytic poisons get preferentially adsorbed on the active centres of the catalyst as explained earlier. Due to the decrease in the number of active centres the catalyst is rendered ineffective.

3.2 Factors affecting hydrogenation process of ball-milled alloy through the catalyst

The hydrogen absorption process has the following steps:

- The physisorption of hydrogen molecule on the alloy surface
- The chemisorption of hydrogen molecule on the alloy surface
- The dissociation of hydrogen molecule into hydrogen atoms
- The formation of metal hydrides at nucleation sites
- The diffusion of hydrogen atom inside the bulk from the nucleation site.

Reverse processes occur during the desorption of hydrogen. All those factors of the catalyst which may affect positively these steps may be considered for improvement in hydrogenation behaviour. Such factors are listed below:

a) Spillover effect
b) Defects introduced in hydrogen storage alloy during ball-milling
c) Defects introduced to the catalyst during ball-milling
d) Nature of catalyst
e) Hardness of catalyst
f) Size of catalyst
g) The elasticity of the metal hydride matrix
h) Number of unpaired electrons in the catalyst
i) Variable valency of catalyst
j) Electronegativity difference between the catalyst and metal hydride
k) Electron distribution and orbital structure
l) The ability of the catalyst to transfer stable diatomic hydrogen into the desired ionic configuration
m) Binding between H atoms and catalyst
n) Lowering of activation energy due to catalyst

All these factors are discussed in detail in the following:

3.2.1 *Spillover effect.* In the case of $MmNi_5$-type alloy, normally the surface of hydrogen storage material is covered by oxides. This oxide layer acts as a poison for the physisorption and chemisorption of the hydrogen molecule. Because of this few absorption-desorption cycles are needed to break the particles into smaller size through pulverization. The smaller particles created with fresh and oxide-free surfaces due to pulverization may also get oxidized if the oxygen content is present. Hence the process of ball-milling to create fresh and oxide-free surfaces may fail if new surfaces again get oxidized. Here comes the role of catalyst. The most important feature of catalyst is that the particles of catalyst get attached to the oxide layer of intermetallic alloy. Now the hydrogen molecules prefer to physisorbed and chemisorbed on the surface of catalyst rather than on the surface of hydrogen storage alloy. Thus hydrogen molecules break into hydrogen atoms at the surface of the catalyst particle. After that hydrogen atoms may diffuse inside the hydrogen storage alloy through the catalyst particle or the interphase between catalyst particle and hydrogen storage alloy. The second process is more probable. Hence catalyst particles attached to the surface of hydrogen storage alloy act as active sites for breaking hydrogen molecules into hydrogen atoms. These hydrogen atoms are now available to be diffused at interstitial sites through the interphase boundary. This phenomenon is known as the spillover effect. A graphical model representing the spillover effect due to the addition of the catalyst is shown in figure 4.

3.2.2 *Defects introduced in hydrogen storage alloy during ball-milling.* This factor has been already discussed in detail in previous sections. Ball-milling introduces various defects in the structure of hydrogen storage alloy. These defect centres act as active nucleation sites for hydrogenation, thus improving the hydrogenation properties.

3.2.3 Defects introduced to the catalyst during ball-milling. The catalyst particle acts as an active chemisorptions site in the hydrogenation process. The defects created in the catalyst particle make it a

more active site for participating in the hydrogenation process. During the ball-milling process defects are introduced at the structural level of hydrogen storage alloys as well as to the added catalyst particle. Thus the defects created to the catalytic particle synergize the catalytic process.

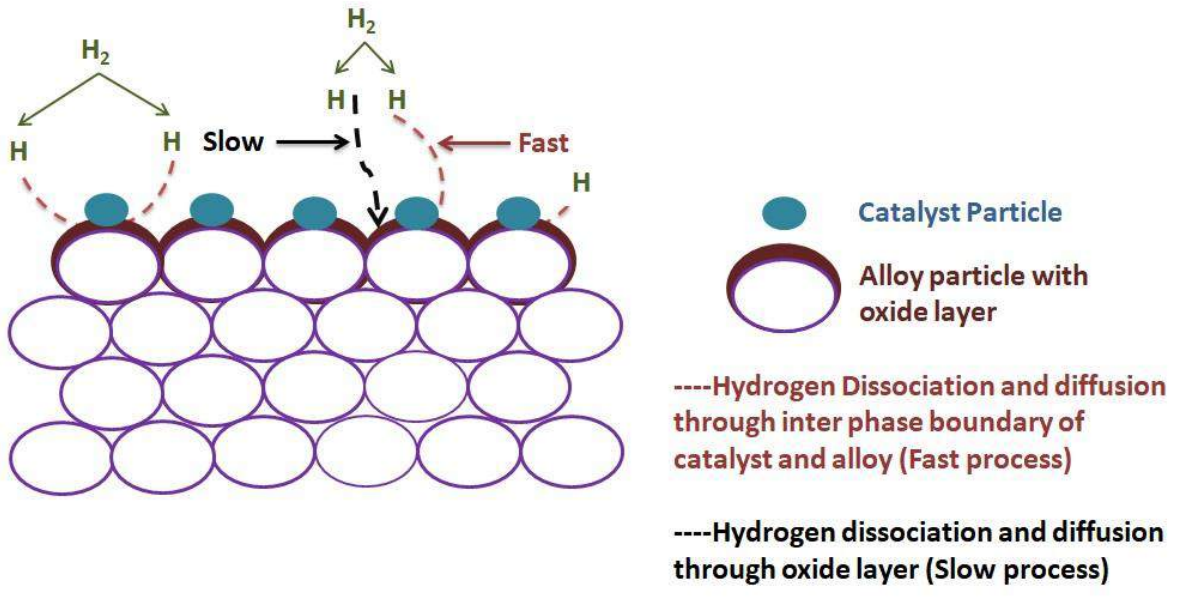

Figure 4. Spillover effect due to the addition of the catalyst.

3.2.4 Nature of catalyst. The reason behind the improved hydrogenation process by adding catalyst is the surface of catalyst acting as an active site for chemisorptions. Normally the surface of hydrogen storage alloy is covered with a layer of oxide. This creates an adverse effect on the hydrogenation process. The catalytic particles attached to the oxide layer offer an active site for breaking hydrogen molecule into hydrogen atoms. For proceeding forward with this step successfully, the catalyst should be free from the oxide layer. Hence only those elements and compounds may be chosen to act as catalysts that do not get oxidized easily.

3.2.5 Hardness of catalyst. The hardness of the added catalyst gives a synergetic effect to the ball-milling process for creating an optimum microstructure [18]. It may be mentioned here that the catalyst particles themselves get ruptured during the ball-milling process and turns into smaller particles. These smaller catalyst particles are responsible for the enhancement of the hydrogenation reaction. The hardness of the catalyst is an extra factor added to the ball-milling process of hydrogen storage alloy.

It is also noteworthy that the ductile nature of catalyst is not a favourable one. Due to ductility catalyst particles will not break into smaller particles. For better result of the catalytic process, the catalyst should have following ability.

- It should be finely dispersed and be able to mix closely and homogeneously onto the powder of hydrogen storage alloy.
- Catalyst should not react chemically with the alloy powder.
- The surface to volume ratio of the catalyst and of alloy particle should be optimized to get large interaction among them with hydrogen.
- The catalyst particles should not agglomerate.

3.2.6 *Initial size of the catalyst.* Smaller be the initial size of catalyst it will play a more effective role. Starting with the fixed concentration of catalyst smaller particles will disperse in the larger area. Hence, more active sites will be created in the overall material. When the catalyst is added its fine particles cover the fresh surface of hydrogen storage alloy powder milling and preserve it from further oxidation and act as an active nucleation site.

3.2.7 *Elasticity of metal hydride matrix.* Elasticity of the MH matrix is another favourable condition for hydrogenation. The absorption of hydrogen at the interstitial site in the lattice results in volume expansion of the lattice. This volume expansion of the lattice further helps in absorbing more hydrogen atoms with favoured H-H interaction. In absence of the lattice expansion the already present hydrogen atom may repeal the further absorption of hydrogen atom. In catalyst added ball-milled alloy, the metal hydride elasticity is comparatively large at the interface of catalyst and MH matrix. This situation favours the hydrogenation process [19].

3.2.8 *Number of unpaired electrons in the catalyst*. Unpaired electrons give reactivity to the elements. Larger be the number of unpaired electrons, it will act as more active sites. With unpaired electrons, the catalyst may make temporary bonding with hydrogen during chemisorptions by exchanging electrons to empty energy levels.

3.2.9 *Variable valency of catalyst.* The presence of variable valency in catalyst creates more active sites. This is similar to the case of e^- in semiconductor; where empty energy states are available, conduction is more likely to occur. In the same way, variable valency creates more active sites on the surface of the catalyst for hydrogen dissociation. Defects introduced to the catalyst during ball−milling also behave like active sites.

The local electronic structure of the catalyst plays an important role. With the help of electron exchange phenomenon, hydrogen molecules are adsorbed at the surface of the catalyst. After adsorption at catalytic surface, hydrogen molecule breaks into hydrogen atoms. The transition elements have property to show multiple valence states. This nature of catalyst explains the excellent catalytic activity of transition metals. In a similar way, defects in the electronic structure of the catalyst behave as catalytically active sites. During ball-milling process, the defect density is increased at the surface of transition metal.

3.2.10 Electronegativity difference between the catalyst and metal hydride. Hydrogen is widely applicable in heterogeneous catalysis. The relation of catalysts with hydrogen is of complex nature. The decomposition of hydrogen molecule is not straight forward. The hydrogen molecule may decompose into four different species. These different hydrogen species may be formed and transported further. These are: the radical H*, the bonded species H^-, or the charged species H^+ and H^- [20]. The creation of a specific hydrogen species depends on the local electronic environment.

Due to the presence of variable valency states in the catalyst, anionic vacancies are created at their surface. These vacancies behave like active sites. Therefore H_2 molecule is dissociated at the surface of the catalyst and H^- get absorbed at the active sites. H^- will further transfer from transition metal surface to less electronegative or more electropositive sites present as M^+ in metal hydride. Larger is the difference of electronegativity between M^+ in metal hydride and catalyst, more likely H^- will transfer to M^+ sites to form Metal hydride (MH).

The larger is the difference between the electronegativity factor between catalyst and M in MH the lesser be the driving force. Hence the difference between applied hydrogen pressure and equilibrium pressure of hydrogen during absorption also reduces. This also enhances the kinetics for H^- transfer from active sites present on the catalyst to interstitial sites of the AB_5 compound. Hence the presence of the catalyst will form active sites for the nucleation of the metal hydride. Further, the cracks and grain boundaries created due to ball−milling in the nano−crystalline material acts as a channel to suck hydrogen and these active sites present on the catalyst behave like a window.

The electronegativity difference between the catalyst and the alloy affects the storage capacity. In metal hydride matrix (MH) metal is electropositive and hydrogen is electronegative. After dissociation of hydrogen molecule at the surface of catalyst particle, hydrogen may be stored as an ion in the MH matrix. The larger be the electronegativity of catalyst, H^- ion will be repelled strongly. This forces the hydrogen ion to go towards M^+ ion. H^- ion may adopt straight and favoured path if the electronegativity difference between M and catalyst is enough. It may be mentioned here that this factor will not create any extra vacancies for hydrogen, but it mayfavour the hydrogen ion to populate all the vacancies created by any process. This type of guided path has been utilized by Im et al. in the metal-carbon-fluorine system for improving hydrogen storage using different level of electronegativity of metal and fluorine [21].

3.2.11 Electron distribution and orbital structure. It is well known that for hydrogen absorption and desorption the first step is decomposition and association of hydrogen molecules during absorption and desorption respectively. Catalyst plays an important role during this step. The choice of catalyst to perform well at this step is very crucial. It has been reported that for decomposition of hydrogen molecule, first the σ electron of hydrogen is transferred to the vacant d-orbital of the catalyst [13]. To favour this step, commonly transition elements are used as catalyst. In the next step electron from the filled d-orbital of the catalyst is transferred to the anti−bonding orbital (σ*) of the hydrogen. This combined process of donation and back donation of electron gives stability to the binding. The back transfer of electrons to σ* favours the breaking of the H−H bond to form H atoms. During desorption inverse process occurs; where H atoms are combined to form an H_2 molecule. Hence, the dissociation and association of hydrogen molecule is strongly related with the orbital structure and electron configuration of the catalyst employed. The availability of vacant d−orbital in the catalyst will promote this process.

3.2.12 Ability of catalyst to transfer stable hydrogen molecule into the desired ionic configuration. The catalyst chosen for the reaction should have ability to dissociate the hydrogen molecule into hydrogen atoms during absorption and combine the hydrogen atoms into hydrogen molecules during desorption process. These dissociated species of hydrogen should be able to move and enter inside the metal hydride matrix to occupy interstitial space available in the solid to form hydride. Initially the hydrogen molecule is stable due to paired electron. After dissociation into hydrogen atoms, comparatively less stable states are created. The ionic state of hydrogen is more stable in comparison to atomic state. In the ionic state of hydrogen, it has either paired or no electron. Hence, hydrogen shows unique dual ionic nature in the form of positive (without electron) or negative (with paired electron) ions. When hydrogen combines with oxygen, it transfers its electron to oxygen behaving like positive hydrogen ion. In case of the alkali atoms, hydrogen takes one electron from alkali atom and behaves as negative ion. Commonly in metal hydride matrix, hydrogen is present in the form of hydridic ion (negative ion). Moreover, the degree of hydridization, is correlated with the electropositive nature of the intermetallic alloy. The stability of the metal hydride matrix is related with the difference between the electropositivity of the metal and electronegativity of the hydrogen. It may be mentioned here that the delocalized hydridic co-ordination of hydrogen in hydrides does not necessarily contradict the postulated protonic mechanism of hydrogen diffusion, which can be explained by electrons being provided locally by the matrix. This explanation does not restrict the occurrence of positive ionic form of hydrogen, which depends on the nature of the electronic surrounding.

The choice of possessing different ionic character by hydrogen is related with the specific condition. This unique nature of hydrogen plays a key role in catalysis mechanism. The realisation of the dual nature of hydrogen requires the presence of electropositive and electronegative species simultaneously in the vicinity of hydrogen to combining with both the protonic and hydridic type of bonding. The catalyst performs the action of dissociating hydrogen and to stimulate them to acquire ionic state. Hence, the catalyst should be able to convert hydrogen into desired stable ionic state.

Whereas, during desorption of hydrogen, catalyst should be able to neutralize and recombine the hydrogen species to form molecular hydrogen. Therefore, the manipulation of local electronic environment is critical issue to be performed by the catalyst. With the proper choice of catalyst, the postulated ambivalent state of hydrogen may be achieved.

3.2.13 Binding between H atoms and catalyst. In a study of H_2 dissociation and subsequent atomic H diffusion on catalyst doped hydrogen storage alloy surfaces strength of binding between H atom and catalyst (maybe transition metal) is very important [22]. The dissociation of the H_2 molecule is only the first step for the absorption of hydrogen. A second fundamental step is the diffusion of the H atoms away from the catalytic site. Few elements used as a catalyst may reduce the H_2 dissociation barrier, while others may reduce the diffusion barrier. The best catalyst will be that which may reduce both dissociation and diffusion barrier. When H atoms bind too strongly with the catalyst, it will obstruct diffusion inside the MH matrix away from the catalytic site. Under such condition, the catalyst is deactivated quickly and slows down the absorption process. On the other hand, the transition metals, which do not bind too strongly the H atoms, allow early diffusion. The report suggests that the degree of binding between hydrogen and catalyst is correlated to the position of the d−band centre [22]. The activation energy barrier for dissociation of H_2 on Ni, Fe and Co is 0.06, 0.03 and 0.03 eV respectively [22]. Similarly, the activation energy barrier for diffusion of H atom is 0.27, 0.30 and 0.41 eV for Ni, Fe and Co respectively. There is an inverse correlation between the height of the diffusion barrier E_{diff} and the height of the dissociation barrier. Hence a compromise is needed to combine a low activation barrier for both the dissociation and diffusion process.

3.2.14 Lowering of activation energy due to catalyst. All the factors affecting the catalysis process for hydrogenation behaviour must be followed by lowering the activation energy at every step of hydrogenation as mentioned at the starting of this section. There are several steps of hydrogenation and reverse steps for dehydrogenation. Larger is the number of steps involving low activation energy, more efficient is the overall hydrogenation-dehydrogenation process.

4. Conclusions

From the above discussions, it is clear that the addition of catalyst during the ball-milling process may further improve the hydrogenation characteristics. On the addition of catalyst during ball-milling of the alloy, the following conclusions may be drawn:

- Ball-milling introduces various defects in terms of vacancies, dislocations and grain boundaries together with strain in the original bulk alloy as well as in added catalyst.
- The increased defects and smaller size of ball-milled alloy and catalyst result in a fresh oxide-free surface with more channels for hydrogen diffusion through inter-phase and grain boundaries, acting as hydride nucleation centres. This eventually enhances the activation and kinetic process of hydrogenation-dehydrogenation in the ball-milled alloy.
- Ball-milling also introduces the defects in the electronic structure of the alloy and catalyst, because of which more hydrogen may be trapped at these defects sites by exchanging the electrons.
- There are several factors and effects which are responsible for the improved hydrogenation process. These are mainly the spillover effect, nature of the added catalyst and electronic structure of catalyst for the parent alloy matrix. All such factors help in lowering the activation energy for the hydrogenation process.
- The improved hydrogenation behaviour of ball-milled alloy due to the addition of catalyst in terms of hydrogen storage capacity, activation process, and kinetics may be attributed to all these phenomena discussed above.

References

[1] Shahi RR, Bhatanagar A, Pandey SK, Shukla V, Yadav TP, Shaz MA and Srivastava ON 2015 MgH_2-$ZrFe_2H_x$ nanocomposites for improved hydrogen storage characteristics of MgH_2 *Int. J. Hydrogen Energy* **40** 11506-13.

[2] Pukazhselvan D, Gonzalo Otero-Irurueta GO, Perez J, Singh B, Bdikin I, Singh MK and Fagg DP 2016 Crystal structure, phase stoichiometry and chemical environment of $Mg_xNb_yO_{x+y}$ nanoparticles and their impact on hydrogen storage in MgH_2 *Int. J. Hydrogen Energy* **41** 11709-15.

[3] House SD, Vajo JJ, Ren C, Zaluzec NJ, Rockett AA and Robertson IM 2017 Impact of initial catalyst form on the 3D structure and performance of ball-milled Ni-catalyzed MgH_2 for hydrogen storage *Int. J. Hydrogen Energy* **42** 5177-87.

[4] Zhang Y, Li Y, Shang H, Yuan Z, Qi Y, Dong X and Guo S 2018 Hydrogen storage performance of the as-milled Y-Mg-Ni alloy catalyzed by CeO_2 *Int. J. Hydrogen Energy* **43** 1643-50.

[5] Pighin SA, Coco B, Troiani H, Castro FJ and Urretavizcaya G 2018 Effect of additive distribution in H_2 absorption and desorption kinetics in MgH_2 milled with $NbH_{0.9}$ or NbF_5 *Int. J. Hydrogen Energy* **43** 7430-9.

[6] Oelerich W, Klassen T and Bormann R 2001 Comparison of the catalytic effects of V, V_2O_5, VN, and VC on the hydrogen sorption of nanocrystalline Mg *J. Alloys Compd.* **322** L5-9.

[7] Uchida HH, Wulz HG and Fromm E 1991 Catalytic effect of Nickel, iron and palladium on hydriding titanium and storage materials *J. Less Comm. Met.* **172-174** 1076-83.

[8] Tessier P and Akiba E 1999 Catalysed reactive milling *J. Alloys Compd.* **293-295** 400-2.

[9] Liang G, Huot J, Boily S, Neste AV and Schulz R 1999 Catalytic effect of transition metals on hydrogen sorption in nanocrystalline ball milled MgH_2-Tm (Tm=Ti, V, Mn, Fe and Ni) systems *J. Alloys Compds.* **292** 247-52.

[10] Duhamel LJ, Carpentier J and Ponchel A 2007 Catalytic hydrogen storage in cerium nickel and zirconium (or aluminium) mixed oxides *Int. J. Hydrogen Energy* **32** 2439-44.

[11] Checchetto R, Bazzanella N, Miotello A and Mengucci P 2007 Catalytic properties on the hydrogen desorption process of metallic additives dispersed in the MgH_2 matrix *J. Alloys Compds.* **446-447** 58-62.

[12] Ershova OG, Dobrovolsky VD, Solonim YM, Khyzum OY and Koval AY 2008 Influence of Ti, Mn, Fe, and Ni addition upon thermal stability and decomposition temperature of the MgH_2 phase of alloys synthesized by reactive mechanical alloying *J. Alloys Compds.* **464** 212-8.

[13] Xie L, Liu Y, Zhang X, Qu J, Wang Y and Li X 2009 Catalytic effect of Ni nanoparticles on the desorption kinetics of MgH_2 nanoparticles *J. Alloys Compds.* **482** 388-92.

[14] Zaluski L, Zaluska A, Tessier P, Strom-Olsen JO and Schulz R 1995 Catalytic effect of Pd on hydrogen absorption in mechanically alloyed Mg_2Ni, $LaNi_5$ and FeTi *J. Alloys Compds.* **217** 295-300.

[15] Oelerich W, Klassen T and Bormann R 2001 Metal oxides as catalyst for improved hydrogen sorption in nanocrystalline Mg-based materials *J. Alloys Compd.* **315** 237-242.

[16] Zaluska A and Zaluski L 2005 New catalytic complexes for metal hydride systems *J. Alloys Compd.* **404-406** 706-11.

[17] Srivastava S and Panwar K 2015 Effect of transition metals on ball-milled $MmNi_5$ hydrogen storage alloy *Materials for Renewable and Sustainable Energy* **4** 19.

[18] Rivoirard S, Rango PD, Fruchart D. Charbonnier J and Vempaire D 2003 Catalytic effect of additives on the hydrogen absorption properties of nano-crystalline MgH_2(X) composites *J. Alloys Compd.* **356-357** 622-5.

[19] Pasquini L, Sacchi M, Brighi M, Boelsma C, Bals S, Perkisas T and Dam B 2014 Hydride destabilization in core-shell nanoparticles *Int. J. Hydrogen Energy* **39** 2115-23.

[20] Duhamel LJ, Carpentier J and Ponchel A 2007 Catalytic hydrogen storage in cerium nickel and zirconium (or aluminium) mixed oxides *Int. J. Hydrogen Energy* **32** 2439-44.
[21] Im JS, Park SJ and Lee YS 2009 The metal-carbon-fluorine system for improving hydrogen storage by using metal and fluorine with different levels of electronegativity *Int. J. Hydrogen Energy* **34** 1423-8.
[22] Pozzo M and Alfe D 2009 Hydrogen dissociation and diffusion on transition metal (= Ti, Zr, V, Fe, Ru, Co, Rh, Ni, Pd, Cu, Ag) -doped Mg(0001) surfaces *Int. J. Hydrogen Energy* **34** 1922-30.

Acknowledgements
the authors are grateful to the Department of Physics (Solid State Laboratory) BHU India and Prof. I.P.Jain (Rajasthan University, INDIA) for helpful discussions.